



Review

Iron oxide copper-gold (IOCG) deposits – A review (part 1): Settings, mineralogy, ore geochemistry and classification



Roger G. Skirrow

Geoscience Australia, GPO Box 378, Canberra, ACT Australia 2601, Australia

A B S T R A C T

Characteristics of ten of the world's metallogenic provinces hosting iron oxide Cu-Au (IOCG) deposits have been critically assessed, including their geological and tectonothermal evolution, alteration-mineralisation parageneses, and ore geochemistry. A new classification framework is proposed in which IOCG deposits form the major part of a family of deposits within Cu-Au-Fe (CGI) mineral systems. Other family members include Fe-sulfide Cu-Au (ISCG) deposits lacking significant iron oxides. The classification combines three criteria: geological and tectonic settings, oxide-sulfide mineralogy, and ore geochemical characteristics. These criteria form the basis for defining deposit subtypes, and also distinguish deposits in CGI mineral systems from porphyry Cu (-Au), skarn Fe-Cu (-Au) and iron oxide-apatite (IOA) deposits, although there are some shared features.

CGI mineral systems with IOCG deposits occur in three geological and tectonic settings. Two settings are closely linked and are termed orogenic and post-orogenic settings. Syn-deformational IOCG and related deposits in orogenic settings formed during regional tectonothermal events at mid- to shallow-crustal levels at generally brittle-ductile conditions. Available data are consistent with a model in which provinces hosting orogenic IOCG deposits experienced tectonic switching from compression to extension, which was also commonly marked by regional bimodal magmatism. This review shows that many of world's IOCG provinces are hosted in such orogenic settings. The rarer post-orogenic extensional setting, often previously described as 'anorogenic', hosts the super-giant Olympic Dam deposit. Andean-type continental margin magmatic arcs undergoing extension comprise the third important setting of IOCG provinces. All major IOCG metallogenic provinces are characterised by the coincidence in space and time between pre-IOCG sedimentary ± volcanic basins and *syn*-IOCG intrusive ± volcanic regional magmatism.

IOCG and ISCG deposits in CGI mineral systems are characterised by an association of Cu and Au with highly elevated Fe (e.g. 15–60 wt% Fe) in the form of abundant Fe oxides and/or Fe sulfides and/or Fe-rich silicates, and with sufficient Cu-Au to be classed as a resource. Deposits in CGI mineral systems exhibit distinctive enrichments of elements in the chalcophile-siderophile suite (Co, Ni, Bi, Se, Te) and/or elements in the LILE-HFSE suite (REE, U, F, Ba, Mo), the ratios of which vary greatly between deposits and define a continuum. A key finding is the correlation of these geochemical variations with the range of oxidation-reduction (redox) characteristics of the ore-related hydrothermal minerals, and also with the three geological-tectonic settings. The causes of these variations are likely fundamental in the formation of IOCG and related deposits.

CGI mineral systems are characterised by paragenetically early Na ± Ca-rich hydrothermal alteration (generally in regional-scale zones), followed by combinations of Fe-, Ca- and K-rich minerals that preceded or accompanied Cu-Au mineralisation. This review has shown that volatile-bearing minerals (e.g. carbonate (CO₂), apatite (P), fluorite (F), barite (SO₄), tourmaline (B)) were deposited with the Cu-Au mineralisation in almost all IOCG provinces, albeit less abundantly in the continental arc-hosted deposits.

It is argued that the special combinations of basinal-derived and magmatic/igneous-derived inputs to ore formation produces the distinctive range of characteristics of IOCG and related deposits in CGI mineral systems.

1. Introduction

The diverse group of iron oxide copper-gold (IOCG) deposits has been one of the most contentious classes of ore deposits since its recognition as a new type in the mid 1980s to early 1990s. Central to the debates have been the issues of definition, classification, the roles of magmatic versus and non-magmatic sources of fluids and metals, and tectonic settings. Early studies (e.g. Meyer, 1988) noted similarities between the giant Olympic Dam Cu-U-Au deposit, discovered in 1975 in South Australia, and iron oxide-apatite-rich deposits of the southeast

Missouri and Kiruna areas (USA, Sweden), and the Bayan Obo magnetite-REE deposit in China. Hitzman et al. (1992) included a number of other iron oxide-rich deposits in first defining the 'Proterozoic iron oxide (Cu-U-Au-REE)' class of ore deposits, and proposed a preliminary model involving extensional tectonic settings. Subsequently, a large number of highly diverse deposits, some newly discovered and others re-classified, have been included within an expanding group of IOCG deposits.

Despite major efforts to clarify and tighten the definition of IOCG deposits and to understand their settings (e.g. reviews by Sillitoe, 2003;

E-mail address: roger.skirrow@gmail.com.

Williams et al., 2005; Corriveau, 2007; Groves et al., 2010; Barton, 2013), there remain many unresolved first-order problems of definition and classification. Some of these issues stem from the IOCG name itself, which describes the mineralogy (iron oxide) associated with the principal ore metals (copper, gold) in the deposits. This terminology contrasts with many other well known deposit types such as porphyry Cu, volcanic-hosted massive sulfide Zn-Pb-Cu, orogenic Au, epithermal Au, etc, which include their principal ore metals and an aspect of either their mode of origin or the ore depositional environment. As a consequence of the wide-embracing IOCG name, deposits of likely fundamentally different origins (e.g. magmatic-hydrothermal versus non-magmatic fluid or metal sources) have been included by some workers in the IOCG group of deposits.

Also problematic has been the variance in the definitions of the required grades of copper and gold to qualify as IOCG deposits. Several workers have proposed broad definitions of IOCG deposits such that some iron oxide-rich deposits with little or no copper or gold are considered part of the IOCG ‘family’ as possible ‘end-members’ or as ‘affiliated’ deposits (e.g. Hitzman et al., 1992; Williams et al., 2005; Corriveau, 2007; Barton, 2013). For example, Barton (2013) included a range of iron oxide-rich deposits lacking, or with sub-economic levels of, Cu-Au-REE-P-Ag-U-Co as part of an ‘iron oxide (-Cu-Au-REE-P-Ag-U-Co) clan’. Groves et al. (2010) addressed this and other problems relating to the extreme diversity of deposits previously classified as IOCG deposits by defining a sub-group of ‘IOCG sensu stricto’ containing > 100 Mt of economic Cu and Au ore, within a broader group of ‘iron oxide-associated’ deposits. Their broader group included some alkaline intrusion- and carbonatite-related deposits such as Palabora (Cu) and Vergenoeg (magnetite-fluorite), considered to be end-members of the ‘iron oxide-associated deposits’. The definition of IOCG deposits by Williams et al. (2005) was revised by Groves et al. (2010) as follows: (1) Cu + Au as economic metals, (2) hydrothermal characteristics and structural controls, commonly with breccias, (3) abundant low-Ti Fe oxides (magnetite, hematite) and/or Fe silicates (grunerite, Fe actinolite, fayalite), (4) LREE enrichment and low-S sulfides, including chalcopyrite-bornite-chalcocite and pyrrhotite, (5) lack of abundant *syn*-sulfide quartz veins and alteration that commonly includes a decreased SiO₂ content of wall rocks, and (6) a temporal relationship with magmatism, yet no close spatial association with causative intrusions.

While consistent with the definition of IOCG deposits of Williams et al. (2005), the classification scheme of Williams (2010) included ‘hematite-group’ and ‘magnetite-group’ IOCG deposits, and differentiated these from several types of ‘affiliated deposits’ (low-Fe-oxide Cu-Au; Co-As ± Au ± Ag ± U ± Fe-oxide deposits with low Cu; and Fe oxide-U deposits with low Cu). Iron oxide-apatite (IOA) deposits of the Kiruna type were excluded from the ‘IOCG and affiliated deposits’ grouping of Williams (2010), as were several types of ‘orthomagmatic/magmatic-hydrothermal iron oxide ± apatite ± Cu ± Au ± rare metal deposits’ such as Palabora (Cu), Bayan Obo (Fe, REE), magnetite-rich porphyry-related Cu-Au deposits such as Ertsberg-Grasberg, and the Vergenoeg magnetite-fluorite deposit. Following Groves et al. (2010), yet another grouping was proposed by Porter (2010a) termed ‘iron oxide associated-alkali altered (IOAA) mineralised systems’, which incorporate: IOCG sensu stricto deposits, IOA deposits, carbonatite and alkaline igneous-related iron oxide deposits, and a subgroup of ‘miscellaneous deposits sharing characteristics of both iron oxide alkali-altered systems and another ore system’. Finally, Corriveau et al. (2010a,b, 2016) refined the IOAA scheme of Porter (2010a) and considered ‘iron oxide and alkali-calcic alteration ore systems’ as including IOCG deposits (with economic Cu ± Au, Ag, REE, U) and five other deposit subtypes (iron oxide ± apatite ± REE deposits; albite-hosted U or Au; skarn-hosted + K-skarn ± Fe oxides with base and precious metals; low-Cu IOCG variants with Au, Co, As, Bi, Ag; and ‘skarn’ alteration).

The foregoing overview of previous classifications of IOCG and ‘affiliated’ deposits highlights the challenges in defining and categorising the highly diverse deposits of Cu-Au associated with iron oxides and/

or iron sulfides. As noted by Groves et al. (2010) the ‘IOCG group of deposits … has progressively become too-embracing …’, and ‘consideration of this broad group as a whole obscures the critical features of the IOCG sensu stricto deposits …’. This appears still to be the case. The aim of this two-part review is to critically re-examine IOCG deposits from a fresh perspective using newly available data so as to identify the diagnostic geological and geochemical characteristics and ore-forming processes of deposits previously included in the IOCG class. Ultimately, it is intended to clarify the issues of ‘what is an IOCG deposit’ and ‘what controls where they occur’ based on an improved understanding of the fundamental processes of ore formation, using a mineral systems framework. A mineral system is defined as ‘all geological factors that control the generation and preservation of mineral deposits’ (Wyborn et al., 1994). The ‘essential ingredients’ in a mineral system are the sources of ore metals, transport of those metals, and their deposition in a mineral deposit. The scales of these geological components and processes range from crustal and regional to deposit and micro scales. A mineral system may generate a range of deposit types and subtypes that are genetically related to the same shared ore-forming processes and geological ‘ingredients’ of the system. Fossil mineral systems can be mapped by identifying (1) the energy sources or ‘drivers’ of the mineral system, (2) the sources of the ore metals, fluids and sulfur, (3) the architecture or structure of the fluid flow pathways, and (4) the physico-chemical gradients of ore deposition. The present contribution addresses aspects of components (1), (3) and (4) by focussing on the regional geological and tectonic settings of IOCG mineral systems, and the mineralogical and geochemical characteristics of the hydrothermal systems, so as to improve the mapping of mineral systems with IOCG deposits and the discovery of new resources. This builds on previous efforts to map the potential for IOCG mineral systems (Skirrow et al., 2019).

This contribution commences with a summary of the general features and definition of IOCG and related deposits and then describes CGI mineral systems containing IOCG deposits from the broad (regional) scale geological context to the deposit- and micro-scale features. First, a synthesis of the geological characteristics and tectonic settings of IOCG deposits is presented, based on detailed descriptions of ten of the world’s IOCG metallogenic provinces and geochronological constraints presented in the *Supplementary Information*. This is followed by descriptions of hydrothermal mineral assemblages and their paragenetic sequences, including proximal and regional alteration and zoning. The next section addresses the ore geochemistry of IOCG and related deposits using published data, and links this to the geotectonic settings and mineralogical variations. Finally, the findings are integrated within a new classification of the global family of IOCG and related deposits. An accompanying contribution reviews the sources of ore components and discusses the ore-forming processes and origins of these enigmatic deposits (Skirrow, in prep.).

2. General features and global distribution of IOCG deposits

2.1. General features

This review considers a group of Cu-Au-Fe-rich deposits that have been variously described as IOCG deposits as well as iron oxide-poor Cu-Au deposits occurring in the same metallogenic provinces. The latter deposits are commonly Fe-sulfide- rather than Fe-oxide-rich and were termed iron sulfide Cu-Au or ISCG deposits by Haynes (2000). In the current study IOCG and ISCG deposits have been grouped together to form a family of Cu-Au-Fe or CGI deposits with a specific set of characteristics that distinguish them from other well known Cu (-Au) and/or Fe ore deposit types such as porphyry Cu (-Au), skarn Fe and Cu, and IOA deposits. These characteristics, listed below, form a descriptive definition of IOCG and related ISCG deposits within CGI mineral systems. They are based on the current review of the geology and deposits in ten global provinces together with previous reviews (e.g. Hitzman et al.,

1992; Haynes, 2000; Sillitoe, 2003; Williams et al., 2005; Corriveau, 2007; Barton, 2013).

- IOCG and ISCG deposits display a deposit- and orebody-scale spatial association of Cu-Au resources with Fe-rich rocks (e.g. 15–60 wt% Fe), with Fe hosted by low-Ti oxides (magnetite and/or hematite), and/or sulfides and/or other Fe-rich minerals; Fe-oxide/Fe-sulfide ratios vary greatly between and within deposits.
- Copper sulfides and Au are associated with moderate to strong enrichments of several of the following groups of elements which may attain ore grade in some deposits: Ag, Co, Ni, Bi, Se, Te, In and/or U, LREE, F, Ba, Mo; in most deposits there are little or no significant enrichments in Zn, Pb, Cd, As, Sb, W, Sn, Ta, Nb or Li, although rare examples of outer/distal Zn-Pb-As-rich zones are known.
- Copper and Fe-sulfides and Au either post-dated, or were deposited synchronously with, the Fe-oxides and Fe-silicates; Fe-sulfides are pyrrhotite and/or pyrite, whereas the Cu-sulfides include chalcopyrite, bornite and chalcocite which are spatially zoned in some deposits; provinces with IOCG and related deposits may contain a wide range of oxide-sulfide assemblages and from reduced pyrrhotite ± magnetite to pyrite ± magnetite to oxidised hematite ± pyrite; IOCG deposits that lack Fe-sulfides are also known.
- Deposit- and orebody-scale hydrothermal alteration in higher temperature settings generally comprises variants of iron, potassic and calcic mineral assemblages including magnetite, biotite, Ca-amphibole (e.g. actinolite-tremolite), Ca- and/or Fe-carbonate, K-feldspar, and much less common Ca-Fe-rich clinopyroxene, garnet, and iron silicates.
- In lower temperature settings the proximal alteration with Fe-Cu-Au minerals comprises combinations of hematite, sericite/phengite, chlorite, and Ca- and/or Fe-carbonate.
- Some IOCG and related deposits contain hydrothermal barite, fluorite, apatite, allanite, molybdenite, tourmaline, and a range of U- and REE-bearing minerals accompanying Cu-Au mineralisation; anhydrite is rarely reported, and epidote is generally inconspicuous although allanite is a key host of REE in some deposits.
- Paragenetically early sodic alteration (albitic plagioclase, scapolite) is uncommon in most Cu-Au ore zones but is characteristic of distal and regional alteration zones where it may be accompanied by Ca-amphiboles, Ca-clinopyroxenes, and minor titanite and magnetite; breccias and brittle-ductile structures commonly control the sites of regional Na (-Ca) alteration; calcic-iron (Ca-Fe) and potassic-iron (K-Fe) alteration typically overprints sodic alteration.
- Hydrothermal quartz is generally not abundant with iron oxide-rich Cu-Au mineralisation but may be present within iron oxide-poor, iron sulfide-rich, Cu-Au zones of the same deposits or in separate ISCG deposits.
- The higher temperature deposits that formed in mid-crustal settings are commonly hosted by brittle-ductile shear zones and related deformation structures including breccias, whereas deposits in lower temperature shallow-crustal settings occur in brittle deformation structures such as faults, veins and breccia zones.
- Two (or more) fluids have been identified as related to Fe-rich alteration and Cu-Au mineralisation in many deposits, including hypersaline and lower salinity brines; CO₂-rich fluids are also commonly present; isotopic and geochemical evidence suggests contributions of water, halogens and sulfur from non-magmatic as well as magmatic or leachedigneous rock sources.
- Proximal intrusive igneous rocks contemporaneous with Cu-Au-Fe mineralisation are not present at many deposits or are volumetrically minor; however, in specific settings (e.g. Andean) there are close spatial and temporal relationships with intrusions of generally intermediate composition; in other IOCG provinces regional magmatism that was broadly coeval with Cu-Au mineralisation tends to be bimodal in composition.

- Almost all IOCG and related deposits occur within volcano-sedimentary basinal host rocks that have been metamorphosed at low to medium grades either before or during Cu-Au-Fe ore formation; local host rocks are highly variable and include metasedimentary, metavolcanic, and igneous rocks ranging from mafic to felsic in composition.

Any proposed holistic genetic and exploration model(s) for this group of IOCG and related deposits must account for all of the key features listed above. This review leads to the conclusion that there are two fundamentally different types of IOCG deposits that formed in separate geotectonic settings (orogenic to post-orogenic versus arc-hosted Andean-type), yet both types involved the coincidence in time and space between pre-IOCG basins and *syn*-mineralisation regional igneous activity. It is proposed here and in the companion paper that the great diversity of deposits in the CGI family is a result of these variations in geological settings and differing contributions of fluids and metals from the basinal and magmatic/igneous sources.

2.2. Global distribution

The major IOCG deposits occur widely in space and time, as previously recognised (e.g. Groves et al., 2010) and summarised in Fig. 1. The ten IOCG metallogenic provinces and their mineral deposits considered in this review include (in age order from Archean to Mesozoic): Carajás province (northern Brazil); Guelb Moghrein deposit (Mauritania); Kiruna province (northern Sweden); Great Bear magmatic zone (northwest Canada); Tennant Creek province (northern Australia); Kangdian province (southwest China) and possible extension in Vietnam including the Sin Quyen deposit; eastern Gawler Craton and subjacent Curnamona Province (southern Australia); Cloncurry province (northeastern Australia); Khetri province (northwest India); and the Andean province (Chile and Peru). The background image in Fig. 1 shows global seismic velocity (shear wave) anomalies at a depth of 165 km (Lu et al., 2019), which is a proxy for the present day boundaries of cratonic blocks at this depth. Although the spatial resolution is relatively low, it is strikingly evident that almost all of the major IOCG provinces occur close to the gradient (highlighted in white) between ‘fast’ and ‘slow’ velocity. This relationship is less evident for the Mesozoic IOCG provinces in South America and, arguably, the Kangdian province in southwest China. Groves et al. (2010) noted a similar relationship between craton margins and the Precambrian IOCG ‘sensu stricto’ deposits defined in that study; the current investigation supports this proposal with additional provinces and data. Furthermore, in Australia this spatial relationship has been shown more precisely by Hoggard et al. (2020) who demonstrated that the large Cu-Au deposits of the eastern Gawler Craton and the Cloncurry provinces lie within ~100 km of the surface projection of the 170 km depth contour of the lithosphere-asthenosphere boundary (LAB). The same spatial association of the LAB with the IOCG and related deposits considered in the present review is evident globally (K. Czarnota, M. Hoggard, R. Skirrow, unpublished data), as it is for sedimentary basin-hosted resources of Zn, Pb and Cu (Hoggard et al., 2020).

In contrast, the locations of major porphyry Cu (-Au) metallogenic provinces are almost all above global domains of relatively low seismic velocity at 165 km depth. The major IOA provinces range in age from Paleoproterozoic (e.g. Kiruna province) and Mesoproterozoic (e.g. southeast Missouri) through Paleozoic (e.g. Bafq, Iran) to Mesozoic (e.g. Chilean Andes, and Middle-Lower Yangtze Belt, China) and even Cenozoic (e.g. El Laco, Chile). Most are situated above relatively low velocity mantle but those in the Urals (Russia) are exceptions, and the IOA deposits of southeast Missouri and the Adirondacks (USA) are located, like the IOCG provinces, close to a cratonic margin.

3. Three regional and tectonic settings of IOCG provinces

The timing of regional geological events in relation to Cu-Au-Fe

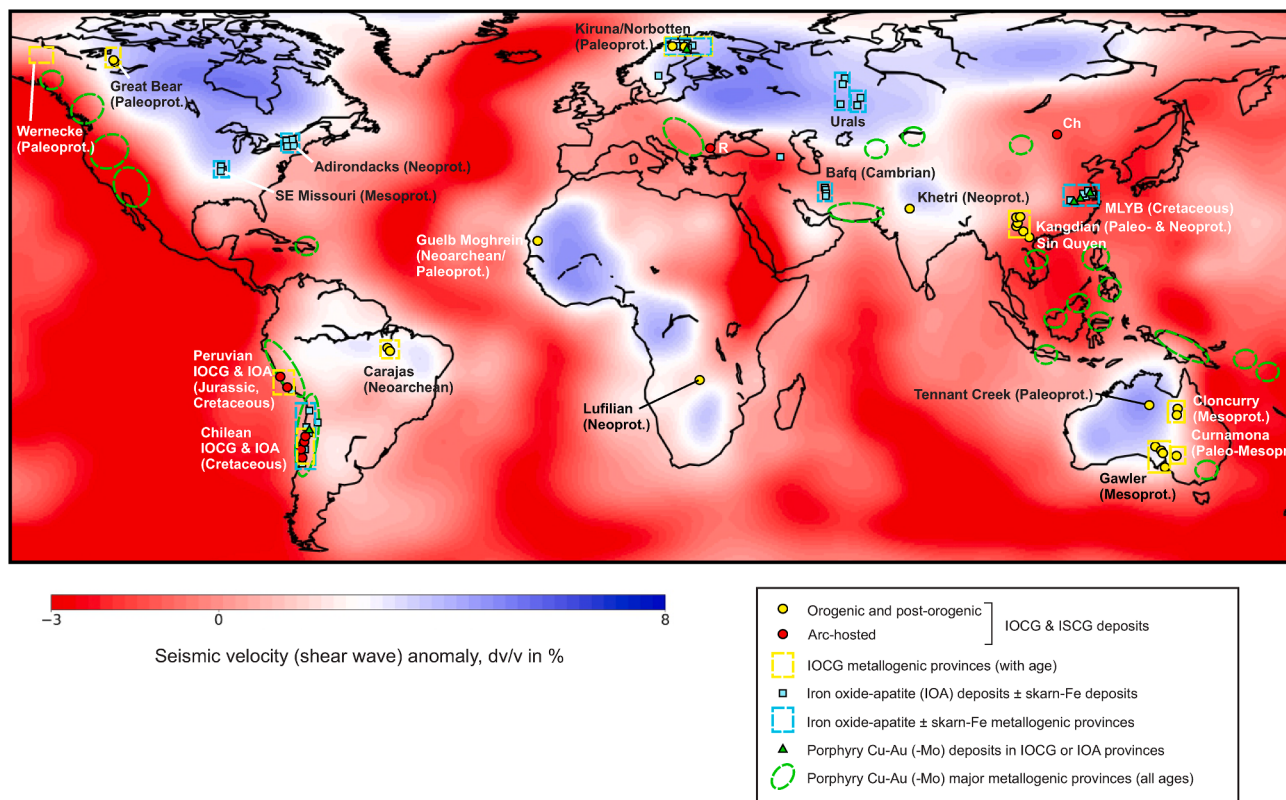


Fig. 1. Locations of global major IOCG deposits and provinces, compared to iron oxide-apatite (IOA) and porphyry Cu-Au (-Mo) deposits and provinces, plotted on a background image of seismic velocity (shear wave) anomalies at 165 km depth relative to the ak135 reference model (from TX2019slab-S model of Lu et al., 2019). Blue areas represent anomalous fast seismic wave speeds representing depleted cratonic lithospheric mantle beneath Archean and Proterozoic cratons. Locations of deposits and metallogenic provinces based on references cited in the text and in the Supplementary Information, and Sillitoe (2010). Abbreviations: Ch – Chandmani Uul deposit (Oyunjargal et al., 2020), R – Rosen deposit (Sillitoe et al., 2020). (For interpretation of the references to colour in this figure legend, the reader is referred to the web version of this article.)

mineralisation is summarised in Fig. 2 for six of the world's major IOCG metallogenetic provinces. Detailed descriptions of regional and hydrothermal events in these provinces along with four others are presented in the *Supplementary Information*, and summary information is given in Table 1. Event time spans shown in Fig. 2 represent the main bodies of available geochronological data for each event, with emphasis on ages determined with robust geochronometers such as U-Pb and U-Th-Pb isotope ages for zircon, titanite and monazite, and Re-Os isotope ages of molybdenite. Additional constraints from $^{40}\text{Ar}/^{39}\text{Ar}$ dating have been utilised for hydrothermal minerals in some provinces. Uncertainties on individual ages are given in the detailed compilations of geochronological data in the *Supplementary Information*. The timing and character of deformation/tectonic events have been largely taken from the literature, supplemented by further interpretation by the author in some provinces as described in the *Supplementary Information*.

This global review of ten IOCG metallogenetic provinces has revealed three distinct lithostratigraphic-tectonothermal settings for the major IOCG and related deposits: two associated with major orogenic/tectonothermal events, and a third where continental margin arcs were undergoing extension (Andean type). The orogenic-related setting of IOCG and related deposits is subdivided into 'orogenic' and 'post-orogenic' settings. These settings are partly similar to the three tectonic settings proposed by Hitzman (2000), namely 'intra-continental orogenic basin collapse', 'intra-continental anorogenic magmatism' and 'extension along a subduction-related continental margin'. Groves et al. (2010) emphasised the latter two of these settings for their IOCG sensu stricto deposits of Precambrian and Phanerozoic ages, respectively. However, the 'intra-continental anorogenic magmatism' setting of Hitzman (2000) and Groves et al. (2010) is considered in the present study to be a post-

orogenic setting, typified by the eastern Gawler Craton. Moreover, the examples of IOCG provinces assigned to each setting differ between this and previous studies.

The three settings and possible hybrids are summarised below; for full referencing see the *Supplementary Information*.

3.1. Orogenic settings

The Cloncurry province was given by Hitzman (2000) as an example of an IOCG province with an 'orogenic basin collapse' setting, along with the Grenville province (with IOA deposits) and the Lufilian Orogen of southern Africa. In the past two decades many more IOCG deposits and provinces have been recognised worldwide, and it is suggested here that in fact many of the world's major IOCG provinces occur in orogenic tectonic settings. These include the Carajás, Guelb Moghrain, Cloncurry, Sin Quyen, Tennant Creek and probably Kangdian and Khetri provinces. The term 'orogenic' is appropriate because the IOCG and related deposits in this setting are interpreted to have formed during regional deformation and tectonothermal events at mid-upper-crustal, low to medium grade metamorphic, conditions within brittle-ductile structures such as shear zones. Where sufficient data are available it is evident in many cases that *syn-tectonic* IOCG and related deposits in this setting post-dated peak metamorphism by millions to tens of millions of years, and hence can be described as having 'late-orogenic' timing. Notwithstanding, until more comprehensive geochronological and structural data are available the broader term 'orogenic' is used herein for such settings.

Moreover, this review (as detailed in the *Supplementary Information*) indicates that the settings of the orogenic IOCG and related

Timing / setting of IOCG deposits

Pre-orogenic transtensional:

Orogenic: Carajás Kiruna Tenant Ck

Post-orogenic:

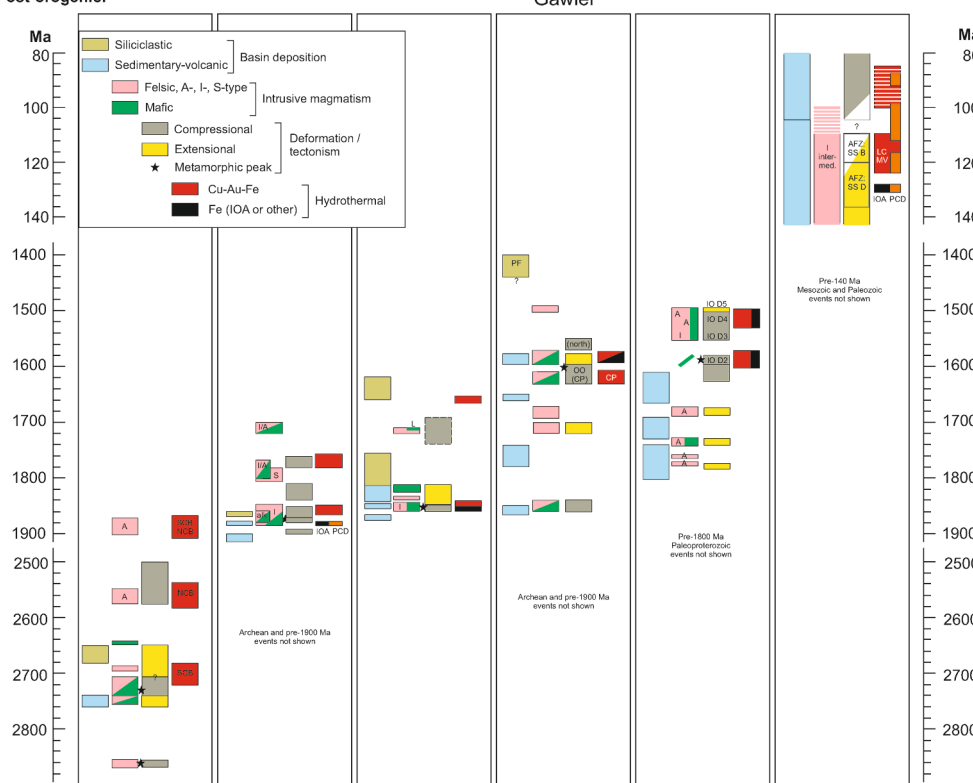


Fig. 2. Synthesis of geochronological data for mineralisation, tectonic, magmatic and supracrustal depositional events in key provinces with IOCG deposits. The Kiruna and Mesozoic Andean provinces also contain well known IOA deposits and small-medium sized porphyry Cu (-Au) deposits. Note breaks in time scale. For sources of data and named rock units see the Supplementary Information. Abbreviations for intrusive magmatism: A – A-type felsic, I – I-type felsic, L – lamprophyre, S – S-type felsic, alk – alkaline. Other abbreviations: AFZ – Atacama Fault Zone, CP – Curnamona Province Cu-Au deposits, IO – Isan Orogeny, IOA – iron oxide apatite deposits, LC – La Candelaria Cu (-Au), MV – Mantoverde Cu (-Au) deposit, NCB – Northern Copper Belt, OO (CP) – Olarian Orogeny in Curnamona Province, PCD – porphyry Cu deposits, SCB – Southern Copper Belt, SS B – strike-slip brittle, SS D – strike-slip ductile.

Table 1

Summary of IOCG metallogenic provinces and their mineral deposits. Data sources are given in the Supplementary Information. Deposit type abbreviations: IOCG – iron oxide Cu-Au deposits, ISCG – iron sulfide Cu-Au deposits, IOA – iron oxide apatite deposits, PCD – porphyry Cu deposits, SSC – sediment-hosted stratiform Cu deposits.

Metallogenic province	Basin rocks hosting CGI mineral systems	Magmatism syn-IOCG (name of suite)	Deposit types in province	Age of Cu-Au deposits	Setting of Cu-Au deposits (# of events)
Carajás	siliciclastics, BIF, felsic & mafic volcanics	Bimodal, alkali-calcic (I-type) felsics & A-types (Planalto)	IOCG, Au-PGE, Ni, Fe (BIF) & late granite-related Cu-Au	Neoarchean & Paleoproterozoic	orogenic (2, Neoarchean); post-orogenic (1, Paleoprot.)
Guelb Moghrein	siliciclastics, BIF, carbonate-rich, mafic volcanics	none recognised	IOCG/ISCG	Neoarchean/early Paleoproterozoic, Paleoproterozoic	orogenic (1)
Kiruna/Norbotten	Intermediate-mafic-felsic volcanic-rich, minor siliciclastics, carbonate & graphite	Calc-alkaline to alkaline, bimodal (Haparanda & Perthite-Monzonite)	IOCG, ISCG, IOA, PCD, VHMS, orogenic Au	Paleoproterozoic	orogenic (2)
Great Bear magmatic zone	Intermediate-mafic-felsic-volcanic-rich, minor siliciclastics	Calc-alkaline to alkaline I-type, and A-type (various GBMZ)	IOCG, IOA, skarn, albitite-U	Paleoproterozoic	orogenic to post-orogenic (1)
Tennant Creek	Siliciclastics, hematitic shale, minor felsic volcanics, minor carbonate	I-type, bimodal (Tennant Creek)	IOCG, ISCG	Paleoproterozoic	orogenic to post-orogenic (2)
Gawler-Curnamona	Siliciclastics, minor mafic & felsic volcanics, minor BIF, calc-silicates & scapolite	Bimodal, high-temperature I- and A-type; minor alkaline (Hiltaba-GRV)	IOCG, minor Mo & Au-Mo (orogenic Au or IRG & epithermal Ag to west; Pb-Zn-Ag to east)	Early Mesoproterozoic	Major deposits: post-orogenic (1)
Cloncurry	Siliciclastics, calcsilicates & scapolite, mafic & felsic volcanics, minor BIF; minor graphite	Bimodal, high-temperature I- and A-type (Williams-Naraku)	IOCG, ISCG, Mo, Pb-Zn-Ag (albitite-U, skarn-REE-U and orogenic? Au to west)	Early Paleoproterozoic	orogenic (2)
Kangdian	Siliciclastics, carbonate-rich, minor graphite	Mafic intrusive	IOCG, SSC, Fe	Paleo- to Neoproterozoic	?orogenic (2)
Khetri	Siliciclastics, calcsilicates & scapolite	Bimodal (Erinpura, timing unclear)	IOCG, SSC (Pb-Zn-Ag and albitite-U to south)	Neoproterozoic	?orogenic (1)
Chilean Iron Belt and south coastal Peru	Mafic-intermediate-felsic volcanic-rich, marine sediments	Calc-alkaline (Coastal Batholith)	IOCG, IOA, Fe-skarn, PCD, manto Cu-Ag	Cretaceous	Syn-extensional pre-orogenic to early-orogenic (1)

deposits in many cases exhibit similar and distinctive patterns of evolution. This involves: basin formation; then tectonic/orogenic processes leading to inversion of the basins and regional metamorphism of commonly high-temperature low-pressure style; and I- and/or A-type felsic and mafic bimodal magmatism that temporally overlaps with particularly the latter stages of the tectonic/orogenic events. A key hypothesis in the present review, building on an earlier proposal (Skirrow, 2010; Skirrow et al., 2018, 2019), is that IOCG mineral systems in orogenic settings preferentially develop during a switch in tectonic style from early compressional to transpressional and thence in some cases to transtensional or extensional regimes. The fully extensional setting is described separately in the next section, as the post-orogenic setting. This switch in tectonic style can explain the apparent dilemma of bimodal magmatism associated with orogenic events, if such magmatism commenced late within the tectonic event, during the tectonic switching from compression to extension. This is consistent with the available geochronological data for the IOCG provinces in orogenic settings, although further testing of this hypothesis is required.

The sedimentary-volcanic basins hosting orogenic IOCG and related deposits typically are of continental to shallow marine rather than deep marine character, and commonly contain oxidised facies and strata with evidence of former evaporites, as well as Fe-rich lithologies such as mafic volcanics and banded iron formation (Barton, 2013; Haynes, 2000; Hitzman, 2000). Carbonaceous units are volumetrically minor or absent in the host sequences but may be locally present at some deposits (Haynes, 2000). The host volcanic-sedimentary-volcanic basins generally formed in extended continental margin including passive margin settings. Later basins that post-date the IOCG deposits in some provinces, such as the Águas Claras Formation in the Carajás province and Ooradidgee Group in the Tennant Creek province, tend to be sedimentary-siliciclastic in character or contain bimodal volcanic rocks (Fig. 2) and may be indicative of extensional tectonic regimes.

Regional magmatism was broadly coeval with the formation of most orogenic IOCG and related deposits although *syn*-mineralisation intrusions are rarely present within or subjacent to the Cu-Au mineralisation. A few examples of orogenic IOCG and related deposits appear to lack major *syn*-mineralisation magmatism (e.g. Osborne deposit, Cloncurry district; Guelb Moghrein, Mauritania). A- and/or high-temperature I-type felsic intrusive ± volcanic rocks are commonly coeval with less voluminous (at the exposed crustal level) mafic to ultramafic intrusive rocks that are weakly to moderately K-rich; calc-alkaline intermediate compositions are generally absent or minor, as are highly alkaline igneous compositions, within the *syn*-mineralisation igneous complexes. The Kangdian province is unusual in the apparent very low abundance of felsic as compared to mafic intrusive magmatism around the period(s) of IOCG deposit formation.

As noted above, *syn*-deformational Cu-Au mineralisation occurred synchronously with, and generally late within (e.g. post-peak-metamorphic), the associated orogenic event as demonstrated by the available radiometric ages (Supplementary Information) and by the structural controls described in the literature for IOCG and related deposits in each province. The author's field observations support such timing in the following provinces: Tennant Creek, Gawler Craton, Curnamona Province, Cloncurry, Kiruna, Kangdian and Khetri. For example, brittle-ductile shear zones and breccias associated with dilatant jogs in shear zones, as well as fold hinges at various scales, are common sites for *syn*-deformational hydrothermal alteration and Cu-Au mineralisation in the orogenic IOCG setting. Geochronological and geological data indicate that some provinces experienced multiple Cu-Au mineralising events 10–100 s of millions of years apart as well as multiple tectonothermal events. This raises the possibility of 'remobilisation' of early Cu-Au mineralisation during later tectonothermal events, which may be difficult to distinguish from the introduction of 'new' Cu-Au during the later events. However, several lines of evidence based on descriptions in the literature and the author's observations support the proposal of *syn*-deformational, *syn*- to late-orogenic

introduction of Cu-Au-Fe mineralisation in the orogenic setting. First, ore-related hydrothermal mineral assemblages are largely confined to zones of deformation such as shear zones, en-echelon and sigmoidal extension veins sets related to shearing, saddle reef-style infillings in fold hinges, attenuated fold limbs, breccias with clasts and hydrothermal matrix exhibiting a tectonic foliation, and hydrothermal veinlets and replacements along a tectonic foliation. Second, there is little or no evidence for extensive Cu-Au mineralisation outside of such *syn*-deformation features in the orogenic IOCG and ISCG deposits that could be described as pre-tectonic mineralisation (except in several provinces with possible SSC mineralisation; see below). Third, as discussed in later sections, the geochemical compositions of IOCG and ISCG deposits in orogenic settings are different to those in the post-orogenic and arc-hosted settings where the ores are not controlled by mid-crustal brittle-ductile structures but by shallow-crustal generally brittle deformation structures. Therefore, if some/all deposits in orogenic settings were simply the deformed, metamorphosed, equivalents of the post-orogenic or arc-hosted deposits then their ore geochemistry may be expected to be similar, which they are not (although Sin Quyen is a possible exception). These arguments do not rule out the possibility of multiple Cu-Au-Fe mineralising events or some degree of 'remobilisation' of Cu-Au during second or later tectonothermal events.

Other deposit types that may or may not be present in the same metallogenic provinces as the orogenic IOCG deposits include: ISCG deposits, (Davidson & Large, 1994; Haynes, 2000); sedimentary and/or hydrothermal Fe oxide deposits and Fe-oxide-rich alteration of various origins; and less common mafic-ultramafic intrusion-hosted Ni-Cu sulfide mineralisation (e.g. Carajás province). The ISCG mineralisation is represented variously as deposits separate from the IOCG deposits (e.g. Greenmount, Mt Dore in the Cloncurry province, Haynes, 2000) or as zones within deposits with otherwise abundant Fe oxides (e.g. Eloise, Osborne in Cloncurry province, Haynes, 2000; Cu-Au-Bi zones outside ironstones at the Orlando East and Gecko ironstone-hosted deposits, Tennant Creek province, Skirrow, 2000). The ISCG deposits show similar structural controls, relative timing, and alteration (notwithstanding differences in Fe-oxide/Fe-sulfide ratios and quartz abundances) to the IOCG deposits in the same metallogenic provinces. Several provinces with orogenic IOCG deposits also host sediment-hosted stratabound Cu deposits that are known as 'SSC' deposits in the Kangdian and Khetri provinces, and which contain no or minor Fe oxides (Chen & Zhou, 2012; Zhao et al., 2012; Mukhopadhyay et al., 2019). Some stratabound Cu (Co) and polymetallic mineralisation in the Olary Domain of the Curnamona Province also may be of SSC affinity (Cook & Ashley, 1992). In some provinces there is evidence for early, possibly *syn*-diagenetic, stratabound Cu mineralisation and Fe-sulfides overprinted by epigenetic, *syn*-deformational, Cu (-Au) of IOCG affinity (e.g. Khetri province, Sharma et al., 2020). Although this scenario also seems plausible in the Kangdian and Curnamona provinces (e.g. Bierlein et al., 1995; Skirrow et al., 2000; Teale & Fanning, 2000a,b), other interpretations have been advanced (e.g. early stratabound IOCG mineralisation overprinted by deformation, Armistead et al., 2018). However, the relative importance of 'remobilised' mineralisation versus introduction of new Cu-Au during the *syn*-deformational stages is unclear in these provinces (e.g. Su et al., 2021). This is also a problem in some provinces with multiple stages of IOCG and/or ISCG mineralisation, and requires further careful textural and paragenetic work to resolve the timing of Cu-Au particularly in relation to deformation fabrics.

The Fe oxide deposits and Fe-oxide-rich alteration zones are important features of all of the IOCG provinces in orogenic settings, and variously occur as zones with little or no Cu-Au mineralisation within some IOCG deposits and as Fe-oxide accumulations spatially quite separate from the Cu-Au mineralisation. For example, in the Carajás province giant Fe ore deposits related to sedimentary BIF formed prior to the IOCG deposits (Grainger et al., 2008), whereas massive magnetite deposits of hydrothermal origin occur in the Southern Copper Belt, separately from the large IOCG deposits and also in some cases occur

within the deposits associated with albite-actinolite alteration (e.g. Sequeirinho orebody in the Sossego deposit, Monteiro et al., 2008). In most orogenic IOCG provinces hydrothermal Fe-oxide bodies with little or no Cu-Au represent alteration within IOCG mineral systems where physico-chemical conditions and/or availability of suitable fluids were unfavourable for significant Cu-Au deposition.

Although uranium is anomalous in some IOCG deposits in orogenic settings (e.g. Salobo deposit in Carajás province, de Melo et al., 2017; Ernest Henry, E1 and Monakoff deposits in Cloncurry province, Mark et al., 2006, Williams et al., 2015; Juno deposit in Tennant Creek province, Large, 1975), significant U enrichments in IOCG deposits in these settings are evidently quite rare. In the Mt Isa Inlier the Mary Kathleen U-REE deposit and albitite-hosted U deposits such as Valhalla occur in separate metallogenic provinces to the west of the Cloncurry IOCG province. Available geochronology suggests that uraninite mineralisation formed at 1550 ± 15 Ma at Mary Kathleen (Page, 1983), and between ~ 1555 Ma and ~ 1530 Ma at the Valhalla albitite-hosted U deposit (Polito et al., 2009). The youngest ages of this U mineralisation are within uncertainty of the oldest ages of the second major Cu-Au ore-forming event in the Cloncurry province at ~ 1530 – 1490 Ma (Perkins & Wyborn, 1998; Duncan et al., 2011). These relationships are permissive of a link between U in some of the IOCG deposits of the Cloncurry province and the late-stage U in deposits to the west in the Mount Isa Inlier, but more clarification is required. Albitite-hosted U mineralisation in the Great Bear magmatic zone may be a further example where U mineralisation formed coevally with IOCG deposits, in this case within the same iron oxide-alkali alteration systems according to (Corriveau et al., 2010a,b, 2016; Montreuil et al., 2015).

3.2. Post-orogenic settings

The prime example of this setting is the eastern Gawler Craton hosting the giant Olympic Dam Cu-U-Au deposit; the subjacent Curnamona Province to the east, with minor known Cu-Au (\pm Fe-oxide) deposits, shared a similar evolution around the period of Cu-Au-Fe mineralisation in the early Mesoproterozoic. Whereas the eastern Gawler Craton and Curnamona Province experienced similar early (Paleoproterozoic) histories to those of the orogenic IOCG provinces (basin formation; inversion related to major orogenic events; temporally overlapping felsic and mafic magmatism; and syn-tectonic IOCG-related hydrothermal alteration) the eastern Gawler Craton and probably the Curnamona Province appear to have undergone a further stage of geo-dynamic development. This involved a switch from a broadly compressional (orogenic) to an extensional tectonic regime, referred to here as post-orogenic and which was marked by voluminous felsic-dominated bimodal igneous activity. The major IOCG deposits such as Olympic Dam, Prominent Hill and Hillside are interpreted to have formed during this tectonic switching at ~ 1595 – 1575 Ma (Skirrow, 2010; Skirrow et al., 2018, 2019). Unlike the orogenic settings, volcanic and sedimentary rocks of roughly similar age to the deposits are preserved in the post-orogenic setting of the Gawler Craton IOCG deposits. The associated magmatism is characteristically A- and/or high-temperature I-type with weakly to moderately K-rich mafic to ultramafic intrusive and volcanic rocks, and there are few igneous rocks of intermediate composition (Budd, 2006). Broadly syn-mineralisation alkaline igneous rocks appear to be more abundant in post-orogenic compared to orogenic settings of IOCG and related deposits. For example the ultramafic dykes at the Olympic Dam deposit (Johnson & Cross, 1995) and picrite dykes at the Wirrda Well prospect (Huang et al., 2016) have affinities with alkaline magmatism, compared with less alkaline compositions of similar aged mafic igneous rocks in other parts of the Gawler Craton (Skirrow et al., 2018).

Other deposit types in the eastern Gawler Craton and Curnamona Province that formed within a few 10 s of millions of years of the ~ 1595 – 1575 Ma period of IOCG mineralisation include: small low-Fe-oxide Cu-Au deposits in the Moonta-Wallaroo district, associated with

quartz veins and K-feldspar-chlorite-sericite alteration; low-Fe-oxide Cu-Mo (-Au) stratabound mineralisation adjacent to Fe-oxide-rich alteration zones (e.g. Kalkaroo and Portia deposits, Curnamona Province); Au-Mo-bearing quartz veins (e.g. White Dam deposit, Curnamona Province) and Mo-greisen type mineralisation (Moonta-Wallaroo district); Ag- and Pb-rich epithermal-like quartz vein mineralisation and shear-hosted Au-quartz vein deposits in the central Gawler Craton to the west of the IOCG metallogenic province. In addition there are numerous Fe oxide bodies of hydrothermal origin in both the eastern Gawler Craton and western Curnamona Province, as well as BIF-related Fe ore deposits that pre-date the Cu-Au mineralisation (e.g. Middleback Ranges, Gawler Craton). Many of the hydrothermal Fe oxide bodies, which are largely barren of Cu-Au, appear to represent alteration within CGI mineral systems (Skirrow et al., 2002; Bastrakov et al., 2007). Finally, the giant Paleoproterozoic Broken Hill Pb-Zn-Ag deposit occurs in the eastern Curnamona Province. This spatial relationship between early basin-hosted Zn-Pb-Ag and later IOCG deposits is similar to that observed in the eastern Mt Isa Inlier where the Broken Hill-type Cannington and Pegmont Pb-Zn-Ag deposits occurs immediately to the east of the Cloncurry IOCG deposits.

Other possible examples of post-orogenic settings of CGI mineral systems include the paragenetically late stages of Cu-Au-Bi mineralisation in the Tennant Creek province which, like the IOCG mineralisation in the Gawler Craton, is characterised by brittle deformation fabrics and a dominance of hematite-rich (rather than magnetite-rich) iron oxide alteration. Examples include: Gecko K44 upper zone of Au-rich Cu-Bi mineralisation, and the Au-Bi-Se-rich Eldorado deposit (Huston et al., 1993; Skirrow, 2000; Skirrow & Walshe, 2002). Also, the Cu-U- and hematite-magnetite-bearing breccias at the Sue-Dianne deposit in the Great Bear magmatic zone (Goad et al., 2000) may represent a post-orogenic overprint on an orogenic metallogenic belt (see also hybrid settings, below).

3.3. Continental margin arc (Andean type) settings

In contrast to the Neoarchean to Neoproterozoic orogenic settings, Cretaceous IOCG deposits in the Chilean and Peruvian Andes formed within a continental margin magmatic arc, either during extensional tectonism (Sillitoe, 2003) or during a switch from extension to inversion (Chen et al., 2013). Moreover, available geochronological data reviewed in the Supplementary Information indicate that the Cretaceous Andean IOCG deposits formed up to ~ 15 million years prior to the onset of a major inversion event, rather than during such an event as in the orogenic IOCG deposits or immediately following an orogenic event as in the post-orogenic setting of the eastern Gawler Craton deposits. Host rocks in the Cretaceous Andean settings are dominated by volcanic and intrusive rocks of mainly intermediate to felsic and minor mafic compositions and with relatively minor sedimentary or metamorphic components. The abundance of calc-alkaline intermediate compositions in this setting, and the close spatial-temporal relationships between intrusions and IOCG mineralisation (Sillitoe, 2003), differ from the settings of orogenic and post-orogenic IOCG deposits. The Cretaceous Andean metallogenic provinces containing the IOCG deposits also host small to medium size porphyry copper and skarn, large iron oxide-apatite (IOA), and 'manto' Cu-Ag deposits that comprise stratabound, epigenetic, Fe-oxide-poor mineralisation.

Based on the few available high-precision ages using robust geochronometers for the Cretaceous Fe and Cu deposits, most of the dated IOA deposits formed at ~ 131 – 127 Ma along with some porphyry Cu deposits. Importantly, the limited available geochronology indicates that the dated IOA deposits significantly predated the major IOCG deposits, which formed at ~ 122 – 110 Ma (e.g. Mantoverde, Candelaria, Raúl-Condestable, early alteration at Mina Justa). The few available dates for Cretaceous manto Cu (-Ag) deposits indicate alteration at ~ 106 – 101 Ma, based on K-feldspar ^{40}Ar - ^{39}Ar dating (e.g. El Soldado deposit, Wilson et al., 2003). However, the significance of these K-

feldspar ages, along with other ^{40}Ar - ^{39}Ar ages of $\sim 104\text{--}95$ Ma for adularia associated with copper mineralisation at the Mina Justa IOCG deposit (Chen et al., 2010), remains unclear and they may represent cooling rather than formation ages. By comparison, at the latitudes of the Chilean Cretaceous IOCG deposits (e.g. $20^\circ\text{--}33^\circ$ S) the onset of inversion of the Jurassic arc and basin system hosting many of the IOCG deposits occurred at $\sim 107\text{--}105$ Ma, with a main phase of compression at $\sim 100\text{--}95$ Ma (Bascuñán et al., 2016; Fennell et al., 2019; Boyce et al., 2020).

These timing constraints indicate that the major Andean IOCG deposits formed during periods of extension or transtension up to ~ 15 m.y. prior to the Cretaceous major inversion event, although there may be some overlap with the initial stages of orogenesis as previously suggested by Chen et al. (2013). In conclusion, the setting and timing of the Andean IOCG deposits, as well as some manto Cu deposits, can be described as pre- to early-orogenic in their timing.

3.4. Possible hybrid settings

The setting of the Paleoproterozoic Kiruna province and the broader region of northern Fennoscandia has been interpreted as an evolving Andean-type continental margin magmatic arc, that was subjected to a series of collision-related tectonothermal or orogenic events (as discussed by Lahtinen et al., 2015, 2018; see also references therein). Like the Cretaceous Andean setting, the Kiruna province experienced the development of large IOA deposits and probable porphyry Cu deposits (e.g. Aitik, Wanhainen & Martinsson, 2010) during arc-related magmatism ($\sim 1884\text{--}1876$ Ma), with later development of IOCG and related mineralisation, commencing at ~ 1862 Ma (see review of geochronology, Supplementary Information and references therein). A key difference between the Kiruna and Andean IOCG settings is that in the Kiruna province the earliest IOCG deposits appear to have formed during and/or late within (rather than prior to) a major collision-related orogenic episode that post-dated arc magmatism and related IOA and porphyry Cu deposits. A second period of IOCG deposit formation at $\sim 1782\text{--}1757$ Ma or as early as ~ 1820 Ma (Bauer et al., 2021) also appears to have occurred during and/or late within another orogenic event affecting northern Fennoscandia (see Supplementary Information). It is notable that the Kiruna province is dominated by magmatic arc-related igneous host rocks with volumetrically minor (meta)sedimentary rocks, and although containing world-class IOA deposits the known IOCG deposits are all small. Overall, the Kiruna province can be interpreted to represent a hybrid setting where an early continental margin magmatic arc setting was overprinted by multiple orogenic events, two of which were associated with the formation of syn- to late-orogenic IOCG and related deposits.

The Paleoproterozoic Great Bear magmatic zone (GBMZ) in north-western Canada hosts well documented but under-explored hydrothermal alteration and diverse types of mineralisation (Cu, Au, U, Co, Mo, V, etc) including small known Au, Cu and U resources (Corriveau et al., 2010a,b, 2016; Montreuil et al., 2016b; Mumin et al., 2007, 2010). Like the Andean and Kiruna settings described above, much of the igneous rocks of the GBMZ are interpreted to have formed in a continental margin magmatic arc setting (Hildebrand et al., 1987; Ootes et al., 2017). Arc magmatism, initiated at ~ 1876 Ma, was preceded by the short-lived Calderian orogeny. Rather than fully postdating the Calderian orogeny, as previously thought, early phases of the GBMZ magmatism ($\sim 1876\text{--}1873$ Ma) are now interpreted as *syn*-deformational within a transpressional tectonic regime late within the Calderian orogeny, and exhibit ‘syn-collisional’ and ‘volcanic arc’ calc-alkaline geochemical signatures (Montreuil et al., 2016a; Ootes et al., 2017). The later magmatic phases ($\sim 1869\text{--}1866$ Ma) have compositions indicating a transition from collisional to post-collisional and extensional settings (Montreuil et al., 2016a; Ootes et al., 2017). The overall setting therefore appears to be one where *syn*-orogenic magmatism was overprinted by magmas with continental arc-like character yet in an extensional,

post-orogenic, setting. Accordingly, the GBMZ may share features (and represent a hybrid?) of the orogenic to post-orogenic type IOCG settings combined with an Andean type continental margin magmatic arc IOCG setting.

3.5. Synthesis: tectonic settings and geodynamic evolution of IOCG provinces

Fig. 3 illustrates the three proposed regional geological and tectonic settings of different types of IOCG and related deposits in CGI mineral systems and their host provinces. The upper panel shows the setting of arc-hosted Andean-type IOCG deposits within a continental margin magmatic arc that is undergoing extension, similar to those proposed by Hitzman (2000), Sillitoe (2003) and Groves et al. (2010). The rifting arc and back-arc basinal environments host not only the IOCG deposits but also (earlier) IOA, small porphyry Cu, skarn-related and (coeval to later?) ‘manto’ Cu deposits. This panel also shows subduction-related metasomatism of mantle lithosphere along a continental margin or root of a lithospheric block which may have occurred in multiple episodes over 10 s or 100 s of millions of years. A sedimentary \pm volcanic basin system is illustrated at the right side where the continental margin has undergone extension and thinning. This lithospheric and basin architecture is based partly on the Gawler Craton – Curnamona Province (Skirrow, 2010; Skirrow et al., 2018) but is herein proposed to be more generally applicable to the settings of other orogenic and post-orogenic CGI mineral systems.

The middle panel of **Fig. 3** illustrates inversion of the basin and magmatic arc during an orogenic event, triggered for example by collision of an oceanic plateau, island arc or microcontinent at a plate margin relatively distal from the basin setting. Crucially for IOCG deposit formation, in this model gravitational instabilities at the LAB triggered by the collisional processes led to melting of previously metasomatized lithospheric mantle (represented by alkaline mafic igneous rocks, Groves et al., 2010; Skirrow et al., 2018) and consequent crustal melting. These occurred late within the orogenic event, during a switch from compression to transtension or extension. The juxtaposition of this mantle-derived magmatism with a pre-existing basin at an extended continental margin is the key setting for the formation of orogenic IOCG and related deposits. These *syn*-deformational deposits form at generally mesothermal conditions within basinal \pm igneous host rocks. The orogenic setting with a tectonic switch from compression to extension is proposed to be applicable to many of the world’s major orogenic IOCG provinces.

The lower panel (**Fig. 3**) shows how in some cases the orogenic setting evolves from a compressional (collisional) to a fully extensional, post-orogenic, tectonic regime. This may be driven by further and major thinning of the mantle lithosphere, for example via wholesale removal or foundering of large parts of the lithospheric mantle (Skirrow et al., 2018) or via slab roll-back (Tiddy & Giles, 2020). The post-orogenic setting hosts the super-giant Olympic Dam IOCG deposit in the eastern Gawler Craton. Because the orogenic and post-orogenic settings form a continuum, earlier mesothermal orogenic IOCG deposits and/or alteration can be exhumed and overprinted by post-orogenic IOCG mineral systems in sub-volcanic to volcanic settings.

4. Hydrothermal alteration and IOCG mineralisation

Hydrothermal minerals in CGI mineral systems occur within assemblages that show a characteristic sequence through time, commonly known as a paragenetic sequence. The general features of such sequences in IOCG deposits of different types have been known for some time (since Hitzman et al., 1992), yet the interpretation of the hydrothermal mineral assemblages has not been well understood in terms of links with geotectonic settings or origins of the hydrothermal fluids. A review of published paragenetic sequences of 29 representative IOCG and ISCG deposits in 9 provinces, summarised in **Fig. 4**, provides a

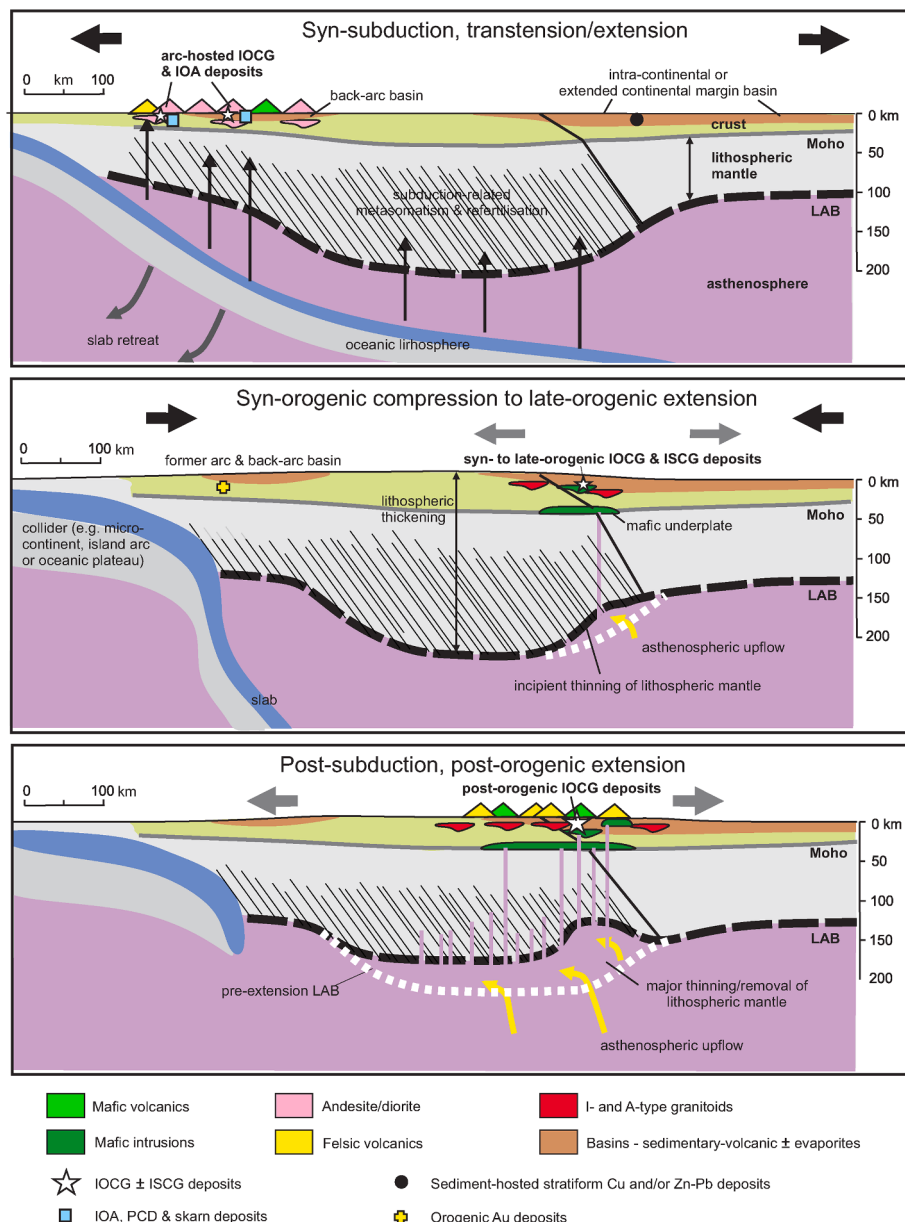


Fig. 3. Schematic tectonic settings and geodynamic evolution of IOCG deposits in CGI mineral systems. Top panel: arc-hosted IOCG and IOA deposits; middle panel: orogenic IOCG and ISCG deposits; lower panel: post-orogenic IOCG deposits (see text). Other indicated deposit types may or may not be present in the IOCG provinces.

framework for comparison with other deposit types and for discussion of the origins of the hydrothermal minerals. The next section focuses on hydrothermal alteration and mineralisation assemblages proximal to the deposits, and then the hydrothermal assemblages are compared with other ore deposit types, before a brief description of regional-scale alteration. The chemical/metamorphic descriptors (e.g. Na-Ca, Ca-Fe, Fe-K) generally correspond to the types previously described by Corriveau et al. (2010a,b, 2016), Hitzman et al. (1992), and Barton (2013).

4.1. Proximal mineral assemblages and paragenetic sequences

The mineral assemblages in CGI mineral systems can be represented by their dominant chemical composition, which change systematically through paragenetic time at a given location. Although there is an influence on mineralogy by the local host rock compositions, which are highly variable in each province, the remarkably consistent mineralogy of the hydrothermal assemblages and their sequences suggests that the

hydrothermal assemblages dominantly reflect the physico-chemical characteristics of the hydrothermal fluids. This is particularly the case in the most intensely altered proximal/central parts of deposits, where it can be assumed that fluid/rock ratios were higher than in peripheral zones. The approach taken here is to identify assemblages of hydrothermal minerals that formed at broadly the same time and therefore represent possible equilibrium chemical conditions or an approach to equilibrium. This concept of an equilibrium mineral assemblage is similar to that used in metamorphic petrology. Accordingly, the focus is on the presence or absence of particular minerals during a particular paragenetic stage rather than on their relative abundance, although the modal amounts of the dominant minerals are taken into account in assigning an assemblage to particular chemical groupings and stages (i.e. Na, Na-Ca, Ca-Fe, K-Fe, etc). Published paragenetic sequences have been critically assessed and minerals assigned to stages and chemical groupings shown in Fig. 4. In some cases the reported mineral assemblages do not fit neatly within the generalised sequence in Fig. 4, in

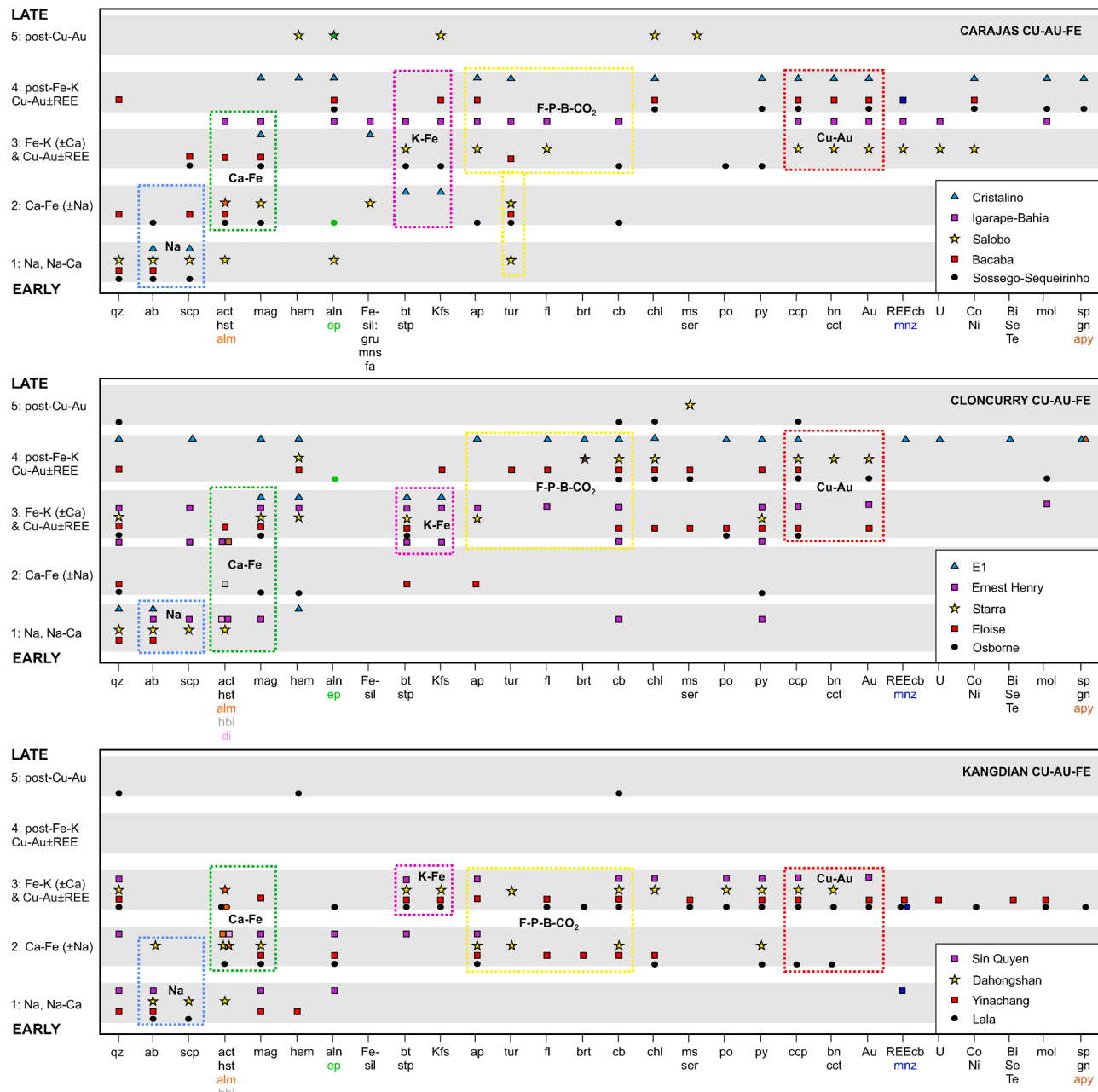


Fig. 4. Paragenetic sequences of hydrothermal minerals for major and representative deposits in selected IOCG provinces. Relative timing of major stages is shown numbered on left axis from early to late. References are listed in Appendix A. Mineral abbreviations (after Whitney & Evans, 2010): ab – albite, act – actinolite, aln – allanite, alm – almandine, anh – anhydrite, ap – apatite, apy – arsenopyrite, Au – gold, brt – barite, bn – bornite, Bi – bismuth sulfides and/or native Bi, bt – biotite, cct – carbonate, cct – chalcocite, chl – chlorite, Co – cobalt-rich sulfides, CCP – chalcopyrite, di – diopside, ep – epidote, fa – fayalite, Fe-sil – Fe-Mg-rich silicates (e.g. fayalite, greenalite, grunerite, minnesotaite), fl – fluorite, gl – galena, gru – grunerite, hbl – hornblende, hem – hematite, hst – hastingsite, Kfs – K-feldspar, mnz – monazite, mns – minnesotaite, mol – molybdenite, mag – magnetite, ms – muscovite, Ni – nickel-rich sulfides, po – pyrrhotite, py – pyrite, qz – quartz, REE – REE-rich minerals (carbonate-rich and/or P-rich including monazite and alumino-phosphate-sulfide REE minerals), scp – scapolite, Se – selenium-rich minerals, ser – sericite, sp – sphalerite, stp – stilpnomelane, Te – tellurium-rich minerals, tur – tourmaline, U – uraninite/pitchblende).

which cases they may be shown between stages (e.g. an assemblage with Ca-rich as well as Fe-K-rich minerals is plotted between stage 2 Ca-Fe and stage 3 Fe-K assemblages).

4.1.1. Alteration-mineralisation stages

The texturally earliest assemblages in CGI mineral systems are almost invariably of sodic character, with or without calcic minerals (Na, Na-Ca in Fig. 4) in deposits from all three of the geotectonic settings described above. Exceptions include the Tennant Creek province where

no Na or Na-Ca alteration is evident at the deposits, although Na and K alteration of regional igneous rocks has been documented in whole-rock geochemical data, albeit without isotopic age constraints (Donnellan et al., 1995). The Na and Na-Ca alteration is represented mainly by albitisation ± scapolitic alteration ± Ca-amphibole (e.g. actinolite) alteration, which are less commonly accompanied by diopside or magnetite or allanite.

In deposits in the orogenic and post-orogenic settings (i.e. all provinces in Fig. 4 except Andes) the Na and Na-Ca alteration transitions to

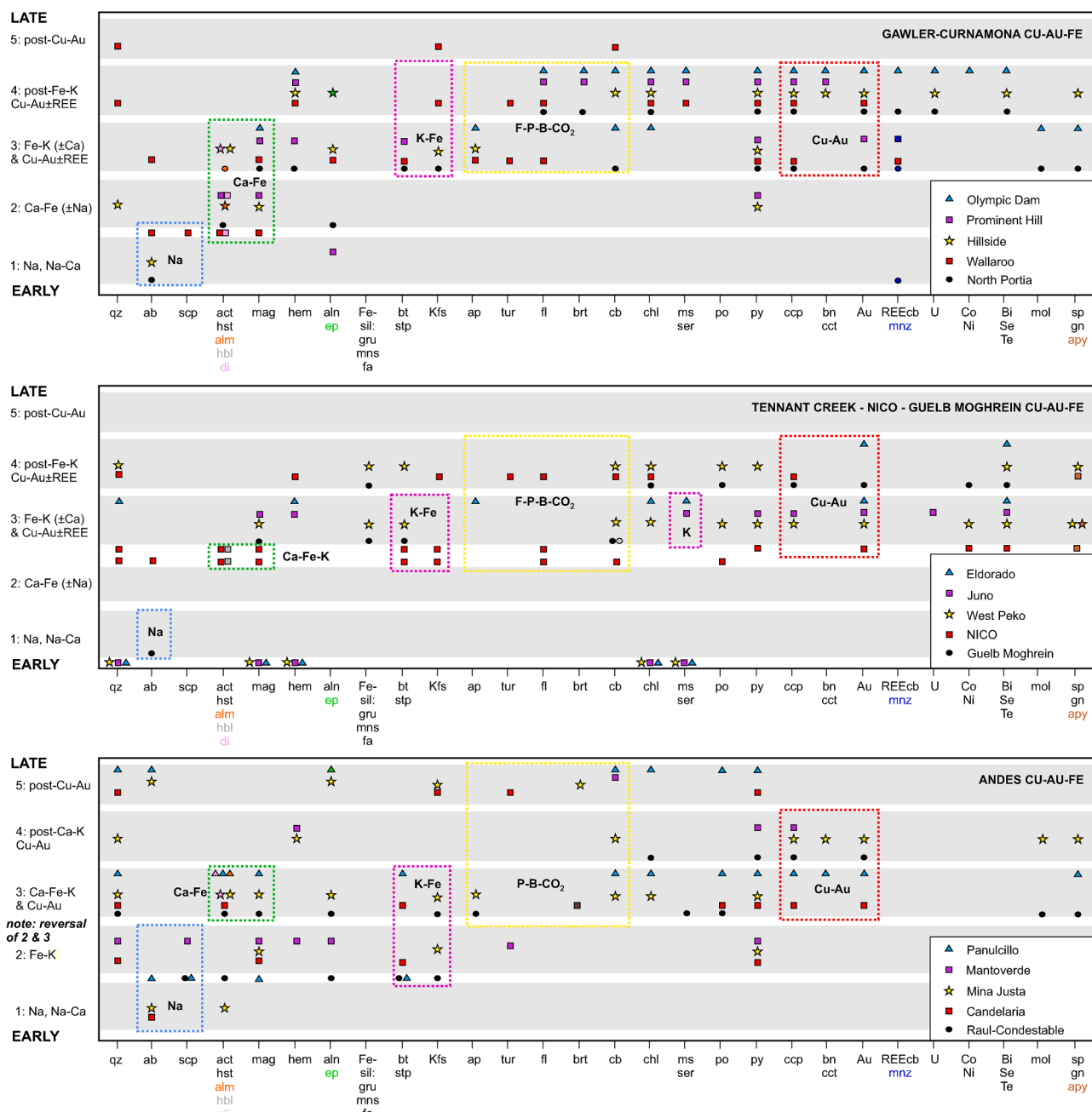


Fig. 4. (continued).

assemblages of Ca-Fe-rich hydrothermal minerals, in some cases with continued formation of sodic minerals. The Ca-Fe assemblages (stage 2 in Fig. 4) are dominated by Fe oxides (generally magnetite) and Ca-amphiboles such as actinolite or hastingsite, and less commonly contain Ca-Fe-rich garnet such as almandine. A few deposits also contain Fe-silicates such as grunerite, minnesotaite, or fayalitic olivine that formed during the Ca-Fe stage (e.g. Guelb Moghrein; West Peko, Tenant Creek province; Salobo, Carajás province). Additionally, skarn-like Ca-Fe alteration is prominent in some orogenic and post-orogenic IOCG and related deposits, and is typically dominated by clinopyroxene or amphibole ± garnet (generally minor), with or without magnetite, scapolite and apatite. The early anhydrous skarn-like alteration is almost invariably barren of coeval Cu-Au mineralisation but may be overprinted by Cu-Au. Examples in the eastern Gawler Craton include: the Hillside deposit where early prograde magnetite-garnet skarn was overprinted by clinopyroxene-actinolite-biotite-allanite-K-feldspar and

thence by hematite-chalcopyrite-chlorite-bornite-chalcocite with rare Bi, U and Pb minerals (Conor et al., 2010). A key example in the Cloncurry province is the Mt Elliott/SWAN deposit where early diopside-scapolite was overprinted by amphibole-calcite-chalcopyrite-scapolite ± magnetite, andradite, tourmaline, allanite, apatite, pyrite and pyrrhotite (Wang & Williams, 2001; Brown & Porter, 2010). Anhydrite and fluorite also have been reported from the Mt Elliott-SWAN system, which is hosted by metamorphic calcsilicate, siliciclastic (including graphitic) metasedimentary rocks and meta-mafic/intermediate igneous rocks that were Na-altered prior to skarn alteration (Brown & Porter, 2010).

The appearance of K-rich minerals marks an important chemical transition in the hydrothermal evolution, represented by K-feldspar, biotite or white mica. This K-metasomatism may commence during the Ca-Fe alteration stage or form a discrete and later Fe-K stage (stage 3 in Fig. 4) with assemblages such as magnetite-biotite or magnetite-K-

feldspar. Crucially the first appearance of Cu sulfide and Au mineralisation generally overlaps with the Fe-K alteration stage, which may continue with some calcic mineral formation in a few cases. Interestingly, the available evidence for the Andean IOCG deposits shows a possible reversal of the Fe-K and Ca-Fe stages in comparison with the orogenic and post-orogenic IOCG deposits, such that the main Cu mineralisation appears with the paragenetically later Ca-Fe alteration in some Andean cases (e.g. with amphibole at Candelaria and Panulcillo; Fig. 4).

A key finding from this review of paragenetic sequences is that Cu-Au mineralisation is in every province accompanied by the deposition of volatile-rich minerals such as fluorite (F), apatite (P), carbonate (CO_2), tourmaline (B), and/or sulfates (S). The amounts and combinations of such minerals accompanying Cu-Au mineralisation are highly variable between and even within deposits. This close temporal and textural association is particularly apparent in all of the orogenic and post-orogenic provinces. The main variations to this observation are in the Carajás province where tourmaline deposition preceded and then accompanied the deposition of Cu-Au mineralisation in some deposits. Also, in some deposits of the Kangdian province and Sin Quyen deposit some of the volatile-rich minerals pre-dated as well as accompanied Cu-Au (Fig. 4). By comparison, fluorite, apatite, carbonate, tourmaline or sulfates appear to be overall less abundant with Cu-Au mineralisation in the Andean IOCG deposits.

The hematite-sericite-chlorite-carbonate assemblage is by far the most important Cu-Au-U-REE-related hydrothermal assemblage in the post-orogenic setting of the Gawler Craton CGI mineral systems. In this province only very minor Cu-Au mineralisation occurs with earlier Fe-K or Ca-Fe alteration. These stage 4 assemblages (hematite-sericite-chlorite-carbonate) are also present in many orogenic IOCG provinces in addition to stage 3 Cu-Au (Carajás, Cloncurry, Guelb Moghrein, Great Bear magmatic zone, Andean), but are generally much less developed than in the Gawler Craton. Examples include: Cristalino (with chalcopyrite) and Salobo (post-chalcopyrite) in the Carajás province; Starra, E1 and Eloise (all with chalcopyrite) in the Cloncurry province; Gecko K44 (with chalcopyrite) in the Tennant Creek province; and NICO (with chalcopyrite) in the GBMZ. The hematite-sericite-chlorite-carbonate assemblage with Cu-Au is evidently lacking in the Kangdian province and at Guelb Moghrein.

4.1.2. Uranium and REE mineral parageneses

The occurrence of REE- and U-bearing minerals varies fairly systematically between provinces, settings and deposit parageneses. The main REE-rich phases reported in the literature are allanite, REE-carbonates and monazite, whereas uraninite is the main reported U-rich phase. Certain groups of deposits and provinces have no reported or trace REE or U minerals, including many of the pyrrhotite-bearing deposits, most of the Andean deposits (although Mantoverde has anomalous REE, Rieger et al., 2010), and most Au-Cu-Bi deposits in the Tennant Creek province (except U at Juno, Large, 1975). A sub-group of deposits with magnetite-pyrite-chalcopyrite contain allanite as a REE host at various stages in the paragenetic sequences from pre-Cu-Au to syn-Cu-Au mineralisation, commonly with apatite and/or fluorite and/or carbonate. Where allanite-bearing deposits contain significant hematite, this oxide is almost always late in the paragenetic sequence and post-dates the allanite which appears to be more closely associated with earlier magnetite and Ca-mineral formation (e.g. Gawler Craton and Curnamona deposits). Like allanite, the REE-carbonates are generally associated with apatite and/or fluorite and/or carbonate assemblages with Cu-Au mineralisation, but unlike allanite they are also associated with uraninite and do not tend to occur in pre-Cu-Au assemblages. The largest resource of REE in IOCG deposits is contained in the Olympic Dam deposit, where REE-carbonates are associated with the hematite-pyrite-chalcopyrite-bornite-chalcocite assemblages that also contain volatile-rich phases such as fluorite, carbonate and barite (Ehrig et al., 2012).

4.2. Comparison of hydrothermal assemblages in IOCG and other ore deposit types

Generalised sequences of hydrothermal mineral assemblages and major-element geochemical character for orogenic and post-orogenic IOCG deposits are compared in Fig. 5 with those for Andean-type magmatic arc-hosted IOCG and selected other Fe and Cu (-Au) deposit types. First, as noted above, the relative timing of K-Fe and Ca-Fe assemblages are probably reversed in syn-late-post-orogenic versus Andean-type IOCG deposits, and the relative abundances of volatile-rich minerals accompanying Cu-Au mineralisation are evidently greater in the orogenic and post-orogenic than in the Andean-type arc-hosted IOCG deposits, based on available paragenetic data.

Second, and with few exceptions, IOCG and related deposits in all settings contain well developed early stages of Na and/or Na-Ca alteration, whereas such alteration is rare and poorly developed in porphyry Cu and skarn Fe/Cu/Au deposits. Within proximal alteration zones at IOA deposits Na-rich alteration is generally not well developed. Interestingly, those IOA provinces with well developed and intense sodic alteration at the regional scale also contain IOCG deposits (e.g., Kiruna, Andes). In contrast, IOA provinces with poorly developed sodic alteration at any scale contain few if any significant Cu-Au deposits of IOCG type, although some contain porphyry Cu (-Au) and skarn Fe and Cu (-Au) deposits (e.g. Middle-Lower Yangtze Belt, China; Bafq region, Iran; southeast Missouri, USA).

Third, Ca-Fe alteration is well developed as an early stage in many orogenic and post-orogenic IOCG, IOA and skarn Fe/Cu/Au deposits but the accompanying mineral assemblages differ in each deposit type. In IOA deposits the magnetite-actinolite \pm clinopyroxene \pm garnet Ca-Fe assemblages are generally accompanied by prominent apatite and minor pyrite, and also by anhydrite in some provinces (e.g. Middle-Lower Yangtze Belt). In contrast, apatite is not a common mineral in early assemblages (Na, Na-Ca, Ca-Fe) in orogenic, post-orogenic and Andean-type IOCG deposits but forms part of later volatile-rich assemblages accompanying Cu-Au mineralisation. Nevertheless, there are examples where apatite is locally abundant with magnetite in early alteration at IOCG deposits, including the Sequeirinho orebody (Carajás province, Monteiro et al., 2008), deep parts of the Olympic Dam deposit (Ehrig et al., 2012; Apukhtina et al., 2017), the Acropolis and other magnetite-rich prospects near Olympic Dam (Bastrakov et al., 2007; Krneta et al., 2017; McPhie et al., 2020), and some magnetite-rich zones in deposits in the Kangdian province (e.g. Dahongshan deposit, Zhao et al., 2017). In the Olympic Dam district many of the sub-economic prospects with magnetite-rich and apatite-bearing alteration have assemblages including pyrite, carbonate, quartz, Ca-amphibole and K-feldspar (Bastrakov et al., 2007). Although apparently lacking amphibole, the apatite-bearing magnetite-rich veins at the Acropolis and Wirrda Well prospects are otherwise similar to those of the aforementioned occurrences, and contain variable amounts of hydrothermal K-feldspar, siderite, quartz, pyrite and biotite/phlogopite (Oreskes & Einaudi, 1992; Cross, 1993) as well as paragenetically later chalcopyrite, barite, fluorite, chlorite and sericite (Krneta et al., 2017). These magnetite-rich assemblages in the Olympic Dam district differ from the typically carbonate- and K-feldspar-biotite-poor hydrothermal assemblages in most IOA deposits. Moreover, geochronological, stable and radiogenic isotope and fluid inclusion data may indicate different timing and origins of apatite-bearing magnetite alteration in IOCG hydrothermal systems of the Gawler Craton compared to IOA deposits, as discussed further below and in the accompanying paper (Skirrow, in prep.).

Magmatic-hydrothermal skarn Fe and Cu deposits developed in carbonate-bearing host rocks generally contain garnet-rich as well as clinopyroxene- and amphibole-rich zones, whereas garnet is not abundant in most orogenic, post-orogenic and Andean-type IOCG deposits. Exceptions include several of the IOCG deposits in the Kangdian province where carbonate-rich host rocks are more abundant than in many other IOCG provinces (e.g. Dahongshan deposit, Zhao et al., 2017), and

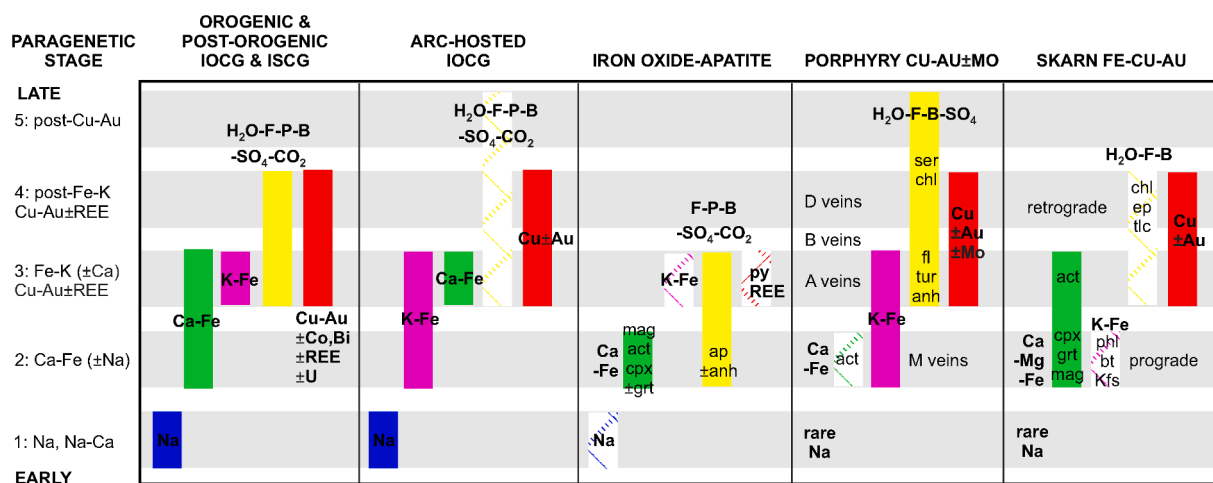


Fig. 5. Generalised paragenetic sequences of hydrothermal mineral assemblages and their chemical character for orogenic and post-orogenic IOCG deposits, compared with arc-hosted IOCG, IOA, porphyry Cu-Au-Mo and skarn Fe-Cu-Au deposits. Hatchured boxes represent weakly developed assemblages compared with full-coloured boxes. Mineral abbreviations: act – actinolite, anh – anhydrite, ap – apatite, bt – biotite, chl – chlorite, cpx – clinopyroxene, fl – fluorite, grt – garnet, Kfs – K-feldspar, mag – magnetite, ms – muscovite, phl – phlogopite, py – pyrite, ser – sericite, tlc – talc, tur – tourmaline. Sources: orogenic and post-orogenic and arc-hosted IOCG deposits; this study (Fig. 4); iron oxide-apatite, porphyry Cu (-Au-Mo) and skarn Fe and Cu (-Au) deposits: Oyarzun et al. (2003); Meinert et al. (2005); Sillitoe (2010); Day et al. (2016); Li et al. (2015a,b); Tornos et al. (2016); Rojas et al. (2018); Bonyadi & Sadeghi (2020).

a few other deposits (e.g. Hillside, Gawler Craton, Conor et al., 2010). Moreover, one of the distinctive features of hydrothermal assemblages in IOCG deposits including those with skarn-like alteration is the generally poor development of Mg-rich alteration relative to Na, Ca, Fe and K alteration, whereas in carbonate-replacement skarn deposits Mg-rich minerals may be common, such as Mg-bearing clinopyroxenes, tremolitic amphibole, phlogopite, Mg-chlorite and talc (Meinert et al., 2005). Further differences between the orogenic + post-orogenic IOCG deposits and classic magmatic-hydrothermal skarn Fe and Cu-Au deposits are the abundances of some of the volatile-rich phases. In particular the abundances of apatite, fluorite and barite appear to be higher in orogenic + post-orogenic IOCG deposits than in skarn Fe and Cu-Fe deposits. However, there appear to be fewer differences between the Andean arc-hosted IOCG deposits and some skarn Fe-Cu deposits, in terms of settings, hydrothermal mineralogy and ore geochemistry.

Whereas many aspects of the paragenetic sequences of orogenic, post-orogenic IOCG and Andean-type arc-hosted IOCG deposits and porphyry Cu-Au deposits are superficially similar there are several important aspects of the geology and mineralogy that distinguish particularly the orogenic IOCG deposits from porphyry deposits. First, the mesothermal crustal settings of orogenic IOCG deposit formation at depths where brittle-ductile deformation is characteristic are significantly deeper than the subvolcanic settings of most porphyry deposits (Sillitoe, 2010). Second, the spatial association of Cu-Au mineralisation with coeval igneous intrusions is much weaker for the orogenic and post-orogenic IOCG deposits compared to the obvious close relationships in porphyry systems as noted by Williams et al. (2005) and Barton (2013) although using different classifications of IOCG deposits. Third, hydrothermal quartz is a major and almost ubiquitous phase in most subduction-related porphyry Cu-Au deposits whereas it is remarkably low in abundance in the most intensely altered and mineralised zones of most orogenic and post-orogenic IOCG deposits. However, orogenic Cu-Au deposits with little or no Fe oxide within IOCG mineral systems commonly contain minor to locally abundant hydrothermal vein quartz.

Fourth, there are differences in the extent and intensity of Na alteration as noted above, as well as differences in REE, U, Co, Ni and other minor-element abundances that will be explored further in subsequent sections. On the other hand, there appear to be many similarities between Andean-type IOCG and porphyry deposits in terms of hydrothermal mineral sequences, spatial relationships to coeval intrusions, and geochemistry (Richards & Mumin, 2013). The key differences are

the lesser development of Na alteration, higher abundance of quartz but lower magnetite, and possibly lower abundances of hydrothermal carbonate and apatite in porphyry compared to Andean-type IOCG deposits. Associated intrusions also may be somewhat more mafic at Andean-type IOCG deposits than at porphyry deposits (Sillitoe, 2003; Richards et al., 2017).

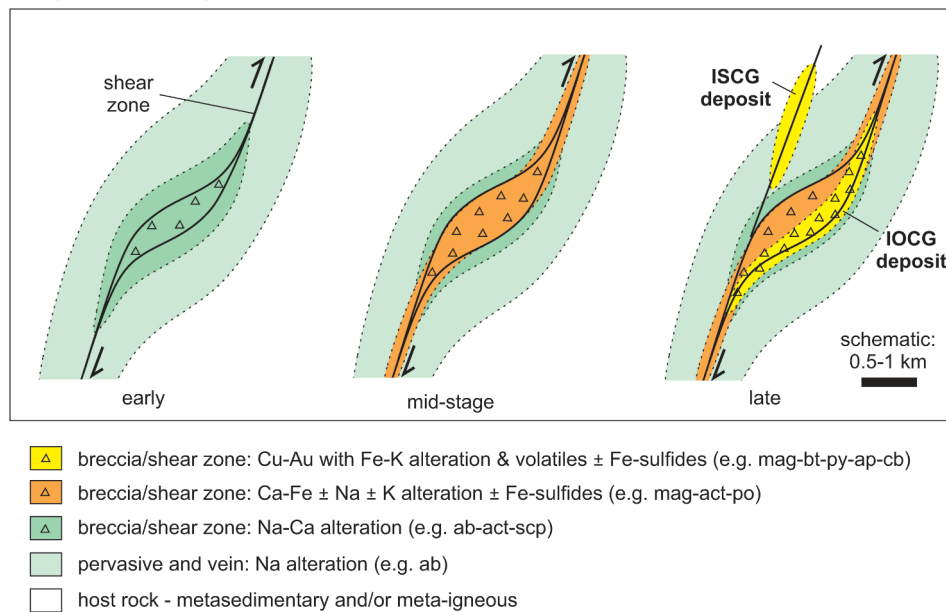
4.3. Alteration zoning – deposit scale

The sequences of hydrothermal mineral assemblages described above for IOCG deposits produce distinctive spatial patterns of alteration-mineralisation zoning which are partly controlled by the structural settings. Based on >30 deposits in 10 metallogenic province these zoning patterns have been generalised for each of the three lithostratigraphic-tectonic settings, in Fig. 6A, B and C.

In orogenic settings structurally favourable sites along ductile to brittle-ductile shear zones (e.g. dilatational jogs at rheological contrasts in local geology) commonly control the overall distribution of alteration-mineralisation. The geometric patterns of overprinting mineral assemblages vary greatly in detail between deposits (Fig. 6A). For example, the size of each zone representing a particular hydrothermal assemblage varies such that a later zone may be smaller than an earlier zone and hence it appears nested within the earlier alteration; alternatively a more extensive later zone may result in ‘enclaves’ of earlier alteration zones, or complete replacement of earlier by later assemblages. It should be noted that some zoning and overprinting effects may simply result from migration of alteration fronts away from fluid channelways, reflecting varying fluid:rock ratios. Also shown in Fig. 6A is an ISCG deposit lacking significant Fe-oxides (at right), which is part of a CGI mineral system.

The post-orogenic setting of the Gawler Craton is typified by breccia-hosted deposits with hydrothermal mineral zoning that can be interpreted in terms of progressive migration of upward-convex shells of alteration-mineralisation towards the paleo-surface. At the Prominent Hill deposit Schlegel & Heinrich (2015) proposed a series of nested upward-convex zones resulting from upflow and migration of hydrothermal fluids, as highly simplified in Fig. 6B. This concept has been extended to other zoned deposits in the eastern Gawler Craton in Fig. 6B. For example at Carrapateena the sub-vertical pipe-like morphology of the hematite-rich breccia zones and Cu-Fe sulfide zones (Porter, 2010b) can be interpreted to indicate migration of alteration-mineralisation

A. Syn- to late-orogenic IOCG and ISCG deposits



B. Post-orogenic IOCG deposits

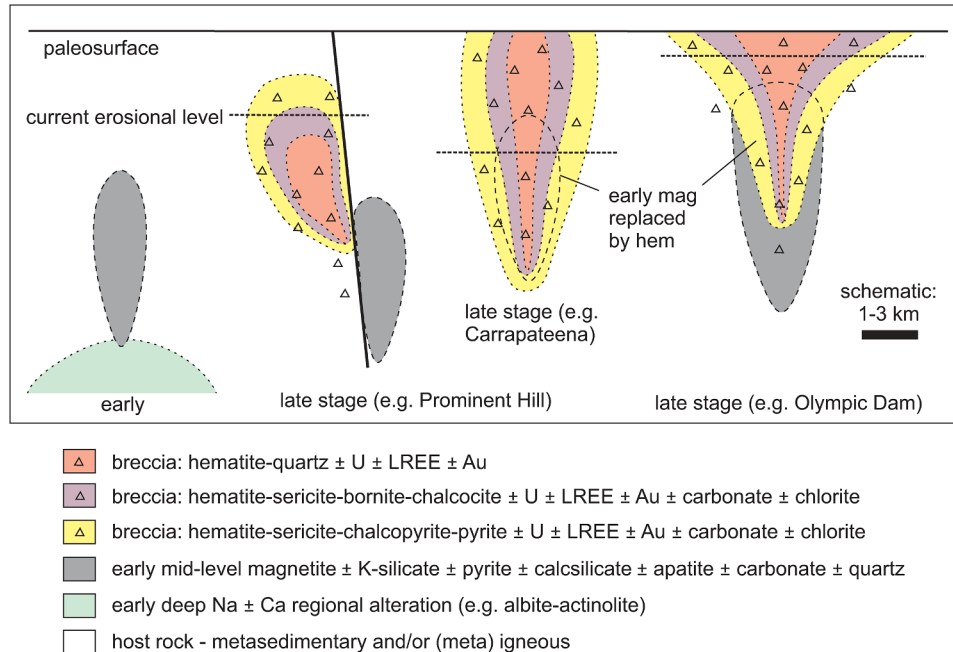


Fig. 6. Schematic cross sections of deposit-scale zoning and paragenetic sequences of hydrothermal alteration-mineralisation assemblages in IOCG and related deposits in CGI mineral systems. A: orogenic settings; B: post-orogenic settings (with example deposits from the Gawler Craton); C: arc-hosted settings (e.g. Chilean and Peruvian Andes deposits, based on [Sillitoe, 2003](#)).

zones to a higher structural level than at Prominent Hill, with subsequent erosion to a mid or lower level in the horizontally zoned system. The flared-upward zoning of Cu-Fe sulfides and other hydrothermal assemblages at Olympic Dam ([Reeve et al., 1990](#); [Haynes et al., 1995](#); [Ehrig et al., 2012](#)) could represent a further progression in which the hydrothermal and breccia system breached the paleosurface to form a broad funnel-shaped body with Cu-poor hematite-quartz alteration in the upper-centre of the deposit.

Schematic zoning within CGI mineral systems in arc-hosted settings is shown in Fig. 6C, based on the model of [Sillitoe \(2003\)](#). A possible spatial and temporal relationship between IOA deposits and IOCG deposits is also illustrated, with structural control by extensional and/or

transtensional mostly brittle fault zones. Reactivation of such fault zones may result in local overprinting of IOA deposits by Cu-Au mineralisation although the two deposit types also occur independently. A close spatial relationship with mafic-intermediate magmatism is also indicated ([Sillitoe, 2003](#)), in contrast to the orogenic and post-orogenic IOCG and related deposits where magmatism is broadly coeval with, but almost invariably distal from, these deposits.

4.4. Regional alteration

Regional-scale hydrothermal alteration, characterised particularly by Na- and Na-Ca-rich mineral assemblages, is a key feature of almost all

C. Arc-hosted IOCG and IOA deposits

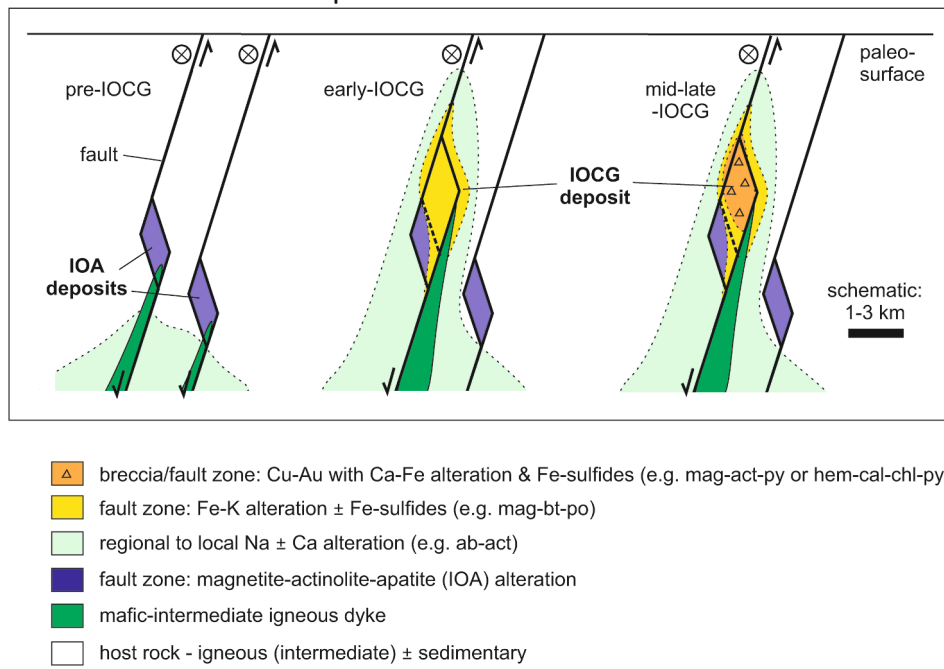


Fig. 6. (continued).

metallogenic provinces hosting CGI mineral systems and their IOCG deposits. Host rocks of widely varying composition are altered to combinations of albite, calcsilicates such as actinolitic amphibole, diopside (commonly salitic) and much less common Fe-Ca garnet, marialitic scapolite, and minor titanite. Sodic alteration with minor or no calcsilicates is commonly dominated by albite-quartz and can result in wholesale ‘bleaching’ of precursor rocks. Calc-silicate-rich domains range in dimensions from 100 s of metres to a few centimetres, and commonly are associated with brecciation. In orogenic IOCG hydrothermal systems such breccias with Na-Ca alteration are typically syn-tectonic, forming for example along brittle-ductile shear zones and in mesoscopic fold hinges. Assemblages transitional between Na-Ca and Fe-K may include biotite or magnetite, but the timing relationships between regional Na-Ca and regional Fe-K alteration are unclear in most provinces where both types of alteration are present, generally because the two regional alteration types are not juxtaposed (e.g. Gawler Craton, Curnamona Province, and Cloncurry province). However, at deposit scales it is more evident that Fe-K overprints Na-Ca alteration, and hence we may assume this to be the case in regional alteration systems. Surprisingly, in only a few provinces have the absolute timing relationships between regional Na-Ca alteration and Cu-Au mineralisation been well constrained by geochronology (see compilation in the [Supplementary Information](#)). For example in the Cloncurry and Curnamona provinces several regional Na ± Ca alteration events have been documented, but only some were coeval with Cu-Au mineralisation events ([Skirrow et al., 2000](#); [Teale & Fanning, 2000a,b](#); [Duncan et al., 2011](#)). The complex magmatic, tectonic and metallogenic-hydrothermal history of the Kiruna province ([Martinsson et al., 2016](#)) is an instructive case study where the few available U-Pb dates for prominent regional Na-Ca alteration show this metasomatism to be coeval with the first of two orogenic IOCG mineralisation events at ~1850–1865 Ma ([Supplementary Information](#)). Importantly, the dated major IOA deposits formed at ~1875–1885 Ma, significantly prior to the dated regional Na-Ca and orogenic IOCG mineralisation. More generally, the extent and intensity of regional Na-Ca alteration in provinces with IOA deposits and that lack significant orogenic, post-orogenic or arc-hosted IOCG deposits (e.g. Middle-Lower Yangtze Belt, Bafq, Southeast Missouri, Adirondacks) appears to be more limited than in the IOCG provinces.

4.5. Mineralogical classification of IOCG and related ISCG deposits

4.5.1. Redox – sulfur – iron mineralogical framework

The compilation of paragenetic sequences of hydrothermal minerals presented in Section 4.1 shows that Fe-rich Cu-Au deposits contain highly variable abundances and ratios of Fe-oxide and Fe-sulfide minerals. Although highly diverse it is apparent that the characteristic Fe-oxide-sulfide mineralogies of different deposits vary systematically with the occurrences of Cu ± Fe sulfides (chalcopyrite, bornite, chalcocite), alteration minerals, and with the relative abundances of key minor elements (e.g. Co, Ni, U, REE, Ba, F, Mo). These geochemical variations are discussed in Section 5. It is possible to describe the patterns of co-variation of hydrothermal minerals in terms of variations in (a) oxidation-reduction (redox) characteristics of the observed mineral assemblages, (b) the ratio of Fe-oxides to Fe-sulfides which relates mainly to the sulfur contents of the hydrothermal fluids relative to Fe, and (c) the relative timing of Fe-oxides and Cu-Fe sulfides. These three parameters are illustrated schematically in [Figs. 7 and 8](#), termed the ‘IOCG-ISCG cube’. Importantly, IOCG and ISCG deposits are shown to form a continuum, with the boundary arbitrarily set where the volumetric abundance of Fe-sulfides equals that of Fe-oxides. The IOCG-ISCG cube also illustrates the hypothesised correlation between the ore-related mineralogy, minor-element geochemistry and the geological-tectonic setting for three subtypes of deposits. In [Fig. 7](#) this is shown by the three volumes outlined in red, orange and green. The three parameters (axes) of the cube and application to classification of deposit subtypes are described below.

[Fig. 8](#) shows the back and front faces of the IOCG-ISCG cube in detail, where the Fe-oxide, Fe-sulfide and Cu ± Fe sulfide mineralogy of the dominant ore assemblages of individual deposits are represented by small areas of the faces (projected from small volumes within the three-dimensional space). Numbered circles represent example deposits, as detailed for some of the major IOCG provinces in [Appendix B](#).

The variations in observed oxide and sulfide mineralogy represented in the IOCG-ISCG cube can be understood in terms of the thermodynamic stabilities of the key Fe-oxides, Fe-sulfides and silicates, as shown in the activity diagram in [Fig. 9](#). Although depicted for specific conditions (300 °C, pH = 5, etc) the topology of the stability fields of the

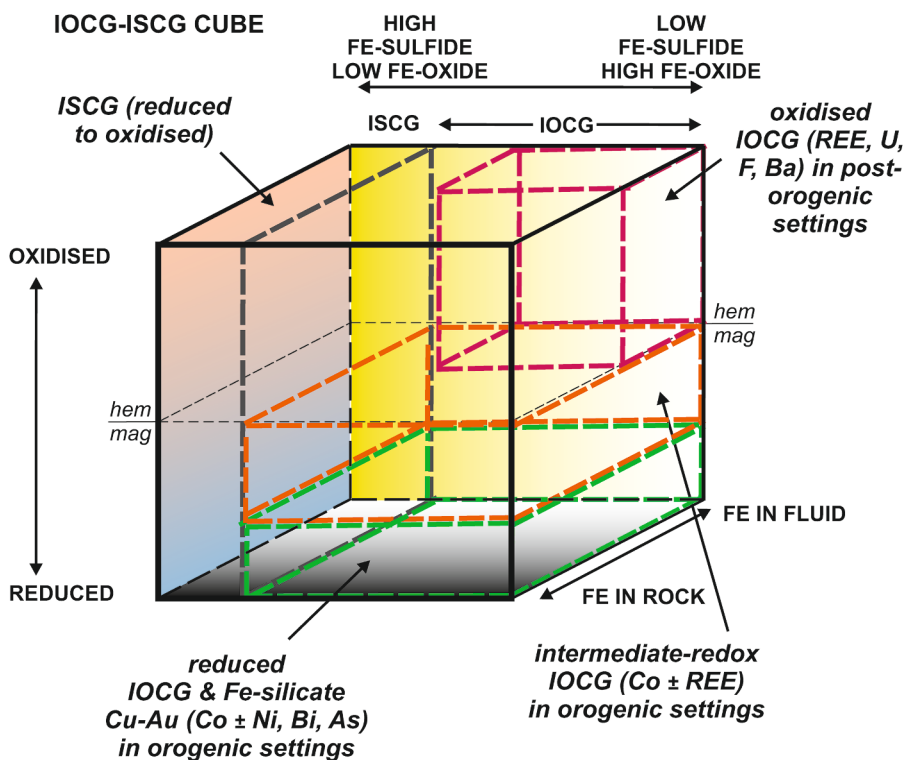


Fig. 7. Three-dimensional depiction of IOCG and ISCG deposit mineralogy (the IOCG-ISCG cube), showing generalised volumes representing three mineralogical-geochemical sub-types of deposits (oxidised, intermediate-redox and reduced) in different tectonic settings. The axes are based on predominance of Fe-oxide versus Fe-sulfide minerals in Cu-Au orebodies (x-axis), interpreted redox formation conditions of key Fe-Cu-O-S minerals (y-axis), and interpreted source/timing of Fe at the ore depositional site (z-axis).

minerals will remain roughly similar at slightly higher or lower temperatures (e.g. 250–350 °C). The y-axis in Figs. 7 and 8 represents the interpreted relative redox characteristics of the observed mineral assemblages, one of the most important parameters in characterising IOCG and ISCG deposits. Oxidised assemblages are defined as those in which hematite is stable at relatively high values of $\log f_{\text{O}_2}$, whereas reduced assemblages are defined as those that formed at relatively low $\log f_{\text{O}_2}$ and where pyrrhotite and/or Fe-silicates such as grunerite or minnesotaite (boundary at ~350–370 °C, Miyano & Klein, 1989) are stable, with or without magnetite and pyrite. Assemblages of intermediate redox contain magnetite and/or Fe-silicates with or without pyrite, but lack either pyrrhotite or hematite. At a fluid pH of 5 and at 300 °C the hematite-magnetite boundary lies close to the predominance field boundary between oxidised sulfur (i.e. aqueous HSO_4^- or SO_4^{2-}) and reduced sulfur (i.e. aqueous H_2S or HS; Fig. 7); this boundary represents another useful demarcation between oxidised and reduced hydrothermal conditions (albeit pH-dependant).

The x-axis in Figs. 7 and 8 represents the observed relative abundances of Fe-sulfides and Fe-oxides in the deposits. This ratio generally reflects the concentrations of sulfur in the fluid relative to the abundances of Fe at the sites of sulfide mineral deposition, as well as redox. At the extreme left side of the IOCG-ISCG cube are ISCG deposits lacking Fe-oxides and containing abundant Fe-sulfides as well as $\text{Cu} \pm \text{Fe}$ sulfides. Examples of ISCG deposits are well known in the Cloncurry province, such as the Eloise deposit (Davidson & Large, 1994; Haynes, 2000). In the Tennant Creek province they have been termed ‘non-ironstone Cu-Au-Bi deposits’ (Skirrow, 1993, 2000; Skirrow & Walshe, 2002). Indeed, many IOCG provinces contain examples of reduced to oxidised Fe-oxide-deficient Cu-Au deposits, which appear to form a continuum in terms of Fe-oxide/Fe-sulfide ratios with otherwise structurally and temporally similar Fe-oxide-bearing Cu-Au deposits (Figs. 7 and 8; Appendix B). Moreover, individual deposits may be internally zoned from massive Fe-Cu sulfide ore zones outwards through Fe-oxide-poor massive sulfide zones to outer Fe-oxide-rich sulfide-poor zones (see grey arrow at ‘WP’ in Fig. 8B, e.g. West Peko deposit, Tennant Creek province). At the extreme right side of the IOCG-ISCG cube (right-hand

face) are Fe-oxide-rich deposits with little or no Fe-sulfide accompanying the $\text{Cu} \pm \text{Fe}$ sulfides and gold (e.g. Salobo, Carajás province, and significant parts of the Olympic Dam and Prominent Hill Cu-Au-U-REE deposits, Gawler Craton). Gold-rich or U-rich Fe oxide deposits with low Cu and minimal sulfides may be variants within CGI mineral systems, and would also occupy parts of the right-hand face of the IOCG-ISCG cube (e.g. Juno and White Devil Au deposits, Tennant Creek province; NICO Au-Co-Bi deposit, Great Bear magmatic zone; Mt Gee U-REE prospect, South Australia).

The z-axis in the IOCG-ISCG cube represents the interpreted timing of Fe-oxide deposition relative to $\text{Cu} \pm \text{Fe}$ sulfides, based on the compilation of paragenetic sequences in Fig. 4 and reported geology of deposits. There are two end-member scenarios represented by the back and front faces of the cube, respectively (Fig. 8A, 8B): (1) all of the Fe-oxides were deposited contemporaneously with the Cu-Au mineralisation during evolution of an hydrothermal system, and (2) all of the Fe-oxides pre-dated Cu-Au mineralisation in separate hydrothermal or sedimentary events (e.g. sedimentary banded iron formation). Examples of scenario (2) include the ‘ironstone’-hosted Au-Cu-Bi deposits of the Tennant Creek province, parts of the Osborne, Starra and Monakoff deposits (Cloncurry province), parts of the Salobo deposit (Carajás province), and the Emmie Bluff prospect (Gawler Craton). In most other IOCG deposits major proportions of the observed Fe-oxides occurring in Cu-Au ore zones were deposited directly from hydrothermal fluids either during Cu-Au mineralisation or immediately beforehand in an evolving system (scenario 1, Fig. 8A). Good examples include the Ernest Henry deposit where chalcocite and pyrite were deposited during the same paragenetic stage as magnetite (Mark et al., 2006), and the Prominent Hill deposit where bornite-chalcocite-chalcopyrite formed with large quantities of hematite (Schlegel & Heinrich, 2015). Cases where both ‘early’ Fe-oxides and syn-Cu-Au Fe-oxides occur within the same deposit (i.e. part way along the z-axis in Figs. 7 and 8) may include the Salobo deposit where banded iron formation was overprinted by hydrothermal magnetite and $\text{Cu} \pm \text{Fe}$ sulfides (de Melo et al., 2017), and in the Gawler Craton where early magnetite ± apatite ± carbonate alteration was overprinted ~4 m.y. later by Cu-Au with abundant hematite (e.g. Olympic Dam deposit and Acropolis prospect, Gawler Craton, Cherry et al., 2018; Ehrig et al., 2012;

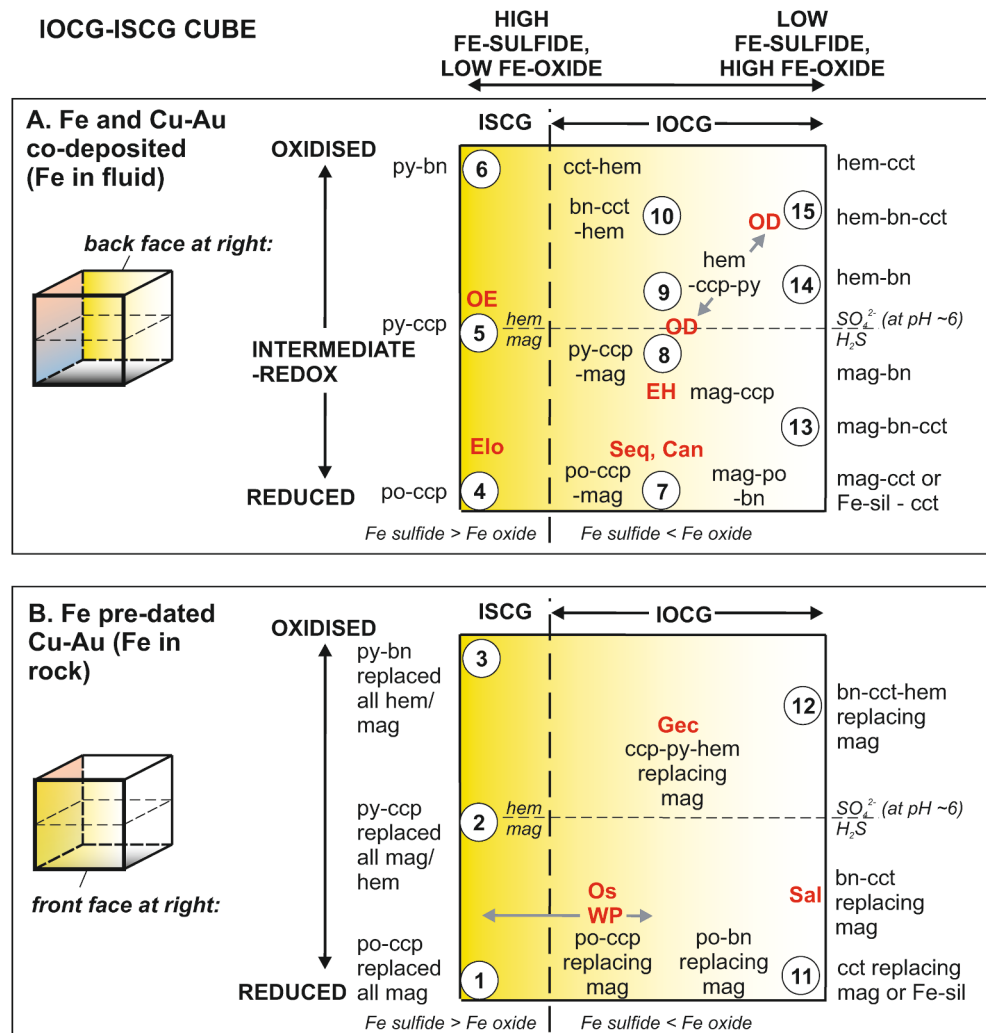


Fig. 8. IOCG-ISCG cube with detail of back and front faces. Axes as in Fig. 7. The back face (Fig. 8A) shows Fe-Cu-O-S mineral assemblages for deposits in which Fe-oxides and/or Fe-sulfides were broadly coprecipitated with main-stage Cu-Au ('Fe in fluid'). The front face (Fig. 8B) shows Fe-Cu-O-S mineral assemblages for deposits where most/all of the Fe-oxides pre-dated the main-stage Cu-Au, such as banded iron formation or hydrothermal ironstones ('Fe in the rock'). Stable mineral assemblages in the Fe-Cu-O-S system are based on Dick (2021), calculated at low to high values of total aqueous S and at 300 °C with differing Fe:Cu ratios (courtesy E. Bastrakov and J. Dick). Numbered circles represent example deposits, as detailed in Appendix B. Key deposits are shown in red text: Cand – Candelaria, EH – Ernest Henry, Elo – Eloise, Gec – Gecko K44 (upper), OD – Olympic Dam, OE – Orlando East, Os – Osborne, Sal – Salobo, Seq – Sequeirinho-Sossego, WP – West Peko. Mineral abbreviations as in Fig. 4. (For interpretation of the references to colour in this figure legend, the reader is referred to the web version of this article.)

Haynes et al., 1995; Johnson & McCulloch, 1995; McPhie et al., 2020; Oreskes & Einaudi, 1990; Reeve et al., 1990).

4.5.2. Oxidised, intermediate-redox and reduced mineralogical subtypes

As noted, both the Cu ± Fe sulfides and silicate alteration mineralogy vary systematically with the Fe-oxide and Fe-sulfide assemblages across the IOCG-ISCG cube. The IOCG and ISCG deposits can be classified into 3 mineralogical subtypes according to their dominant ore-related assemblages, which broadly correlate with the three geological-tectonic settings defined earlier (Fig. 7).

In the oxidised Fe-oxide Cu-Au (REE, U, F, Ba) subtype (red-outlined volume in Fig. 7) highly oxidised and S-poor hematite-white mica zones (top-right edge of IOCG-ISCG cube in Figs. 7 and 8, and top-left part of Fig. 9) may contain little or no sulfides or Cu but can be enriched in U and/or Au and/or REE, for example the upper and/or inner zones at Olympic Dam and Prominent Hill (Ehrig et al., 2012; Schlegel & Heinrich, 2015). These zones also may represent the most acidic conditions (e.g. Prominent Hill, Schlegel & Heinrich, 2015; Schlegel et al., 2018). Moderately oxidised hydrothermal assemblages generally contain hypogene bornite ± chalcocite with hematite ± pyrite and white mica (at low pH) or potentially K-feldspar (at high pH), as shown in Figs. 8 and 9. These bornite ± chalcocite assemblages transition downwards and/or outwards into less oxidised chalcopyrite-pyrite-hematite ± magnetite assemblages where chlorite may be present with white mica (e.g. Olympic Dam, Reeve et al., 1990). Examples are present in many other IOCG-bearing provinces. These include late-stage hematite- and U-

bearing chalcopyrite (-Au) mineralisation at the Sue Dianne deposit (Great Bear magmatic zone), and the paragenetically late hematite-bearing stage at Starra (Cloncurry province) where Au-rich mineralisation is associated with bornite, chalcopyrite, chalcocite, pyrite, chlorite, anhydrite, carbonate and later white mica (Rotherham et al., 1998). However, unlike the oxidised deposits of the Gawler Craton the late-stage Au-Cu at Starra is not REE-U-F-Ba-rich. This also appears to be the case in the hematite-rich examples of Au-Cu-Bi deposits in the Tennant Creek province and at the Cristalino deposit (Carajás province). Similarly, although hematite- and Cu-rich breccia at the Mantoverde deposit (Chilean Andean province) is weakly enriched in the LREE (e.g. up to 10 × local andesitic values), it contains very low U and lacks fluorite, barite, and hypogene bornite and chalcocite (Rieger et al., 2010).

A second mineralogical subtype of IOCG-ISCG deposits has intermediate-redox Cu-Au ore assemblages (green-outlined volume in Fig. 7) with variable modal proportions of magnetite, lack pyrrhotite or hematite, and contain chalcopyrite as the dominant Cu-bearing sulfide. Minor hypogene bornite is commonly present but bornite ± chalcocite dominating over chalcopyrite appears to be rare (e.g. Salobo). Many of the deposits in the Carajás, Cloncurry, Kangdian and Tennant Creek provinces are considered here to be members of the intermediate-redox group of IOCG deposits. Silicate mineralogy in the Cu-Au ore-associated assemblages is generally dominated by Fe-K-rich phases such as biotite or rare stilpnomelane, and/or Fe-Ca-rich phases such as actinolite or garnet, and/or Fe-rich silicates such as chlorite, grunerite, and

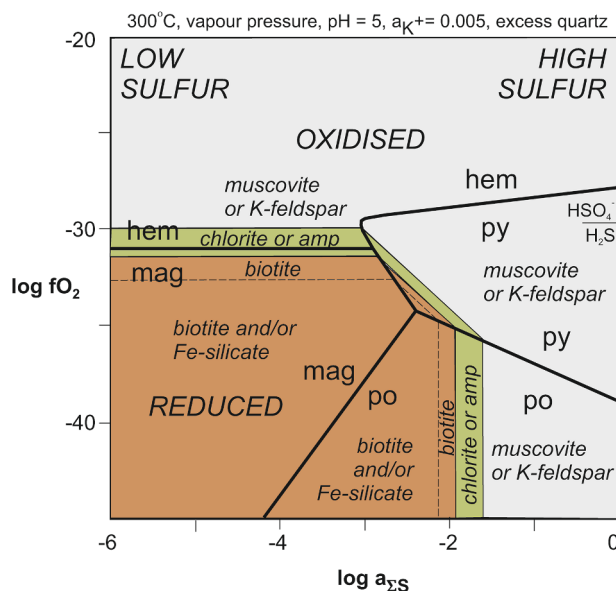


Fig. 9. Activity diagram of oxygen fugacity ($\log f\text{O}_2$) versus total aqueous sulfur activity ($\log a_{\Sigma\text{S}}$) at 300°C , showing stability fields for Fe oxides and sulfides along with silicates in the system Fe-O-H-S-Si-Al-K. This diagram may be used as a ‘legend’ for the IOCG-ISCG cube in Figs. 7 and 8. Muscovite is the stable K-silicate at $\text{pH} = 5$, as illustrated; K-feldspar is stable at $\text{pH} > 6.5$ for activity of $\text{K}^+ = 0.001$, or at $\text{pH} > 5.5$ for activity of $\text{K}^+ = 0.01$. At higher temperatures Fe-amphibole would occupy approximately the field of chlorite. Parts of the biotite field may be occupied by stilpnomelane and/or Fe-silicates such as minnesotaite or grunerite under certain conditions (e.g. differing activity of K^+ or temperature). Figure modified from Skirrow & Walshe (2002).

uncommon fayalite, minnesotaite or greenalite. The stability relationships of some of these minerals is shown in Fig. 9 where it is clear that both the redox conditions and sulfur content of the fluids (among other parameters) are important in determining the particular oxide-sulfide-silicate assemblages at individual deposits. The intermediate-redox IOCG and ISCG deposits are highly variable in the reported occurrences of minerals hosting REE, U, Co, Ni, Bi, Mo and other ore elements, as noted above (Fig. 4). There may be a sub-set of the intermediate-redox deposits that exhibit anomalous to very high REE contents (commonly with allanite as the main REE host) and which may be transitional to the oxidised IOCG-ISCG group (e.g. Sin Quyen, SWAN, Monakoff, E1, Ernest Henry; see also Ore Geochemistry section, below).

The third mineralogical subtype of IOCG-ISCG deposits is represented by the most reduced assemblages, with pyrrhotite and/or Fe-silicates and variable modal proportions of magnetite and pyrite (green-outlined volume, Fig. 7). Chalcopyrite is the dominant Cu sulfide with minor bornite in some deposits. Examples range from magnetite-pyrrhotite-pyrite-rich deposits (e.g. Osborne, Raúl-Condestable, Candelaria, Sin Quyen, Lala, NICO), and some with Fe-silicates such as West Peko (minnesotaite, greenalite), to pyrrhotite-rich ISCG deposits or zones lacking magnetite (e.g. Eloise, Dahongshan, Mt Elliott eastern zone) or containing only minor magnetite (e.g. Guelb Moghraïn, Sequeirinho-Sossego). It is notable that reported occurrences of minor minerals in the reduced IOCG-ISCG deposit group commonly includes phases hosting Co, Ni, As and Bi but very rarely REE- or U-rich phases nor fluorite, barite or anhydrite.

5. Geochemical characterisation of IOCG and related deposits

OSNACA (Ore Samples Normalised to Average Crustal Abundances) is an open-source database of whole-rock geochemical data for ore samples from a large number of ore deposits of different types worldwide (Brauhart et al., 2017; OSNACA, 2020). Consistent analytical

methods have been used for determination of 62 element abundances in all samples, with detection limits at or below average crustal abundances (OSNACA, 2020). Ore samples were assigned by Brauhart et al. (2017) into 15 deposit types or classes including IOCG plus ‘other’. Of the 1165 samples accessed from OSNACA in 2020 a subset of 99 samples were classified as representing IOCG ores. Although OSNACA presently contains only a few samples for any particular deposit, the data are believed to be representative of key ore types, and are sufficient to identify broad similarities and differences between groups and sub-groups of deposits (Brauhart et al., 2017). For example, multi-dimensional scaling and principal component analysis shows that samples from IOCG deposits are geochemically distinct from all of the other ore deposit types in the data set, with closest similarities to porphyry Cu, magmatic Ni-Cu-PGE and sediment-hosted Cu deposits (Brauhart et al., 2017).

However, there are substantial variations in geochemistry within the broad group of samples attributed as IOCG ores in the OSNACA data set. Ore samples from several of the deposits attributed as IOCG type in the OSNACA data set have very different geochemistry and geology to the IOCG and ISCG deposits considered in this review. These include the Vergenoeg fluorite-magnetite deposit (South Africa), the Messina Cu deposit (South Africa), the Kurilla Cu deposit (Australia) and the Merlin Mo-Re deposit (Australia). These samples have been considered separately from the ‘IOCG ores’ data set in the present study, as have a few samples of hydrothermally altered rocks with low-grade mineralisation (omitted). The remaining IOCG-attributed samples have been carefully assessed against the characteristics of the IOCG and ISCG deposits as defined in this review. Samples from deposits qualifying as IOCG or related ISCG deposits have been assigned to mineralogical subtypes according to their dominant ore-related oxide-sulfide-silicate mineralogy, relative redox conditions of oxide-sulfide-silicate mineral formation, and settings, following Figs. 7 and 8. A summary of deposits and subtype attribution is given in Appendix C, which also lists the sources of additional geochemical data for several Andean IOCG deposits. This mineralogical-redox framework was then used to compare the ore geochemistry between (a) mineralogical subtypes within the family of IOCG-ISCG deposits, and (b) between IOCG-ISCG deposits and other selected ore deposit types, as described below.

5.1. Geochemical subdivision of IOCG and related ISCG deposits

Inspection of the OSNACA data for the ore samples attributed as IOCG or ISCG deposits has revealed large variations in the relative abundances of some of the chalcophile-siderophile elements (e.g. Co, Ni, Bi, Se, Te) compared to selected HFSE and LILE (e.g. U, REE, Mo). These striking variations are evident in plots of the ratio $(\text{Co} + \text{Ni} + 10^*\text{Bi} + 10^*\text{Se} + 50^*\text{Te})/(\text{U} + \text{La})$, termed the IOCG discriminator, in which the element values are in ppm. The multipliers for Bi, Se and Te are based on an empirical comparison of their average crustal abundances with Co, Ni, U and La so that the weighted contributions of each element are similar (Fig. 10). An important and surprising finding of this study is that the widely varying values of the IOCG discriminator show a good correlation with the ore-related mineralogy and with the interpreted redox conditions of oxide-sulfide-silicate mineral formation, from reduced to oxidised (Figs. 7 and 10). As the interpreted redox conditions have been determined independently from the geochemical characterisation, the correlations in Fig. 10 are considered to be a fundamental feature of the IOCG and related deposits in CGI mineral systems. Moreover, there appears to be a weak inverse correlation between the Au/Cu ratio and the IOCG discriminator index, such that the relatively oxidised ores tend to have higher Au/Cu ratios than the relatively reduced and Cu-rich ores (Fig. 10).

The variations in key element suites are also clearly evident in plots of individual elements representing the suites, and allow discrimination of four geochemical subtypes of IOCG ores within a continuum of values of the IOCG discriminator. For example, Fig. 11 shows La versus Co

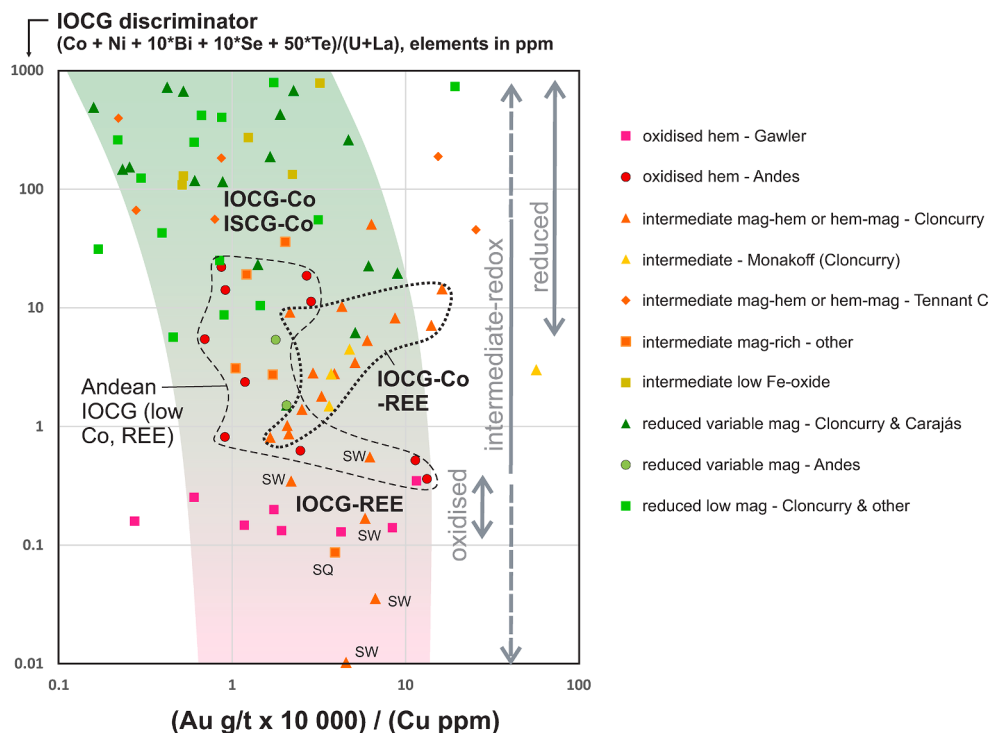


Fig. 10. IOCG discrimination diagram based on whole-rock ore geochemistry, showing Au/Cu ratio versus the IOCG discriminator ratio ($(Co + Ni + 10^*Bi + 10^*Se + 50^*Te)/(U + La)$), with elements in ppm. The subtypes of IOCG and other deposits listed in the legend are based on independently determined mineralogical-redox subdivisions (Fig. 7); the generalised ranges of oxidised, intermediate-redox and reduced mineral assemblages are indicated with arrows. The coloured band encloses most data points. Geochemical data from the OSNACA data set (OSNACA, 2020) with additional data for Mantoverde (Chile, Rieger et al., 2010), Candelaria, Carola and Socavon Rampa (Chile, Marschik & Fontboté, 2001). Abbreviations: SQ – Sin Quyen, SW – SWAN.

concentrations (with symbol size proportional to U content) and a subdivision into four subtypes demarcated by nominal boundaries at 100 ppm Co and 100 ppm La. The four geochemical subtypes are listed below, followed by detailed descriptions. The same subtypes are also labelled on Fig. 10.

Subtype (1): 'IOCG-Co' and 'ISCG-Co' ores with moderate to high enrichments in the chalcophile and siderophile elements $Co + Ni + Bi + Se + Te$, and with low U and REE contents; mineralogical data indicate these deposits also lack fluorite (F) and barite (Ba) with the Cu sulfides (no Ba and F analytical data are available in OSNACA).

Subtype (2): 'IOCG-REE' ores highly enriched in selected HFSE and LILE, in particular REE and/or U, which commonly also have high Mo, F, and Ba contents, and low $Co + Ni + Bi + Se + Te$ contents.

Subtype (3): 'IOCG-Co-REE' ores with geochemistry transitional between subtypes (1) and (2), with moderate to strong enrichments in both the $Co + Ni + Bi + Se + Te$ and REE-U-Mo-F-Ba groups of elements.

Subtype (4): IOCG ores without strong enrichments in either the $Co + Ni + Bi + Se + Te$ group or the REE-U-Mo-F-Ba group of elements (termed the IOCG (low Co, REE) subtype).

The IOCG-Co and related ISCG-Co ores of subtype (1) have moderate to strong enrichments in $Co + Ni + Bi + Se + Te$ but low abundances of REE and U, and are generally characterised by variable quantities of magnetite (from very abundant in IOCG-Co to minor or absent in ISCG-Co variants) with pyrrhotite and/or pyrite, chalcopyrite \pm bornite. They also may contain Fe^{2+} -rich silicates in differing combinations, such as biotite, phlogopite, actinolite, grunerite, fayalite and/or stilpnomelane. Variations in relative abundances of magnetite and sulfides may be considerable even within individual deposits in this subtype. Deposits of subtype (1) lack syn-sulfide hematite and sulfate minerals such as barite and anhydrite, as well as hypogene chalcocite. The mineral assemblages of this subtype are indicative of relatively reduced to intermediate-redox conditions during Cu-Fe sulfide ore deposition (Figs. 7–9). In the Cloncurry district where some of these reduced deposits of subtype (1) are ISCG deposits it has been suggested that local reduction of the ore fluid was effected by reductants in the host rocks such as graphite (Haynes, 2000), and with resultant suppression of magnetite formation (Williams et al., 2005). However, considered globally, almost all of the pyrrhotite-

bearing ISCG and IOCG deposits occur in non-graphitic host rocks (e.g. Osborne, Cloncurry province, Adshead et al., 1998; West Peko, Tennant Creek province, Skirrow & Walshe, 2002; Guelb Moghrein, Mauritania, Kolb et al., 2010; Kolb & Petrov, 2016; Kirschbaum & Hitzman, 2016; and pyrrhotite-bearing deposits in the Carajás, Kangdian and Andean provinces). An alternative explanation is that the reduced character of the mineral assemblages is inherent to the redox properties of the ore fluid prior to ore deposition. It is also reasonable to infer that the enrichments of $Co + Ni + Bi + Se + Te$ and low abundances of REE and U are also a fundamental feature of the hydrothermal fluids involved in the formation of the IOCG-Co and related ISCG deposits. In the special case of the Guelb Moghrein deposit graphite in the orebody is considered to be the product of breakdown of siderite to magnetite plus graphite; the host carbonate and mafic meta-igneous rock sequence is graphite-free (Kirschbaum & Hitzman, 2016). Other examples of reduced to intermediate-redox IOCG-Co and related ISCG deposits include: Eloise, Kulthor, Lorena (Cloncurry province, Australia); Antas, Sossego-Sequeirinho (Carajás province, Brazil); and Warrego (Tennant Creek province, Australia).

Ores of geochemical subtype (2), labelled 'IOCG-REE' in Figs. 10 and 11, have distinctive low values of <1 for the $(Co + Ni + 10^*Bi + 10^*Se + 50^*Te)/(U + La)$ discriminator, in contrast to the IOCG-Co ores of subtype (1). Although there are relatively few deposits represented in OSNACA in this subtype, the main examples are world-class hematite-rich breccia-hosted Cu-Au-U-REE deposits in the Gawler Craton, including the Olympic Dam, Prominent Hill and Carrapateena deposits. In addition to U and LREE, these deposits are also highly anomalous in Ba and F as evident from the abundances of barite and fluorite (Reeve et al., 1990; Belperio et al., 2007; Porter, 2010b; Ehrig et al., 2012). The ore-related mineral assemblages are indicative of relatively oxidised hydrothermal conditions and include hematite, barite, chalcocite and bornite (Figs. 7–9; Reeve et al., 1990; Haynes et al., 1995; Ehrig et al., 2012; Schlegel & Heinrich, 2015; Schlegel et al., 2018). The Olympic Dam deposit has a remarkably wide range of other anomalously enriched elements that in some cases are zoned across the deposit, such as deep and/or peripheral zones with anomalous Mo, W, Sb, As, Te, Ba and Sn (Ehrig et al., 2012). Minerals representing reduced conditions are

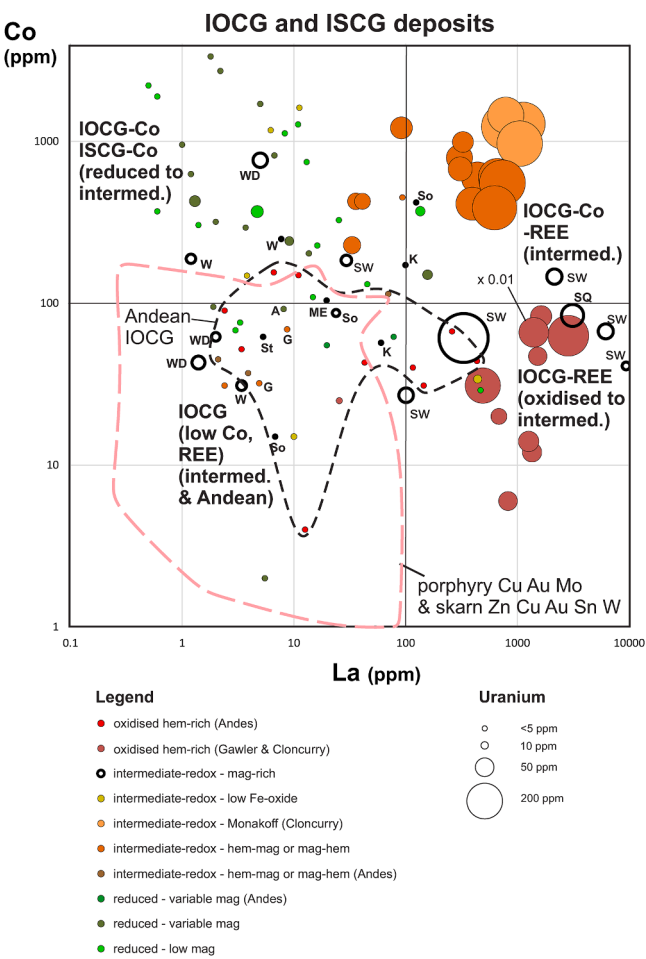


Fig. 11. La (ppm) versus Co (ppm) with U (symbol size) discrimination diagram for geochemical subtypes of IOCG and ISCG deposits (IOCG-Co, IOCG-REE, etc), based on OSNACA ore geochemical data (OSNACA, 2020). Symbol colours correspond to subtypes of IOCG and ISCG deposits defined independently of the geochemical data, on the basis of mineralogy and oxidation-reduction conditions, following Fig. 7. The size of the symbols is proportional to the U (ppm) values; the area of one symbol for an Olympic Dam sample is reduced by a factor of 100 for clarity (labelled $\times 0.01$). Also shown is the field for ores from porphyry Cu-Au and Mo deposits, and various types of skarn deposits (Au, Cu, Zn, Sn, W). Abbreviations for selected deposits: W – Warrego, WD – White Devil, G – Gecko (all Tennant Creek province); SQ – Sin Quyen (Vietnam), SW – SWAN (Cloncurry province); K – Khetri (India); ME – Mount Elliott, St – Starra (Cloncurry province); So – Sossego, A – Antas (Carajás province). Additional data for Mantoverde (Chile, Rieger et al., 2010), Candelaria, Carola and Socavon Rampa (Chile, Marschik & Fontboté, 2001).

absent or rare (e.g. rare pyrrhotite at Olympic Dam, Ehrig et al., 2012). Locally abundant magnetite with siderite, pyrite and chalcopyrite, in the deeper and/or peripheral zones at Olympic Dam, represent hydrothermal conditions of intermediate redox compared to relatively oxidised upper and/or inner zones (Figs. 7–9; Reeve et al., 1990; Haynes et al., 1995; Ehrig et al., 2012).

A third subtype of ores, labelled ‘IOCG-Co-REE’ in Figs. 10 and 11, exhibit geochemical signatures that are transitional between the IOCG-Co and IOCG-REE subtypes, with strong enrichments in both REE + U and Co + Ni + Bi + Se + Te. These ores occur in relatively few deposits as presently represented in the OSNACA data set, all within the Cloncurry district (Ernest Henry, Monakoff, and E1 Group deposits). The Cu-Au ores are characterised by generally high ratios of magnetite/hematite and pyrite/pyrrhotite, and they are all relatively Fe-oxide-rich. They mostly lack minerals indicative of strongly reduced conditions (e.g. graphite, pyrrhotite, fayalite, minnesotaite, loellingite) but contain

minor to locally abundant minerals representing oxidised conditions (e.g. hematite, barite; Mark et al., 2006; Williams et al., 2015). Typical assemblages with Cu-Au mineralisation include magnetite, pyrite, chalcopyrite, biotite, K-feldspar, carbonate, Ca-amphibole, chlorite and quartz. The IOCG-Co-REE ores are therefore represent intermediate-redox conditions of hydrothermal mineral formation (Figs. 10 and 11).

A fourth geochemical subtype of ores is evident from Fig. 11 (labelled IOCG (low Co, REE)), with low Co (<100 ppm), La (<100 ppm) and U (<5 ppm). These ores have IOCG discriminator values spanning the range between the IOCG-Co and IOCG-REE subtypes (similar to the IOCG-Co-REE range) but their REE + U and Co + Ni + Bi + Se + Te contents are relatively low. Most ores in this geochemical subtype are Fe-oxide-rich and contain magnetite-pyrite-chalcopyrite ± hematite assemblages typical of intermediate-redox formation conditions (Figs. 7–9). Importantly, most of the IOCG ores from the Andean deposits plot within this IOCG (low Co, REE) subtype, with the exception of several samples from the hematite-magnetite-rich Mantoverde deposit which contains enrichments in REE but low U (Rieger et al., 2010). It is noteworthy that this deposit also contains relatively abundant hypogene hematite with chalcopyrite (Benavides et al., 2007; Rieger et al., 2010), whereas other Andean IOCG deposits with hematite \gg magnetite (Carola, Socavon Rampa, Barreal Seco) have much lower REE abundances.

The IOCG (low Co, REE) subtype also contains ore samples from parts of some Au-Cu-Bi deposits from the Tennant Creek province, although other samples from the same deposits plot within the IOCG-Co fields in Figs. 10 and 11 (e.g. Warrego, White Devil). When the broader element group of Co + Ni + Bi-Se + Te is considered, most of the Cu-rich Tennant Creek Au-Cu-Bi ores plot within the same geochemical subtype as the reduced IOCG-Co ores from the Cloncurry, Carajás and Guelb Moghrein provinces (Fig. 10), including samples from the West Peko deposit (R. Skirrow, unpublished data, not in OSNACA). This suggests that at least the Cu-rich members of the Tennant Creek Au-Cu-Bi deposits are indeed geochemically very similar to other deposits in the global IOCG family of deposits (cf. Groves et al., 2010). Nevertheless, some ores with extremely high Au/Cu ratios (e.g. White Devil) plot well outside the main trend of IOCG and related ISCG deposits in Fig. 10, and may represent a separate and later Au event (Huston et al., 2020; also see Tennant Creek province section of Supplementary Information).

A few deposits have mineralogical features that are inconsistent with the majority of other deposits in their geochemical subtype. For example, the SWAN Cu-Au ores in the Cloncurry province have low IOCG discriminator values and high La-Co-U contents similar to those of the oxidised IOCG-REE subtype (Figs. 10 and 11), but the deposit has an intermediate-redox mineral assemblage of magnetite-amphibole-pyrite-chalcopyrite-anhydrite with albite and clinopyroxene (Brown & Porter, 2010). The Sin Quyen deposit may be another example. The origin of these mis-matches is not fully understood. Interestingly, the Mt Elliott Cu-Au deposit, which is adjacent to the SWAN deposit, is considered to be part of the same hydrothermal system as the SWAN deposit and shares similar mineralisation and alteration mineralogy including minor anhydrite, pyrrhotite, allanite, tourmaline, apatite, biotite and K-feldspar (Brown & Porter, 2010). Although few data are available in OSNACA, Mt Elliott has a higher IOCG discrimination value (16) than SWAN (0.01–0.55) and significantly lower REE and U contents. These relationships may indicate that fluids of similar sulfate-stable (oxidised) and LREE-rich character to those in IOCG-REE deposits were involved at both SWAN and Mt Elliott, producing local anhydrite and LREE enrichments yet without hematite development, perhaps due to high temperatures. These oxidised magnetite-anhydrite-stable fluids may have overprinted or coexisted with a more reduced (pyrrhotite-bearing) hydrothermal environment represented at the Mt Elliott deposit. This example illustrates the complexities in the mineralogical and geochemical evolution of the IOCG and related deposits considered herein, which in places resulted in features of hybrid (e.g. multi-stage, or multi-fluid) origin.

5.2. Geochemical comparisons of IOCG deposits with other ore types

Comparison of the geochemistry of the IOCG ore samples in the OSNACA data set reveals that, for the IOCG-Co, IOCG-REE and IOCG-Co-REE subtypes, Co + Ni + Bi + Se + Te and/or U + REE are enriched relative to porphyry (Cu ± Au, Mo), skarn deposits of various types (Cu, Fe, Au, W, Sn), intrusion-related gold (IRG), granite-related greisen (Sn, W, Mo, Bi) and pegmatite (Nb, Ta, Li) deposits (Fig. 12). Although there is some overlap between these groups around y-axis values of ~100 the Telfer Au-Cu deposit in northwestern Australia stands out as an exception and has similar Co-Ni-Bi-Se-Te compositions to those of the IOCG-ISCG deposits represented in OSNACA. The overall differences between IOCG-ISCG and these other deposit types are also clearly evident when only La and Co are plotted as key representatives of the REE and Co + Ni + Bi + Se + Te element suites (Fig. 13). The porphyry, skarn and granite-related groups of deposits, widely agreed to be of intrusion-related magmatic-hydrothermal origin, have Co + Ni + U + La (total ppm) values of generally <100 for samples with Cu > 1000 ppm, whereas the IOCG ores mostly have Co + Ni + U + La (total ppm) values >100 for Cu > 1000 ppm (Fig. 12). In the La versus Co diagram the nominal boundaries of 100 ppm La and 100 ppm Co used for subdivision of the IOCG and related deposits appear to also effectively demarcate the fields of the porphyry and skarn deposits (Fig. 13). Notably, the low Co, La and U contents of most of the Andean IOCG ore samples (except some Mantoverde samples) match the low values of porphyry and skarn deposits, which are also mostly located within magmatic arc settings (Sillitoe, 2010). Hence this ore geochemistry is likely fundamental to the

Deposit classification in Cu-Au-Fe (CGI) mineral systems

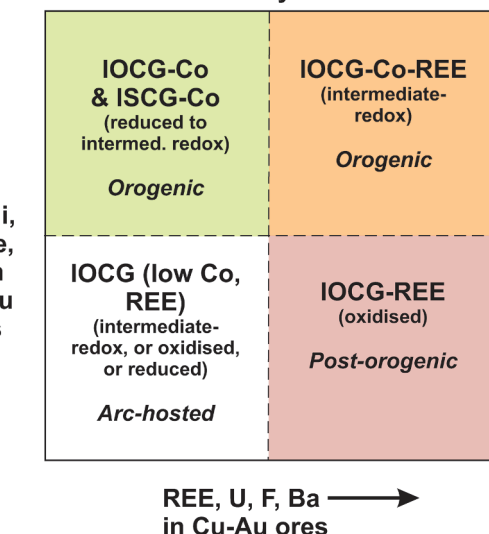


Fig. 13. Classification scheme with ore geochemical axes for subtypes of deposits in the CGI mineral systems including IOCG and ISCG deposits. Note the combined use of ore geochemical, mineralogy-based redox, and geotectonic setting attributes in the proposed scheme.

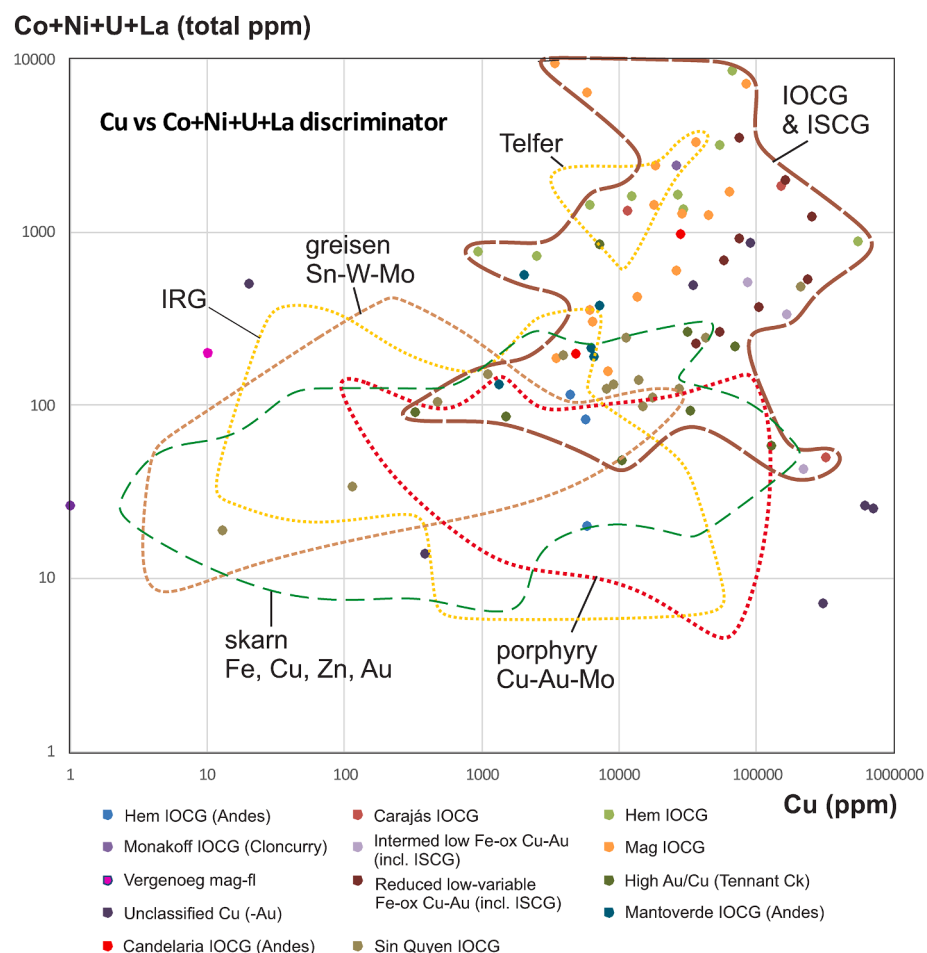


Fig. 12. Copper versus Co + Ni + U + La (in ppm) discriminator diagram comparing IOCG-ISCG deposits with fields for intrusion-related magmatic-hydrothermal deposits (porphyry Cu-Au-Mo, skarn Fe Cu Zn Au, greisen Sn-W-Mo, and intrusion-related gold (IRG) deposits). The subtypes of IOCG-ISCG deposits listed in the legend are based on mineralogical subdivisions shown in Figs. 7 and 8 and listed in Appendix C. Data from the OSNACA database (OSNACA, 2020).

continental arc setting.

In summary, with the exception of the Andean IOCG deposits, most IOCG ores in the OSNACA data set are dissimilar to magmatic-hydrothermal deposit types, in terms of the key minor element suites Co + Ni + Bi + Se + Te and REE + U (Mo, F, Ba), but share some geochemical features of deposits formed by hydrothermal leaching of mafic and other host rocks. The possible reasons for these geochemical similarities and differences are discussed in the accompanying paper (Skirrow, in prep.), where they are suggested to relate to the relative partitioning of compatible and incompatible elements between hydrous fluids, silicate melts, and sulfide melts, and the relative stabilities of the metal complexes and mineral solubilities in hydrothermal fluids. Indeed, the elements Co, Ni, U and La have been chosen as discriminators mainly because of their contrasting behaviours in magmatic and hydrothermal fluid-silicate-sulfide melt systems. It should be noted, however, that the inferred redox conditions (or other geochemical parameters) of the observed ore-related hydrothermal mineral assemblages do not necessarily represent the very earliest redox (or other hydrothermal) characteristics of the fluids along their flow paths to the sites of ore deposition.

6. Discussion

6.1. Relationships between IOCG and IOA deposits

The relationships between IOCG and IOA deposits have been much debated since the 1980s and 1990s when the IOA deposits of Kiruna province were included by Hitzman et al. (1992) in the global family of Proterozoic iron oxide (Cu, U, Au, REE) deposits. While suggesting a genetic link and a continuum between IOA and IOCG end-members, Hitzman (2000) also noted there are fundamental differences between IOA and IOCG deposits and that they did not necessarily form coevally where they occur in the same district. Williams et al. (2005) stated that Kiruna-type iron oxide-apatite ores are not IOCG deposits and may be genetically fundamentally different and yet they may share similar geological environments and sources of some components. The different timing and tectonic settings of the Precambrian IOA and IOCG deposits was also cited by Groves et al. (2010) as evidence of distinct genesis rather than end-members in a continuum. On the other hand, Corriveau et al. (2010a,b, 2016) proposed a generalised alteration zoning model, based on observations in the Great Bear magmatic zone and broader comparisons, in which IOA deposits formed at deeper, higher temperature and earlier stages in the same ‘iron oxide–alkali alteration’ systems as shallower, lower temperature and later IOCG (and albite-hosted U and polymetallic skarn) deposits. Recent studies in the Chilean Iron Belt have also promoted a more direct genetic association between deeper IOA and shallower IOCG deposits than proposed by Sillitoe (2003), as described by Knipping et al. (2015), Reich et al. (2016), Barra et al. (2017), Simon et al. (2018) and Rodriguez-Mustafa et al. (2020).

The availability of considerable new data in recent decades brings new constraints to the issue of the relationship between IOA and IOCG deposits. First, among the world’s 10 major orogenic, post-orogenic and arc-hosted IOCG provinces large IOA deposits of Kiruna type are present only in the Kiruna province itself, and in the Chilean Iron Belt, although large Fe oxide-rich apatite-poor hydrothermal bodies and/or Fe-oxide-rich alteration lacking significant Cu-Au mineralisation are present in many of the other major IOCG provinces. Available geochronological constraints for the Kiruna province and Chilean Iron Belt indicate that the formation of the large IOA deposits preceded the main IOCG mineralisation events by >10–15 m.y. (see review in the Supplementary Information). Moreover, the IOA deposits in both of these provinces contain very low Cu-Au contents, although they generally contain minor pyrite and may host trace chalcopyrite. In rare cases where the IOA deposits contain small Cu (-Au) resources the textural and structural relationships indicate that the main Cu (-Au) mineralisation overprints the IOA deposit (e.g. Cerro Negro Norte, Chile, Salazar et al., 2020),

consistent with the geochronological data for the Chilean Iron Belt indicating a significant time gap. Conversely, the magnetite-rich paragenetically early stages in the main IOCG deposits in the Andean provinces (Chile and Peru) and Kiruna province are not known to be apatite-rich, nor do they contain the coarse-grained (pegmatitic) magnetite-apatite-amphibole intergrowths that are typical of parts of many IOA deposits in both regions. For example, in the Candelaria deposit the paragenetically early magnetite-rich alteration is not apatite-bearing (Marschik & Fontboté, 2001; del Real et al., 2018) despite the evidence of similar magnetite geochemical and isotopic compositions to magnetite in some IOA deposits of the Chilean Iron Belt (Rodriguez-Mustafa et al., 2020). Similarly, at the Mantoverde deposit Rieger et al. (2010) reported only minor apatite (associated with quartz, tourmaline, scapolite and white mica) within the magnetite-hematite-rich deposit, and noted the differences in alteration and magnetite geochemistry between the IOA deposits in the district and the Mantoverde deposit.

Magnetite-rich alteration with in some places local apatite is indeed present in some of the other orogenic, post-orogenic and arc-hosted IOCG provinces but, as in the Kiruna and Andean provinces, it is paragenetically earlier than, and temporally distinguishable from, the Cu-Au mineralisation where data are available. For example, in the post-orogenic Olympic Cu-Au province in the Gawler Craton magnetite-rich alteration with locally abundant apatite at the Acropolis prospect formed ~4 m.y. earlier than the major Cu-U-Au mineralisation event at the Olympic Dam deposit (based on high-precision U-Pb TIMS dating, Cherry et al., 2018; Courtney-Davies et al., 2019; McPhie et al., 2020; see also review in the Supplementary Information). Moreover, the magnetite alteration at Acropolis and elsewhere in the Olympic Dam district is associated with hydrothermal K-feldspar and carbonate as well as actinolite, pyrite and quartz (Oreskes & Einaudi, 1990, 1992; Basstrakov et al., 2007; Cherry et al., 2018). This K-CO₂-Ca-rich character is different to the typically Ca-Na-rich compositions of alteration minerals in and around most magnetite-rich IOA deposits such as those in the Kiruna district, Middle-Lower Yangtze Belt, Chilean Iron Belt, southeast Missouri (USA) and the Bafq district of Iran (Fig. 5; e.g. Oyarzun et al., 2003; Daliran et al., 2010; Zhou et al., 2013; Day et al., 2016; Martinsson et al., 2016; Bonyadi & Sadeghi, 2020). Nevertheless, potassic alteration is present in some peripheral and/or upper alteration zones of some IOA deposits, where it is generally represented by K-feldspar accompanied by hematite (e.g. Kiruna district; southeast Missouri, Day et al., 2016) or by phlogopite ± K-feldspar (e.g. Middle-Lower Yangtze Belt, China, Zhou et al., 2013). Neither of these assemblages have been reported in the IOCG and related deposits considered in the present review of 10 metallogenic provinces globally.

In other orogenic IOCG provinces with paragenetically early magnetite-rich alteration, apatite is either absent/not reported (Guelb Moghrein, Tennant Creek, Cloncurry, Khetri) or is only rarely and locally abundant with magnetite alteration (e.g. Sequeirinho orebody of Sossego deposit, Carajás province, Monteiro et al., 2008). Biotite and carbonate commonly accompany the early magnetite-rich alteration in many orogenic IOCG provinces, but these minerals are rarely present in significant modal amounts in the major IOA deposits in the Kiruna, southeast Missouri, Bafq, Middle-Lower Yangtze Belt and the Chilean Iron Belt IOA provinces. A further example of large hydrothermal magnetite bodies in orogenic IOCG provinces is the Lightning Creek sill complex in the Cloncurry district. Here, the albite-magnetite-quartz ± diopside mineralogy and spherulitic textures of the magnetite-rich bodies within the monzonodioritic intrusion (Perring et al., 2000) are different to the variably apatite-amphibole-albite ± K-feldspar ± pyrite-bearing mineralogy and massive to pegmatoidal textures that are typical of magnetite and/or hematite-rich Kiruna type IOA deposits.

Except for the Kiruna province and Chilean Iron Belt, other major IOA provinces including southeast Missouri, Bafq, and the Middle-Lower Yangtze Belt are not known to contain significant IOCG deposits of the types described herein (ogenic, post-ogenic and arc-hosted) but in some cases host porphyry Cu (-Au) and/or intrusion-related skarn Fe

and/or Cu and/or Au deposits (e.g. Middle-Lower Yangtze Belt, Zhou et al., 2013; Sun et al., 2018). The Boss Cu deposit is the only known significant Cu resource in the southeast Missouri IOA district (40 Mt @ 0.83% Cu), which has been described as an IOCG deposit and lacks significant apatite with the early-stage Fe-oxides (Day et al., 2016). Iron and Cu sulfides overprinted the Fe-oxides and have high $\delta^{34}\text{S}$ values indicating a sulfur source likely external to the spatially associated igneous rocks, possibly related to input of basinal brines (Johnson et al., 2016). Thus it seems likely that in this rare case of significant Cu mineralisation in an IOA province (other than Kiruna and the Chilean Iron Belt, noted above), the late introduction of Cu was not directly related to the formation of the host Fe-oxide-rich body, which is similar to other IOA deposits in the district that are generally considered to be of magmatic-hydrothermal origin (e.g. Johnson et al., 2016).

In summary, available geological and geochronological information strongly points to different timing, tectonic settings, hydrothermal evolution and probably origins of formation of the orogenic and post-orogenic IOCG deposits compared to IOA deposits. The most productive settings for orogenic and post-orogenic IOCG mineralisation appear to be those where inversion of (extended) continental margin basins occurred inboard of prior magmatic arcs, coincident with syn- to post-orogenic magmatism. In contrast, the settings of most large IOA deposits were continental margin magmatic arcs undergoing extension/transtension. Although this same broad setting was shared by the arc-hosted IOCG deposits in the Andes, available data indicate that the major IOA deposits formed >10–15 million years earlier than the IOCG deposits, and hence a direct genetic association of the two deposit types within the same hydrothermal systems is difficult to reconcile. This does not rule out the possibility of IOCG mineralisation overprinting IOA deposits, however.

6.2. Classification of IOCG and related ISCG deposits

The results of the present review of geological and tectonic settings, alteration-mineralisation mineralogy and ore geochemistry of IOCG and related deposits in CGI mineral systems are integrated within the classification scheme shown simplified in Figs. 13 and 14, and in detail in Table 2. A broader classification scheme including other types of

hydrothermal Cu ± Au and/or Fe deposits is presented in Table 3. Whereas there are some similarities between this scheme and the previous classifications of Hitzman et al. (1992), Hitzman (2000), Williams et al. (2005), Williams (2010), Groves et al. (2010) and Barton (2013) there are some significant differences, as follows.

First, this classification distinguishes three tectonic settings: orogenic, post-orogenic and arc-hosted, which only partly correlate with any previous proposals of settings. The *syn-tectonic*, orogenic, settings of many of the IOCG and related deposits have been especially under-emphasised previously, with far more focus on ‘anorogenic’ settings. In the present scheme none of the proposed three settings are ‘anorogenic’; instead a post-orogenic extensional setting is proposed that is intimately linked to the preceding orogenic processes in the same terranes.

Second, this scheme distinguishes IOCG and related ISCG deposits from porphyry Cu (-Au), skarn Fe-Cu-Au, and IOA deposits, although it is recognised that some features of the geology, mineralogy and geochemistry may be shared between these deposit types. In particular, several of the previous classifications consider IOA deposits as ‘end-members’ within a broad family of iron oxide-associated deposits, whereas it is proposed herein that IOA deposits are of fundamentally different origin to the orogenic and post-orogenic IOCG deposits. However, they may be related to the arc-hosted Andean-type IOCG deposits in a way that remains poorly understood.

Finally, mineralogical and geochemical subtypes of the IOCG and related ISCG deposits occurring in particular geotectonic settings are proposed in the new classification scheme – relationships that have been largely unrecognised previously. For example deposits of the IOCG-Co subtype are characterised by correlations between reduced ore-related hydrothermal mineral assemblages and elevated levels of Co, Ni, Bi, Se and/or Te (and low U and REE), and occur specifically within the orogenic tectonic setting (Fig. 13). Whereas the new scheme has some similarities with the mineralogy- and metal-based classification of Williams (2010) a greater focus on redox, geochemistry of minor elements, and geological setting is proposed herein. Williams (2010) included iron oxide Cu-Au ± U (IOCG) deposits within a group of ‘closely affiliated deposits’, along with ‘low Fe-oxide Cu-Au’, ‘Fe oxide-U (low Cu)’ and ‘Co-As ± Fe-oxide ± Au (low Cu)’. Here, emphasis is placed on the IOCG and ISCG members of this family and on their membership of the newly-named CGI mineral system, while not dismissing the possible inclusion of other members of the Williams (2010) family of ‘closely affiliated deposits’.

7. Summary and conclusions

Ten of the world’s most important metallogenic provinces hosting IOCG and other ore deposits have been reviewed in the present contribution, including the geochronology, geological and tectonothermal evolution, alteration-mineralisation parageneses and zoning, and ore geochemistry. Key conclusions are as follows.

- (1) IOCG deposits form the major part of a broader family of deposits within Cu-Au-Fe or CGI mineral systems that also includes iron sulfide Cu-Au (ISCG) deposits with little or no iron oxides.
- (2) CGI mineral systems occur in three distinct tectonic settings, two of which are related to orogenic processes, and host orogenic and post-orogenic IOCG and related ISCG deposits. In the third, arc-hosted Andean-type, setting the IOCG deposits formed during extension/transtension of continental margin magmatic arcs.
- (3) A common theme that links the orogenic and post-orogenic settings is a tectonic switch from compression to extension, during which the development of the CGI mineral systems occurred.
- (4) Metallogenic provinces with IOCG and related deposits in all three tectonic settings are characterised by the coincidence in space and time between pre-IOCG sedimentary ± volcanic basins and *syn*-IOCG intrusive ± volcanic magmatism, although the

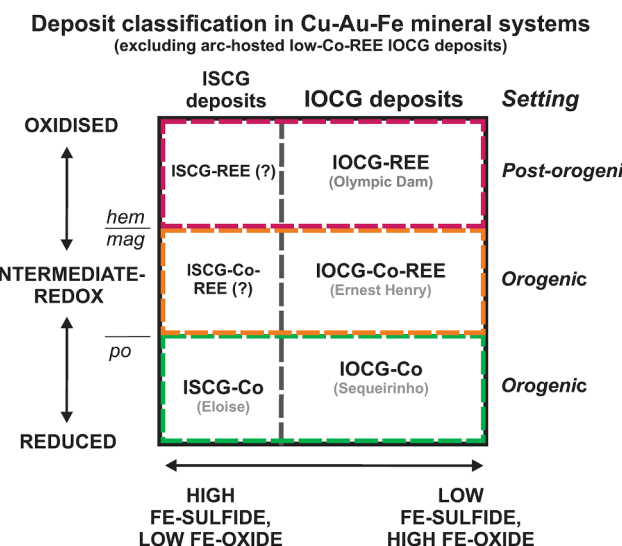


Fig. 14. Classification scheme with redox and sulfide/oxide ratio axes for subtypes of deposits in CGI mineral systems including IOCG and ISCG deposits, with type examples (Olympic Dam, Ernest Henry, Sequeirinho ore body of the Sossego deposit). The boundary between IOCG and ISCG deposits is nominally set where the abundances (by volume) of oxides and Fe sulfides are equal. Some ISCG deposit types have not been documented but are predicted to exist (shown with '?').

Table 2

Classification and key features of orogenic, post-orogenic and arc-hosted IOCG and related ISCG deposits, compared with IOA deposits.

Deposit type	Deposit redox or other subtype	Timing, tectonic setting, deformation	Ore geochem. (subtype)	Dominant Fe ox & Fe-Cu sulfides	Alteration/metamorphism	Example deposits
Orogenic IOCG & ISCG	Reduced to intermediate-redox IOCG to ISCG spectrum	ogenetic, <i>syn-tectonic</i> , brittle-ductile	Cu, Au, Co, Ni; some have minor Zn, Pb, Bi, Se, Te, As <i>(IOCG-Co) (ISCG-Co)</i>	mag, po, py, ccp	early Na ± Ca (ab, scp, act); mid Ca-Fe (amph, mag, di, grt, aln, ap); late Fe-K (mag, bt, Kfs) with Cu-Au & volatiles (CO ₂ , P, B)	<u>IOCG</u> : Osborne, West Peko, some Carajás (Sequeir.), some Kangdian (Dahongshan, Lala), some Khetri, some GBMZ (NICO), <u>ISCG</u> : Guelb Moghrein, Eloise, Greenmount, Mt Dore, parts Mt Elliott
	Intermediate-redox to oxidised IOCG to ISCG spectrum	ogenetic, <i>syn-tectonic</i> , brittle-ductile	Cu, Au with (Co, Ni) or (Mo, F, REE, U, Ba) or both (EH, Monakoff, E1, Salobo) <i>(IOCG-Co-REE)</i>	mag, hem, py, ccp, bn	early Na ± Ca (ab, scp, act); mid Ca-Fe (amp, mt, dp, gt, all, ap); late Fe-K (mt, bt, Kfs) with Cu-Au & volatiles (CO ₂ , P, F, B, SO ₄) (except TCK)	<u>IOCG</u> : Ernest Henry; E1, Monakoff (late F, Ba, Cu?); SWAN?, Sin Quyen?, Salobo, Rakkurijarvi; some Tennant Creek; <u>ISCG</u> : some Kiruna CuAu; some Khetri CuAu (?SSC); Hongnipo? (Kangdian)
	Oxidised IOCG to ISCG spectrum	ogenetic, <i>syn-tectonic</i> , brittle-ductile to brittle; some may be late-orogenic or post-orogenic(?)	Cu, Au, REE, U, F, Ba <i>(some IOCG-Co-REE)</i>	hem, py, ccp, bn, cct	late Fe-K (hem, ms, chl) with Cu-Au & volatiles (CO ₂ , P, F, SO ₄)	<u>IOCG</u> : Starra (hm-Ba-F-Au-bn zones); Gecko K44 upper, & Eldorado (but lack Co, REE, U, F or Ba)
Post-orogenic Cu-Au-Fe (REE)	Intermediate-redox	post-orogenic, switch from compressional to extensional, brittle deformation	Minor P (ap), ± REE, ± Cu	mag, py, minor CCP	early Na ± Ca (ab, scp, act, di); mid Fe-K-Na-Ca (mag, bt, ab, act); or mid Fe-K-Ca (mag, Kfs, act, ap, cb, qz)	<u>IOCG alteration</u> : Acropolis, Titan, Murdie; <u>IOCG deposits</u> : Kalkaroo, Wallaroo
	Oxidised IOCG to ISCG spectrum	post-orogenic, switch from compressional to extensional, brittle deformation	Cu, Au, Ag, REE, U, F, Ba, ± Mo <i>(IOCG-REE)</i>	hem, py, CCP, bn, CCT; minor or no mag	mid Fe (-P-CO ₂) (mag, sd, ap); late Fe-volatiles (-K) (hem, ser, chl, brt, fl, cb) with Cu-Au-REE-U	<u>IOCG</u> : Olympic Dam, Prominent Hill, Wirrda Well, Carrapateena, Sue Dianne?, North Portia <u>ISCG or intrusion-related</u> : Moonta?, White Dam Au-Mo
Magmatic arc- or back-arc-hosted IOCG	Reduced to intermediate-redox IOCG	Syn-subduction; extension before inversion, mostly brittle deformation	Cu, minor Au, (generally low P, Co, Ni, REE, U, F, Ba)	mag, po, py, CCP	early Na (ab); mid Fe-K (mag, bt, Kfs); late Ca-Fe-K (mag, amp, bt, Kfs) with Cu (-Au)	<u>IOCG</u> : Candelaria, Raíl-Condestable?, Marcona?
	Intermediate-redox to oxidised IOCG to ISCG spectrum	Syn-subduction; extension before inversion, mostly brittle deformation	Cu, minor Au, Ag, rare REE, U (generally low P, Co, Ni, F, Ba)	hem, mag, py, CCP, bn, CCT	early-mid Fe (-Na, -K, -Ca) (mag, ab, Kfs, amp); late Fe (-CO ₂) (hem, cb, chl) with Cu (-Au)	<u>IOCG</u> : Mantoverde, Mina Justa? <u>ISCG?</u> : some Chilean manto Cu-Ag ± Fe (Punta del Cobre district, Mantos Blancos)
	Oxidised Cu (-Au) ± iron oxides	Syn-subduction, ?pre- or ? early-orogenic	Cu, Ag (low Au, REE, U)	CCP, bn, CCT, PY ± minor hem	??	<u>ISCG?</u> : some Chilean mantos (El Soldado)
Arc- or back-arc-hosted IOA	Fe-Ca-P	Syn-subduction, extensional / transtensional, rifted arc or back-arc	Ca, P, ± LREE, ± F, ± S	mag ± minor py, anh, (rare CCP, no Au)	Fe-Ca-P (mag, ap, amp, cpx)	Kiruna, MLYB, CIB (ER, LC, EA, EC, EL), SEM (PR, LPK), Bafq
	Fe-K	Syn-subduction, extensional / transtensional, rifted arc or back-arc	K, (low-P) ± S, ± F, ± LREE, Ba, B, ± minor Cu (lack U, Mo)	mag, hem ± minor py, anh (rare to minor Cu, no Au)	Fe-K (mag, hem, Kfs)	SEM (Boss; PR late), IM (late)) Andes (?MV (early), Marcona)

Mineral abbreviations: ab – albite, act – actinolite, aln – allanite, amp – amphibole, anh – anhydrite, ap – apatite, Au – gold, bn – bornite, brt – barite, bt – biotite, cb – carbonate, cct – chalcocite, chl – chlorite, CCP – chalcopyrite, cpx – clinopyroxene, di – diopside, fl – fluorite, hem – hematite, Kfs – K-feldspar, mag – magnetite, ms – muscovite, po – pyrrhotite, py – pyrite, qz – quartz, REE – REE-rich minerals (carbonate-rich and/or P-rich including monazite and alumino-phosphate-sulfide REE minerals), scp – scapolite, ser – sericite, U – uranium-rich minerals (e.g. uraninite/pitchblende), sd – siderite.

Abbreviations: for IOA districts: CIB, Chilean Iron Belt, EA, El Algarrobo, EC El Colorado, EL El Laco, ER El Romeral, IM Iron Mountain, LC Los Colorados, LPK Lower Pilot Knob, MLYB Middle-Lower Yangtze Belt, MV Mantoverde, PR Pea Ridge, SEM southeast Missouri.

compositions of the igneous rocks and relationships to deposits differs between the orogenic, post-orogenic and arc-hosted settings. As argued in the companion paper (Skirrow, in prep.), the variable inputs of basin-derived and magma-derived fluids and ore components (metals, sulfur, etc) is considered to be the main link between deposits in CGI mineral systems but also the principal cause of the observed variations in mineralogy and geochemistry.

(5) In all three tectonic settings the IOCG and related deposits share several features of their alteration-mineralisation, including:

- A metal association of Cu and Au with elevated Fe, whether as low-Ti Fe oxides or Fe sulfides and/or Fe-rich silicates.
- Hydrothermal alteration that includes paragenetically early Na- ± Ca-rich minerals (generally in regional-scale alteration zones but also proximal at some deposits) followed by combinations of Fe-, Ca- and K-rich minerals that accompany or precede Cu-Au mineralisation together with volatile-bearing minerals such as carbonate (CO₂), apatite (P), fluorite (F), barite (SO₄) and tourmaline (B); however, deposits in the arc-hosted settings have less abundant volatile-rich minerals.

Table 3

Classification scheme of selected Cu- and/or Fe-rich deposit classes and types, and the place of IOCG and ISCG deposits (highlighted in yellow). Genetic class interpretations of the 'hybrid' deposit types are based on discussions in the accompanying contribution (Skirrow, in prep.); others after Meinert et al. (2005), Groves et al. (2010), Sillitoe (2003, 2010). Abbreviations: fl – fluorite, IOA – iron oxide-apatite, IR – intrusion-related, mag – magnetite, MH – magmatic-hydrothermal, MLYB – Middle-Lower Yangtze Block, SSC – sediment-hosted stratiform Cu.

Genetic class	Cu and/or Fe deposit types	Timing/tectonic setting	Deposit subtypes	Example deposits and provinces
Intrusion-related magmatic-hydrothermal (IR-MH)	Porphyry	Syn-subduction & post-collisional	Porphyry Cu Porphyry Cu-Au Porphyry Cu-Mo	Many
	Skarn	Syn-subduction	Skarn Fe, Fe-Cu Skarn Cu Skarn Au	Many Marcona Fe (-Cu)?
	Alkaline-igneous /carbonatite associated	anorogenic	Carbonatite-related Cu, REE; Alkaline-igneous-related Fe, REE, U, F	Palabora Cu Bayan Obo REE Fe Vergenoeg fl-mag Kiruna province SE Missouri province Adirondacks province Bafq province MLYB province
Hybrid: mainly IR-MH, minor basinal input	IOA Fe	Syn-subduction		Candelaria Mantoverde Raúl-Condestable Mina Justa Many – see *
Hybrid: mainly IR-MH, minor basinal input	Arc-hosted Andean-type IOCG	Syn-subduction, pre- to early-orogenic	Reduced, intermediate-redox & oxidised IOCG & ISCG	Olympic Dam Prominent Hill Carrapateena Starra Eldorado Sue Dianne?
Hybrid: MH and basinal inputs	Orogenic IOCG & ISCG	Syn-late-orogenic	Reduced IOCG-Co, intermediate-redox IOCG-Co-REE & oxidised IOCG-Co-REE	Mantos Blancos El Soldado Mt Isa Cu Zambian & DR Congo Cu belt Kupferschiefer
	Post-orogenic IOCG & ISCG	Post-orogenic	Intermediate-redox IOCG-REE to oxidised IOCG-REE	
Hybrid: basinal with minor MH inputs	Manto Cu (-Ag)	Pre- or early-orogenic?		
Basinal	Mt Isa Cu type SSC & redbed Cu	Orogenic/syn-tectonic Diagenetic		

*Obsorne, Eloise, Guelb Moghrein, NICO, West Peko, Warrego, Dahongshan, Lala, Sin Quyen, Sequeirinho, Salobo, Igarapé Bahia, SWAN/Mt Elliott, Ernest Henry, E1, Monakoff, White Devil, Juno, Gecko, Starra.

- A paucity of Mg-rich hydrothermal minerals and hydrothermal quartz in the IOCG members of IOCG mineral systems, but minor to abundant quartz in many of the Fe-oxide-poor ISCG members.
 - A wide range of relative redox conditions of formation of ore-associated hydrothermal minerals, from reduced (e.g. pyrrhotite \pm Fe-silicate-bearing) through intermediate-redox (e.g. magnetite-pyrite-bearing) to oxidised (e.g. hematite \pm pyrite \pm sulfate minerals). The Cu sulfide mineralogy varies systematically from chalcopyrite \pm rare bornite in the relatively reduced deposits to chalcocite and bornite in the most oxidised deposits or zones within deposits.
 - IOCG and related ISCG deposits are enriched in distinctive suites of minor elements (Co, Ni, Bi, Se, Te, and/or REE, U, F, Ba) compared to well known magmatic-hydrothermal deposits such as porphyry Cu (-Au), skarn Fe and Cu and granite-related greisen deposits; however, IOCG deposits in arc-hosted settings have lower levels of Co, Ni, Bi, Se, Te, REE, U, F, and Ba than IOCG deposits in orogenic and post-orogenic settings.
 - Among the orogenic and post-orogenic IOCG and related ISCG deposits a correlation has been identified between (a) ore geochemical variations in the ratio $(\text{Co} + \text{Ni} + 10^*\text{Bi} + 10^*\text{Se} + 50^*\text{Te})/(\text{U} + \text{La})$ with element values in ppm (termed the IOCG discriminator), (b) the alteration-mineralisation mineralogy, and (c) the geological-tectonic settings.
 - (6) IOCG and related deposits in each of the three geotectonic settings have distinctive structural, mineralogical and geochemical characteristics, as follows.
- The orogenic setting hosts IOCG and related ISCG deposits that formed during brittle-ductile to brittle deformation in mid-shallow-crustal environments, at conditions compatible with medium to low grade metamorphism. These deposits have alteration-mineralisation mineral assemblages indicating generally reduced to intermediate-redox hydrothermal conditions during Cu-Au ore formation. Sodic \pm Ca regional alteration, present in all provinces except possibly Tennant Creek, is typically overprinted by proximal alteration assemblages representing Ca-Fe metasomatism and then by Fe-K alteration-metasomatism that accompanies the main Cu-Au mineralisation along with volatile-rich minerals. The reduced to intermediate-redox members of the redox spectrum of orogenic deposits form the IOCG-Co and ISCG-Co geochemical subtype. Magnetite is the dominant Fe-oxide where present, but some of the reduced deposits lack significant Fe-oxide and are dominated by Fe-sulfides (ISCG deposits). IOCG-Co-REE ores with intermediate-redox assemblages (magnetite, pyrite) constitute a separate subtype of orogenic deposits (e.g. Ernest Henry).
 - The post-orogenic setting of IOCG mineral systems is apparently rare but hosts the world's largest IOCG deposit at Olympic Dam in the Gawler Craton. This setting represents the full evolution of tectonic switching from compression to extension. The Curnamona Province, Great Bear magmatic zone and Tennant Creek provinces may record similar switches in tectonic regime. Shallow-crustal to near-surface (sub-volcanic to volcanic) environments of ore formation are indicated in the Olympic Cu-Au province of the Gawler Craton. Whereas highly oxidised (hematite, barite, chalcocite, bornite) and low-

pH (sericite ± pyrophyllite) conditions are evident in all of the major deposits (Olympic Dam, Prominent Hill, Carrapateena), some deposits preserve evidence of earlier and generally deeper intermediate-redox (magnetite, pyrite, siderite, chalcopyrite) chemical environments. IOCG ores in the Gawler post-orogenic setting have some of the lowest values of the IOCG discriminator ($\text{Co} + \text{Ni} + 10^*\text{Bi} + 10^*\text{Se} + 50^*\text{Te}/(\text{U} + \text{La})$), and also contain abundant volatile-rich phases such as fluorite (F), carbonate (CO_2), barite (SO_4), and apatite (P) accompanying the Cu-Au-U-REE mineralisation.

- The third, continental margin magmatic arc-hosted, geological and tectonic setting of IOCG deposits and CGI mineral systems is mainly represented by Cretaceous deposits in the Chilean and Peruvian Andes, although hybrid settings involving Paleo-proterozoic continental margin magmatic arc settings may be present in the Kiruna province and Great Bear magmatic zone. Whereas the arc-hosted IOCG deposits share some features of IOCG deposits in orogenic and post-orogenic settings, the former tend to lack abundant volatile-rich minerals coeval with the Cu-Au mineralisation, and have low $\text{Co} + \text{Ni} + \text{Bi} + \text{Se} + \text{Te} + \text{REE} + \text{U}$ values that resemble those of most porphyry and skarn deposits. They also show a sequence of hydrothermal assemblages that may differ from those of the orogenic and post-orogenic IOCG deposits. Moreover, their close spatial and temporal association with intermediate-composition intrusions and pre- to early-orogenic timing contrasts with such relationships and igneous compositions in the orogenic and post-orogenic IOCG provinces. The arc settings also include pre-IOCG IOA, and (small) porphyry Cu (-Au) and skarn deposits of roughly similar age to the IOCG deposits. It is concluded that

the arc-hosted IOCG deposits represent a sub-group of the IOCG family with different origins to the orogenic and post-orogenic IOCG deposits, and which appear to have a greater affinity with calc-alkaline arc-related magmatic-hydrothermal ore deposits that are present in the same metallogenic provinces.

Declaration of Competing Interest

The authors declare that they have no known competing financial interests or personal relationships that could have appeared to influence the work reported in this paper.

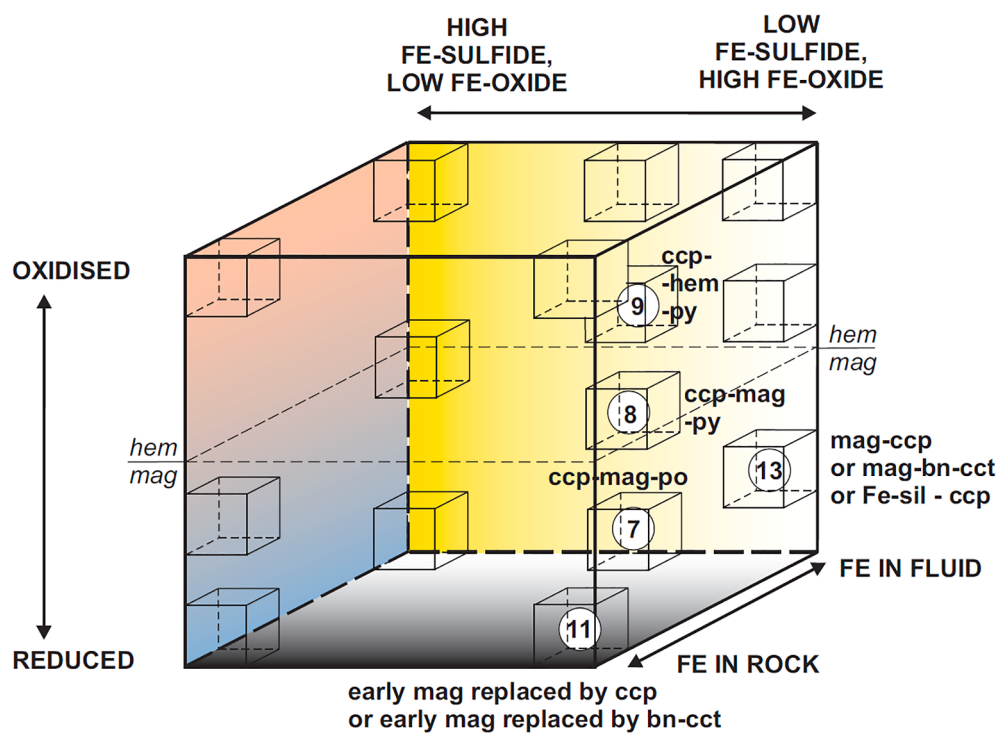
Acknowledgements

This work draws upon discussions with, and support from, many colleagues over the years. In particular the following people are thanked: Evgeniy Bastrakov, David Huston, Karol Czarnota, David Champion, Michael Doublier, Richard Blewett, Anthony Schofield, Simon van der Wielen (all Geoscience Australia) and also John Walshe, Sue Daly, Anthony Reid, Colin Conor, Martin Fairclough, Karin Barovich and Ken Cross. Additionally, David Huston and Evgeniy Bastrakov are thanked for helpful reviews of an early version of the manuscript. Carl Brauhart and Stefan Hagemann are acknowledged for the use of the OSNACA open-source ore geochemical data set. Journal reviews by Xinfu Zhou and an anonymous reviewer improved the manuscript, for which they are thanked. Editorial handling by Huayong Chen and David Lentz is gratefully acknowledged. This study is a contribution towards the Australian Government's Exploring for the Future (EFTF) program. Published with the permission of the CEO, Geoscience Australia.

Appendix A. References for Figure 4, paragenetic sequences

- Carajás province, Brazil** (Cristalino, Igarapé-Bahia, Salobo, Bacaba, Sossego-Sequeirinho deposits): Monteiro et al. (2008); Moreto et al. (2011); de Melo et al. (2017); de Melo et al. (2019); Craveiro et al. (2020); Pestilho et al. (2020)
- Cloncurry province, Australia** (Ernest Henry, E1, Starra, Eloise, Osborne deposits): Rotherham (1997); Baker & Laing (1998); Baker et al. (2001); Mark et al. (2006); Fisher & Kendrick (2008); Williams et al. (2015); Case (2016); Cave et al. (2018)
- Sin Quyen deposit, Vietnam** (possible extension of Kangdian province): McLean (2002); Li & Zhou (2018)
- Kangdian province, China** (Dahongshan, Yinachang, Lala deposits): Chen & Zhou (2012); Li et al. (2015); Zhao et al. (2017)
- Gawler Craton and Curnamona Province, Australia** (Olympic Dam, Prominent Hill, Hillside, Wallaroo, North Portia deposits): Oreskes & Einaudi (1990); Reeve et al. (1990); Conor (1995); Haynes et al. (1995); Teale & Fanning (2000a); Skirrow et al. (2002); Conor et al. (2010); Ehrig et al. (2012); Ismail et al. (2014); Schlegel & Heinrich (2015)
- Tennant Creek province, Australia** (Eldorado, Juno, West Peko deposits): Large (1975); Skirrow & Walshe (2002)
- Guelb Moghrein deposit, Mauritania**: Kolb et al. (2010); Kirschbaum & Hitzman (2016); Kolb & Petrov (2016)
- Great Bear magmatic zone, Canada** (NICO deposit): Goad et al. (2000); Acosta-Góngora et al. (2015)
- Andes province, Chile and Peru** (Panulcillo, Mantoverde, Mina Justa, Candelaria, Raúl-Condestable deposits): Hopper & Correa (2000); Marschik & Fontboté (2001); de Haller et al. (2006); Benavides et al. (2007); Chen et al. (2010); Rieger et al. (2010); del Real et al. (2018)

Appendix B. Fe-oxide and Fe-Cu sulfide mineralogical characteristics of IOCG and related ISCG deposits, listed by IOCG province

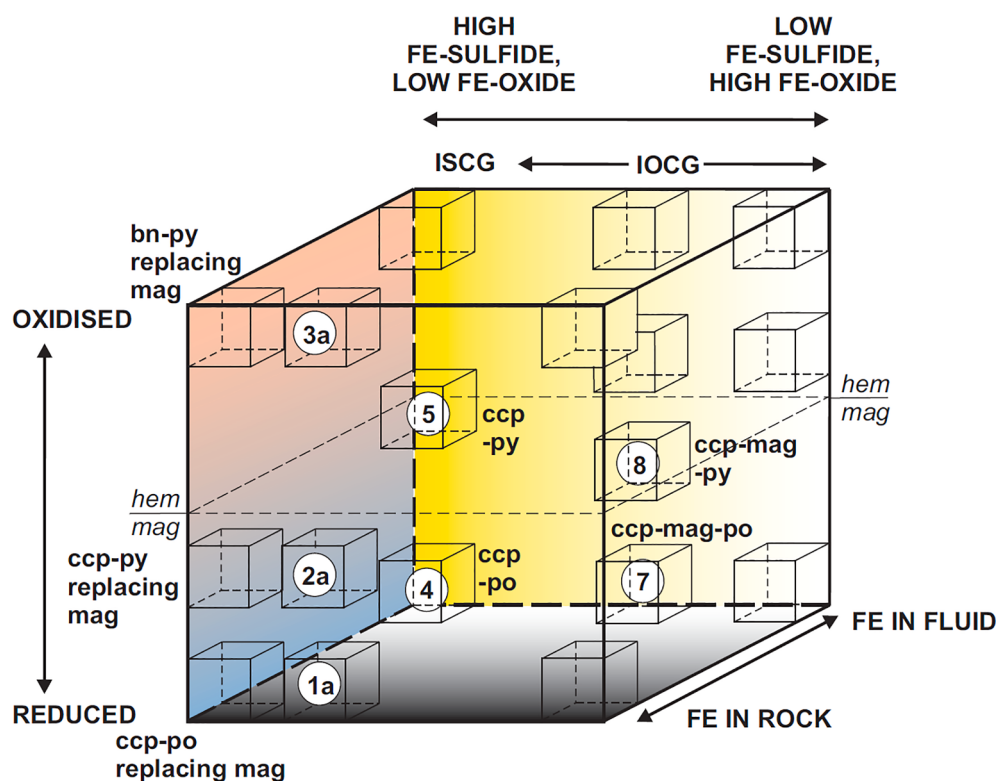


Carajás Neoarchean IOCG deposits

- (7) Sossego-Sequerinho Cu-Au, Castanha Cu-Au (Co, Ni)
- (8) Sossego-Sequerinho Cu-Au, Cristalino (Cu-Au), Borrachudo Cu-Au (Co, Ni, REE), Castanha Cu-Au (Co, Ni)
- (9) Cristalino Cu-Au
- (11) Salobo Cu-Au (Co, REE) (early BIF mag?)
- (13) Salobo Cu-Au (Co, REE) (mag-bn-ccp-cct-fl), Bacaba Cu-Au (mag-ccp), Igarape Bahia Cu-Au (mag-bn-ccp-cct), Igarape Cinzento (GT-46) (mag-ccp-bn)

References for Carajás province:

Monteiro et al. (2008); Moreto et al. (2011); de Melo et al. (2017); de Freitas Toledo et al. (2019); de Melo et al. (2019); Craveiro et al. (2020); Pestilho et al. (2020); Previato et al. (2020)

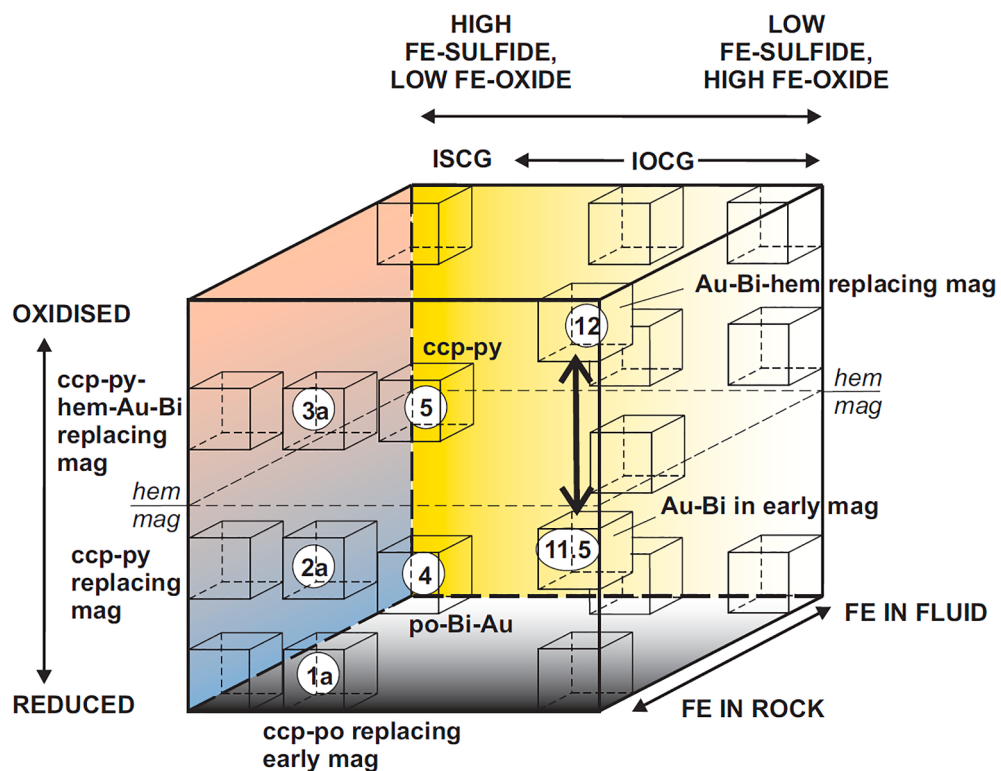


Cloncurry IOCG and ISCG deposits

- 1a Osborne Cu-Au (Co)
- 2a Osborne Cu-Au (Co), Starra Cu-Au (Co) early mag-ccp stage
- 3a Starra late Au-Cu stage
- 4 Eloise Cu-Au (Co), Mt Elliott Cu-Au (east)
- 5 Greenmount Cu-Au (Co)
- 7 Monakoff Cu-Au (Co, REE) early stage, E1N Cu-Au (REE) early stage
- 8 Ernest Henry Cu-Au (Co, REE, brt, fl), Mt Elliott (west) & SWAN Cu-Au (REE), E1N Cu-Au (REE, late brt, fl), Monakoff Cu-Au (REE, late brt, fl)

References for Cloncurry province:

Rotherham (1997); Baker & Laing (1998); Williams & Skirrow (2000); Baker et al. (2001); Mark et al. (2006); Fisher & Kendrick (2008); Brown & Porter (2010); Williams et al. (2015); Case (2016); Cave et al. (2018)

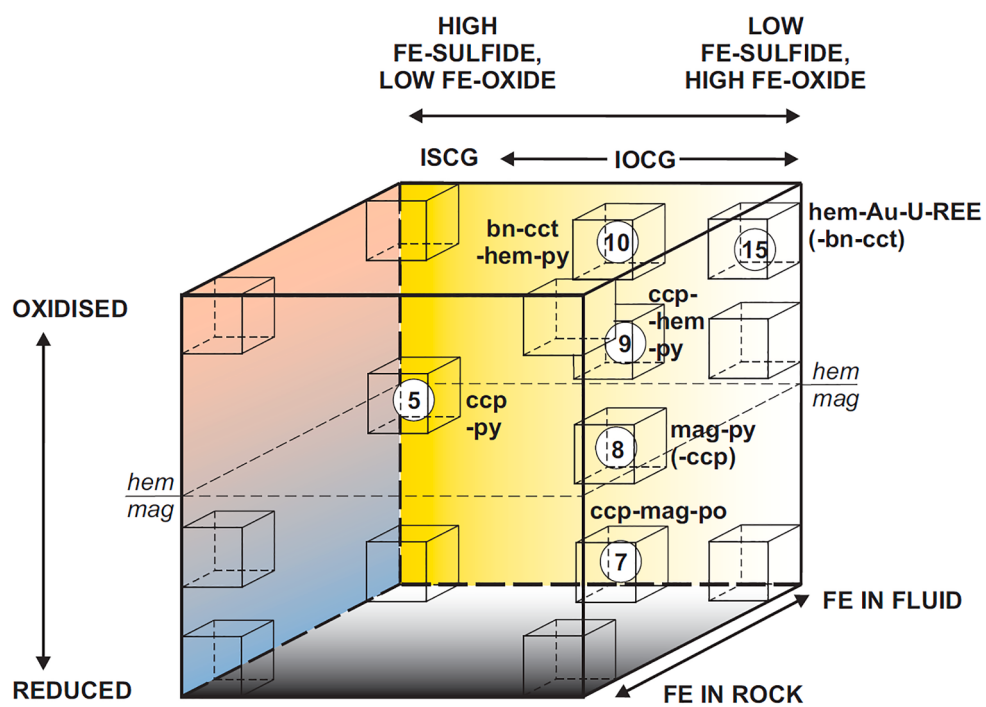


Tennant Creek Au-Cu-Bi IOCG & ISCG deposits

- 1a West Peko Cu-Au-Bi, Warrego Cu-Au-Bi (uncommon po)
- 2a Warrego Cu-Au-Bi, Gecko K44 Cu-Au-Bi (lower zone), Peko Cu-Au-Bi, Orlando Cu-Au-Bi
- 3a Gecko K44 Cu-Au-Bi (upper zoe)
- 4 West Peko shear-hosted Au-Bi outside ironstone
- 5 Orlando East, Gecko (Monitor, Goanna), Bishop Creek Cu-Au-Bi
- 12 Eldorado, Nobles Nob (?) Au (-Bi)
- 11.5 ↔ 12 White Devil, Juno, Argo, TC8, Chariot mag-Au-Bi (variable hem, py, Cu)

References for Tennant Creek goldfield:

[Large \(1975\); Wedekind et al. \(1989\); Skirrow \(1993, 2000\); Huston et al. \(1993\); Skirrow & Walshe \(2002\)](#)

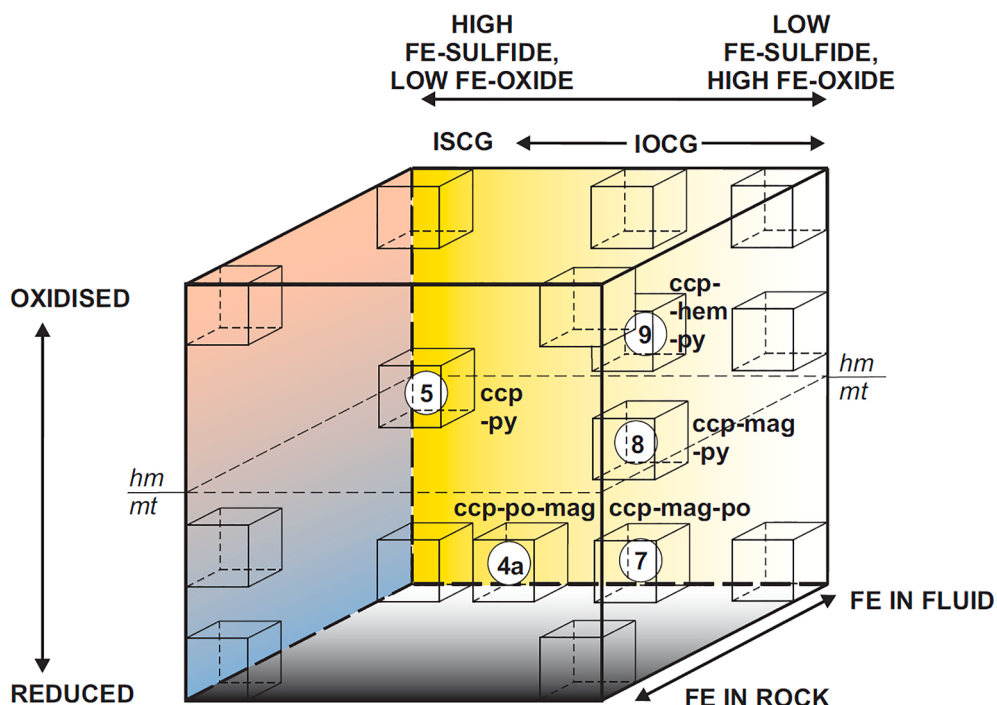


Gawler Craton IOCG and ISCG deposits

- 15 Olympic Dam, Prominent Hill, Carrapateena hem-qtz zones (upper / inner zones)
- 10 Olympic Dam, Prominent Hill, Carrapateena Cu-Au ore zones (upper / inner zones)
- 9 Olympic Dam, Prominent Hill, Carrapateena ore zones (lower / outer zones)
- 8 Olympic Dam, Prominent Hill and barren/low grade prospects (early mag-py ± CCP ± sid ± apatite)
- 7 Joes Dam, Manxman Cu-Au prospects
- 5 Moonta Cu-Au in qz-Kfs veins (ISCG or other deposit type?)

References for Gawler Craton – Olympic Cu-Au province:

Oreskes & Einaudi (1990); Reeve et al. (1990); Conor (1995); Haynes et al. (1995); Skirrow et al. (2002); Conor et al. (2010); Ehrig et al. (2012); Ismail et al. (2014); Schlegel & Heinrich (2015)



Other IOCG & ISCG deposits (Andean in bold)

- ⑦ Dahongshan Cu (-Au), Lala Cu (-Au), Sin Quyen Cu (-Au),
NICO early stage Au-Co-Bi-As, **Candelaria Cu-Au**, Raul-Condestable Cu-Au
- ⑧ Dahongshan Cu (-Au), Lala Cu (-Au), Yinachang Cu (-Au), Sin Quyen Cu (-Au),
Candelaria Cu-Au, Raul-Condestable Cu-Au, Mina Justa Cu-Au
- ⑨ Sue Dianne Cu-Au, NICO Au-Co-Bi-As (late Cu stage), **Mantoverde Cu-Au (REE)**,
Mina Justa Cu-Au
- ⑤ Hongnipo Cu (-Au) (Kangdian),
?manto Cu-Ag deposits (**Chile**), ?some 'SSC' Cu (-Au) deposits (Khetri)
- ④a Guelb Moghrein Cu-Au (Co, Ni, Bi)

References for Chilean and Peruvian Andes province:

Hopper & Correa (2000); Marschik & Fontboté (2001); Boric et al. (2002); Maksaev & Zentilli (2002); de Haller et al. (2006); Ramírez et al. (2006); Benavides et al. (2007); Chen et al. (2010); Rieger et al. (2010); del Real et al. (2018)

References for Kangdian province: Zhao & Zhou (2011); Chen & Zhou (2012); Zhou et al. (2014); Li et al. (2015); Zhao et al. (2017); Lin et al. (2020)

References for Great Bear magmatic zone: Goad et al. (2000); Acosta-Góngora et al. (2015)

References for Guelb Moghrein deposit: Kolb et al. (2010); Kirschbaum & Hitzman (2016); Kolb & Petrov (2016)

Appendix C. Summary of deposits extracted from the OSNACA global ore geochemical data base (Brauhart et al., 2017; OSNACA, 2020) and attributed as IOCG deposits. Sub-types assigned in the present study are based on descriptions in OSNACA together with information from published literature for individual deposits, and correspond to variants in the IOCG-ISCG cube (Figs. 7, 8). Data for several additional deposits are sourced as indicated. The number of samples in OSNACA for each deposit (# samples) differs in some cases from the number of samples plotted in the figures in this contribution (# plotted) due to exclusion of samples of host rock; only ore samples have been used in this study

OSNACA and additional ore geochemistry data set									
Deposit name	Country	State	Metal. Prov.	# samples	# plotted	OSNACA class	Sub-type (this study)	Notes possible ISCG?	Source
Kanmantoo	Australia	South Australia	Adelaide Fold Belt	2	2	IOCG	Reduced - low mt		OSNACA
Antas	Brazil	Pará	Carajás	1	1	IOCG	Reduced - variable mt		OSNACA
Sossego	Brazil	Pará	Carajás	3	3	IOCG	Intermed-redox - mt-rich		OSNACA
Barreal Seco	Chile	Atacama	Chilean Iron Belt	3	3	IOCG	Oxidised - hm-rich (Andes)		OSNACA
Candelaria	Chile	Atacama	Chilean Iron Belt	2	2	IOCG	Reduced - variable mt		Marschik & Fontboté (2001)
Carola	Chile	Atacama	Chilean Iron Belt	3	3	IOCG	Intermed-redox - hm-mt or mt-hm-rich		Marschik & Fontboté (2001)
Manto Verde	Chile	Atacama	Chilean Iron Belt	5	5	IOCG	Oxidised - hm-rich (Andes)	Rieger et al. (2010)	
Socabón Rampa	Chile	Atacama	Chilean Iron Belt	2	2	IOCG	Oxidised - hm-rich (Andes)		OSNACA
Artemis	Australia	Queensland	Cloncurry	6	4	IOCG	Reduced - low mt	Zn-Pb-rich	OSNACA
Barbara	Australia	Queensland	Cloncurry	8	6	IOCG	Reduced - low mt		OSNACA
Blackard	Australia	Queensland	Cloncurry	2	1	IOCG	Cu-Au	oxidation & Fe ox unknown	OSNACA
Cameron River	Australia	Queensland	Cloncurry	9	8	IOCG	Reduced - low mt		OSNACA
Canteen	Australia	Queensland	Cloncurry	4	4	IOCG	Reduced - low mt	Fe ox unknown	OSNACA
E1	Australia	Queensland	Cloncurry	10	10	IOCG	Intermed-redox - hm-mt or mt-hm-rich		OSNACA
Elise	Australia	Queensland	Cloncurry	7	7	IOCG	Reduced - variable mt		OSNACA
Ernest Henry	Australia	Queensland	Cloncurry	12	12	IOCG	Intermed-redox - hm-mt or mt-hm-rich		OSNACA
Great Australia	Australia	Queensland	Cloncurry	2	2	IOCG	Cu-Au	Fe ox unknown	OSNACA
Kaiman	Australia	Queensland	Cloncurry	3	3	IOCG	Intermed? Cu-Au	Fe ox unknown	OSNACA
Kulthor	Australia	Queensland	Cloncurry	3	3	IOCG	Reduced - variable mt		OSNACA
Kurilla	Australia	South Australia	Cloncurry	2	2	IOCG	unknown		OSNACA
Little Eva	Australia	Queensland	Cloncurry	2	2	IOCG	Oxidised - hm-rich		OSNACA
Lorena	Australia	Queensland	Cloncurry	1	1	IOCG	Reduced - low mt		OSNACA
Merlin	Australia	Queensland	Cloncurry	4	4	IOCG		no Fe ox, not Cu-Au-Fe (Co, REE) deposit	OSNACA
Monakoff	Australia	Queensland	Cloncurry	7	7	IOCG	Intermed-redox	hybrid?	OSNACA
Mount Colin	Australia	Queensland	Cloncurry	5	3	IOCG	Cu-Au	oxidation and Fe-ox unknown	OSNACA
Mount Elliot	Australia	Queensland	Cloncurry	1	1	IOCG	Intermed-redox - mt-rich		OSNACA
Osborne	Australia	Queensland	Cloncurry	13	12	IOCG	Reduced - variable mt		OSNACA
Rocklands	Australia	Queensland	Cloncurry	3	3	IOCG	Intermed-redox - low Fe-ox		OSNACA
Starra	Australia	Queensland	Cloncurry	6	4	IOCG	Intermed-redox - hm-mt or mt-hm-rich		OSNACA
Swan	Australia	Queensland	Cloncurry	8	8	IOCG	Intermed-redox - mt-rich		OSNACA
Trekeland	Australia	Queensland	Cloncurry	2	1	IOCG	Cu-Au	oxidation and Fe-ox unknown	OSNACA
Olympic Dam	Australia	South Australia	Gawler Craton	6	6	IOCG	Oxidised - hm-rich		OSNACA
Prominent Hill	Australia	South Australia	Gawler Craton	3	3	IOCG	Oxidised - hm-rich		OSNACA
Wheat Hughes	Australia	South Australia	Gawler Craton	2	2	IOCG	Intermed-redox - low Fe-ox		OSNACA
Guelb Moghrein	Mauritania	Inchiri	Guelb Moghrein	2	2	IOCG	Reduced - low mt		OSNACA
Khetri	India	Rajasthan	Khetri	2	2	IOCG	Intermed-redox - mt-rich		OSNACA
Messina	South Africa	Limpopo	Limpopo	3	3	IOCG	unknown	not Cu-Au-Fe (Co, REE) deposit?	OSNACA
Vergenoeg	South Africa	Limpopo	Limpopo	1	1	IOCG		magnetite-fluorite, not Cu-Au-Fe (Co, REE) de	OSNACA
Sin Quyen	Vietnam	Lào Cai	Red River Fault Zone	1	1	IOCG	Intermed-redox	mag rich	OSNACA
Gecko	Australia	Northern Territory	Tennant Creek	2	2	IOCG	Intermed-redox - hm-mt or mt-hm-rich		OSNACA
Warrego	Australia	Northern Territory	Tennant Creek	3	3	IOCG	Intermed-redox - mt-rich		OSNACA
White Devil	Australia	Northern Territory	Tennant Creek	3	3	IOCG	Intermed-redox - mt-rich		OSNACA
Wernecke Mtn	Canada	Yukon	Wernecke	1	1	IOCG	Intermed-redox - low Fe-ox		OSNACA

Appendix D. Supplementary material

Supplementary data to this article can be found online at <https://doi.org/10.1016/j.oregeorev.2021.104569>.

References

- Acosta-Góngora, P., Gleeson, S.A., Samson, I.M., Corriveau, L., Ootes, L., Taylor, B.E., Creaser, R.A., Muehlenbachs, K., 2015. Genesis of the Paleoproterozoic NICO iron oxide-cobalt-gold-bismuth deposit, Northwest Territories, Canada: evidence from isotope geochemistry and fluid inclusions. *Precambr. Res.* 268, 168–193. <https://doi.org/10.1016/j.precamres.2015.06.007>.
- Adshead, N.D., Vougaris, P., Muscio, V.N., 1998. Osborne copper-gold deposit. In: Berkman, D.A., Mackenzie, D.H. (Eds.), *Geology of Australian and Papuan New Guinean Mineral Deposits* (pp. 793–800). Australasian Institute of Mining and Metallurgy, Monograph 14.
- Apukhtina, O.B., Kamenetsky, V.S., Ehrig, K., Kamenetsky, M.B., Maas, R., Thompson, J., McPhie, J., Ciobanu, C.L., Cook, N.J., 2017. Early, deep magnetite-fluorapatite mineralization at the Olympic Dam Cu-U-Au-Ag deposit, South Australia. *Econ. Geol.* 112 (6), 1531–1542. <https://doi.org/10.5382/econgeo.2017.4520>.
- Armistead, S.E., Betts, P.G., Ailleres, L., Armit, R.J., Williams, H.A., 2018. Cu-Au mineralisation in the Curnamona Province, South Australia: a hybrid stratiform genetic model for Mesoproterozoic IOCG systems in Australia. *Ore Geol. Rev.* 94 (September 2017), 104–117. <https://doi.org/10.1016/j.oregeorev.2018.01.024>.
- Baker, T., Laing, W.P., 1998. Eloise Cu-Au deposit, East Mt Isa Block: structural environment and structural controls on ore. *Aust. J. Earth Sci.* 45 (3), 429–444. <https://doi.org/10.1080/0812099808728402>.
- Baker, T., Perkins, C., Blake, K.L., Williams, P.J., 2001. Radiogenic and stable isotope constraints on the genesis of the Eloise Cu-Au deposits, Cloncurry district, Northwest Queensland. *Econ. Geol.* 96 (4), 723–742. <https://doi.org/10.2113/gsecongeo.96.4.723>.
- Barra, F., Reich, M., Selby, D., Rojas, P., Simon, A., Salazar, E., Palma, G., 2017. Unraveling the origin of the Andean IOCG clan: a Re-Os isotope approach. *Ore Geol. Rev.* 81 (October 2016), 62–78. <https://doi.org/10.1016/j.oregeorev.2016.10.016>.
- Barton, M.D., 2013. Iron oxide-(Cu-Au-REE-P-Ag-U-Co) systems. In: *Treatise on Geochemistry: second ed.*, vol. 13. Elsevier Inc., pp. 515–541. <https://doi.org/10.1016/B978-0-08-095975-7.01123-2>.
- Bascuñán, S., Arrigada, C., Le Roux, J., Deckart, K., 2016. Unraveling the Peruvian Phase of the Central Andes: stratigraphy, sedimentology and geochronology of the Salar de Atacama Basin (22°30–23°S), northern Chile. *Basin Res.* 28 (3), 365–392. <https://doi.org/10.1111/bre.2016.28.issue-310.1111/bre.12114>.
- Bastrakov, E.N., Skirrow, R.G., Davidson, G.J., 2007. Fluid evolution and origins of iron oxide Cu-Au prospects in the Olympic Dam district, Gawler Craton, South Australia. *Econ. Geol.* 102 (8), 1415–1440. <https://doi.org/10.2113/gsecongeo.102.8.1415>.
- Bauer, T.E., Lynch, E.P., Sarlus, Z., Dreijer-Carroll, D., Martinsson, O., Metzger, N., Wanhaninen, C., 2021. Structural controls on iron oxide-copper-gold mineralization and related alteration in a Paleoproterozoic supracrustal belt: Insights from the Nautanen deformation zone and surroundings, northern Sweden. *Econ. Geol.* <https://doi.org/10.5382/econgeo.4862>.
- Belperio, A., Flint, R., Freeman, H., 2007. Prominent Hill: a hematite-dominated, iron oxide copper-gold system. *Econ. Geol.* 102 (8), 1499–1510. <https://doi.org/10.2113/gsecongeo.102.8.1499>.
- Benavides, J., Kyser, T.K., Clark, A.H., Oates, C.J., Zamora, R., Tarnovschi, R., Castillo, B., 2007. The Mantoverde iron oxide-copper-gold district, III Región, Chile: the role of regionally derived, nonmagmatic fluids in chalcocite mineralization. *Econ. Geol.* 102 (3), 415–440. <https://doi.org/10.2113/gsecongeo.102.3.415>.
- Bierlein, F.P., Ashley, P.M., Plimer, I.R., 1995. Sulphide mineralisation in the Olary Block, South Australia – evidence for syn-tectonic to late-stage mobilisation. *Mineral Deposita* 30 (6), 424–438. <https://doi.org/10.1007/BF00196402>.
- Bonyadi, Z., Sadeghi, R., 2020. Hydrothermal alteration associated with magnetite mineralization in the Bafq iron deposits. *Iran. J. Asian Earth Sci.* 189 (February 2019) <https://doi.org/10.1016/j.jseas.2019.104152>.
- Boric, R., Holmgren, C., Wilson, N.S.F., Zentilli, M., 2002. The geology of the El Soldado manto type Cu (Ag) deposit, central Chile. In: Porter, T.M. (Ed.), *Hydrothermal Iron Oxide Copper-gold and Related Deposits: A Global Perspective*, vol. 2. PGC Publishing, pp. 163–184.
- Boyce, D., Charrier, R., Farías, M., 2020. The first Andean compressive tectonic phase: sedimentologic and structural analysis of mid-Cretaceous deposits in the Coastal Cordillera, central Chile (32°50'S). *Tectonics* 39 (2), 1–24. <https://doi.org/10.1029/2019TC005825>.
- Brauhart, C.W., Grunsky, E.C., Hagemann, S.G., 2017. Magmatic-hydrothermal space: a new metric for geochemical characterisation of metallic ore deposits. *Ore Geol. Rev.* 86, 867–895. <https://doi.org/10.1016/j.oregeorev.2016.11.001>.
- Brown, M., Porter, T.M., 2010. The Mount Elliott IOCG system, Eastern Fold Belt, Mount Isa Inlier, northwest Queensland. In: Porter, T.M. (Ed.), *Hydrothermal Iron Oxide Copper-gold and Related Deposits: A Global Perspective*, vol. 3. PGC Publishing, pp. 219–231.

- Budd, A., 2006. The Tarcoola Goldfield of the central Gawler gold province, and the Hiltaba Association Granites, Gawler craton, South Australia: Unpublished PhD thesis, Australian National University.
- Case, G.N., 2016. *Genesis of the E1 Group of iron oxide-copper-gold deposits, Cloncurry district, northwest Queensland*. Unpubl. PhD thesis. James Cook University of North Queensland.
- Cave, B., Lilly, R., Glorie, S., Gillespie, J., 2018. Geology, apatite geochronology, and geochemistry of the Ernest Henry inter-lens: implications for a re-examined deposit model. *Minerals* 8 (9), 405. <https://doi.org/10.3390/min8090405>.
- Chen, H., Clark, A.H., Kyser, T.K., Ullrich, T.D., Baxter, R., Chen, Y., Moody, T.C., 2010. Evolution of the giant Marcona-Mina Justa iron oxide-copper-gold district, south-central Peru. *Econ. Geol.* 105 (1), 155–185. <https://doi.org/10.2113/gsecongeo.105.1.155>.
- Chen, H., Cooke, D.R., Baker, M.J., 2013. Mesozoic iron oxide copper-gold mineralization in the Central Andes and the Gondwana supercontinent breakup. *Econ. Geol.* 108 (1), 37–44. <https://doi.org/10.2113/econgeo.108.1.37>.
- Chen, W.T., Zhou, M.F., 2012. Paragenesis, stable isotopes, and molybdenite Re-Os isotope age of the Lala iron-copper deposit, southwest China. *Econ. Geol.* 107 (3), 459–480. <https://doi.org/10.2113/econgeo.107.3.459>.
- Cherry, A.R., Ehrig, K., Kamenetsky, V.S., McPhie, J., Crowley, J.L., Kamenetsky, M.B., 2018. Precise geochronological constraints on the origin, setting and incorporation of ca. 1.59 Ga surficial facies into the Olympic Dam Breccia Complex, South Australia. *Precambr. Res.* 315 (July), 162–178. <https://doi.org/10.1016/j.precamres.2018.07.012>.
- Conor, C.H.H., 1995. Moonta-Wallaroo Region – An Interpretation of the Geology of the Maitland and Wallaroo 1:100 000 Sheet Areas. Mines and Energy South Australia, Open File Envelope, p. 8886.
- Conor, C., Raymond, O., Baker, T., Teale, G., Say, P., Lowe, G., 2010. Alteration and mineralisation in the Moonta-Wallaroo copper-gold mining field region, Olympic Domain, South Australia. In: Porter, T.M. (Ed.), *Hydrothermal Iron Oxide Copper-gold and Related Deposits: A Global Perspective*, vol. 3. PGC Publishing, pp. 147–170.
- Cook, N.D.J., Ashley, P.M., 1992. Meta-evaporite sequence, exhalative chemical sediments and associated rocks in the Proterozoic Willyama Supergroup, South Australia: implications for metallogenesis. *Precambr. Res.* 56 (3–4), 211–226. [https://doi.org/10.1016/0301-9268\(92\)90102-T](https://doi.org/10.1016/0301-9268(92)90102-T).
- Corriveau, L., 2007. Iron oxide copper-gold deposits: a Canadian perspective. In: Goodfellow, W.D. (Ed.), *Mineral Deposits in Canada: A Synthesis of Major Deposit Types, District Metallogeny, the Evolution of Geological Provinces and Exploration Methods*. Geological Association of Canada, Mineral Deposits Division, Special Publication Volume 5, pp. 307–328.
- Corriveau, L., Montreuil, J.F., Potter, E.G., 2016. Alteration facies linkages among iron oxide copper-gold, iron oxide-apatite, and affiliated deposits in the Great Bear magmatic zone, Northwest Territories, Canada. *Econ. Geol.* 111 (8), 2045–2072. <https://doi.org/10.2113/econgeo.111.8.2045>.
- Corriveau, L., Mumtin, A.H., Setterfield, T., 2010a. IOCG environments in Canada: characteristics, geological vectors to ore and challenges. In: Porter, T.M. (Ed.), *Hydrothermal Iron Oxide Copper-gold and Related Deposits: A Global Perspective*, vol. 4. PGC Publishing, pp. 311–344.
- Corriveau, L., Williams, P.J., Mumtin, A.H., 2010b. Alteration vectors to IOCG mineralization: from uncharted terranes to deposits. In: Corriveau, L., Mumtin, A.H. (Eds.), *Exploring for Iron Oxide Copper-gold Deposits: Canada and Global Analogues*, vol. 20. Geological Association of Canada, Short Course Notes, pp. 89–110.
- Courtney-Davies, L., Ciobanu, C.L., Verdugo-Ihl, M.R., Dmitrijeva, M., Cook, N.J., Ehrig, K., Wade, B.P., 2019. Hematite geochemistry and geochronology resolve genetic and temporal links among iron-oxide copper gold systems, Olympic Dam district, South Australia. *Precambrian Res.* 335 (June), 105480. <https://doi.org/10.1016/j.precamres.2019.105480>.
- Craveiro, G.S., Villas, R.N.N., Xavier, R.P., 2020. A fluid inclusion and stable isotope (O, H, S and C) study of the Archean IOCG Cristalino deposit, Carajás Mineral Province, Brazil: implications to ore genesis. *Ore Geol. Rev.* 127 (August), 103822. <https://doi.org/10.1016/j.oregeorev.2020.103822>.
- Cross, K.C., 1993. Acropolis and Wirrda Well prospects. In: Drexel, J.F., Preiss, W.V., Parker, A.J. (Eds.), *The Geology of South Australia*, 154. Geological Survey of South Australia, Bulletin, p. 138.
- Daliran, F., Stosch, H.-G., Williams, P.J., 2010. Lower Cambrian iron oxide-apatite-REE (U) deposits of the Bafq district, east-central Iran. In: Corriveau, L., Mumtin, H. (Eds.), *Exploring for Iron Oxide Copper-gold Deposits: Canada and Global Analogues. Short Course Notes*, vol. 20. Geological Association of Canada, pp. 143–155.
- Davidson, G.J., Large, R.R., 1994. Gold metallogeny and the copper-gold association of the Australian Proterozoic. *Miner. Deposita* 29 (3). <https://doi.org/10.1007/BF00206864>.
- Day, W.C., Slack, J.F., Ayuso, R.A., Seeger, C.M., 2016. Regional geologic and petrologic framework for iron oxide ± apatite ± rare earth element and iron oxide copper-gold deposits of the Mesoproterozoic St. Francois Mountains Terrane, southeast Missouri, USA. *Econ. Geol.* 111 (8), 1825–1858. <https://doi.org/10.2113/econgeo.111.8.1825>.
- de Freitas Toledo, P.I., Moreto, C.P.N., Xavier, R.P., Gao, J., de Matos, J.H.da.S.N., de Melo, G.H.C., 2019. Multistage evolution of the Neoproterozoic (ca. 2.7 Ga) Igarapé Cinzento (GT-46) iron oxide copper-gold deposit, Cinzento Shear Zone, Carajás Province, Brazil. *Econ. Geol.* 114 (1), 1–34. <https://doi.org/10.5382/econgeo.2019.4617>.
- de Haller, A., Corfu, F., Fontboté, L., Schaltegger, U., Barra, F., Chiaradìa, M., Frank, M., Alvarado, J.Z., 2006. Geology, geochronology, and Hf and Pb isotope data of the Raúl-Condestable iron oxide-copper-gold deposit, central coast of Peru. *Econ. Geol.* 101 (2), 281–310. <https://doi.org/10.2113/gsecongeo.101.2.281>.
- de Melo, G.H.C., Monteiro, L.V.S., Xavier, R.P., Moreto, C.P.N., Santiago, E., 2019. Tracing fluid sources for the Salobo and Igarapé Bahia deposits: implications for the genesis of the iron oxide copper-gold deposits in the Carajás Province, Brazil. *Econ. Geol.* 114 (4), 697–718. <https://doi.org/10.5382/econgeo.4659>.
- de Melo, G.H.C., Monteiro, L.V.S., Xavier, R.P., Moreto, C.P.N., Santiago, E.S.B., Dufrane, S.A., Aires, B., Santos, A.F.F., 2017. Temporal evolution of the giant Salobo IOCG deposit, Carajás Province (Brazil): constraints from paragenesis of hydrothermal alteration and U-Pb geochronology. *Miner. Deposita* 52 (5), 709–732. <https://doi.org/10.1007/s00126-016-0693-5>.
- del Real, I., Thompson, J.F.H., Carriedo, J., 2018. Lithological and structural controls on the genesis of the Candelaria-Punta del Cobre iron oxide copper gold district, northern Chile. *Ore Geol. Rev.* 102 (August), 106–153. <https://doi.org/10.1016/j.oregeorev.2018.08.034>.
- Dick, J.M., 2021. Diagrams with multiple metals in CHNOSZ. *Appl. Comput. Geosci.* 10 (November 2020) <https://doi.org/10.1016/j.acgs.2021.100059>.
- Donnellan, N., Hussey, K.J., Morrison, R.S., 1995. Flynn 5759, Tennant Creek 5758: Explanatory Notes, 1:100 000 Geological Map Series. Northern Territory Geol. Surv.
- Duncan, R.J., Stein, H.J., Evans, K.A., Hitzman, M.W., Nelson, E.P., Kirwin, D.J., 2011. A new geochronological framework for mineralization and alteration in the Selwyn-Mount Dore corridor, Eastern Fold Belt, Mount Isa Inlier, Australia: genetic implications for iron oxide copper-gold deposits. *Econ. Geol.* 106 (2), 169–192. <https://doi.org/10.2113/econgeo.106.2.169>.
- Ehrig, K.J., McPhie, J., Kamenetsky, V.S., 2012. Geology and mineralogical zonation of the Olympic Dam iron oxide Cu-U-Au-Ag deposit, South Australia. In: Hedenquist, J. W., Harris, M., Camus, F. (Eds.), *Geology and Genesis of Major Copper Deposits and Districts of the World: A Tribute to Richard H. Sillitoe*. Special Publication 16. Society of Economic Geologists, pp. 237–267. <https://doi.org/10.5382/sp.17>.
- Fennell, L.M., Iannelli, S.B., Encinas, A., Naipauer, M., Valencia, V., Folguera, A.S., 2019. Alternating contraction and extension in the southern central Andes (35°–37°S). *Am. J. Sci.* 319 (5), 381–429. <https://doi.org/10.2475/05.2019.02>.
- Fisher, L.A., Kendrick, M.A., 2008. Metamorphic fluid origins in the Osborne Fe oxide - Cu - Au deposit, Australia: Evidence from noble gases and halogens. *Miner. Deposita* 43 (5), 483–497. <https://doi.org/10.1007/s00126-008-0178-2>.
- Goode, R.E., Mumtin, H., Duke, N.A., Neale, K.L., Mulligan, D.L., 2000. Geology of the Proterozoic iron oxide-hosted, NICO cobalt-gold-bismuth, and Sue-Dianne copper-silver deposits, southern Great Bear magmatic zone, Northwest Territories, Canada. In: Porter, T.M. (Ed.), *Hydrothermal Iron Oxide Copper-gold and Related Deposits: A Global Perspective*, vol. 1. Australian Mineral Foundation, pp. 249–267.
- Grainger, C.J., Groves, D.I., Tallarico, F.H.B., Fletcher, I.R., 2008. Metallogenesis of the Carajás Mineral Province, Southern Amazon Craton, Brazil: varying styles of Archean through Paleoproterozoic to Neoproterozoic base- and precious-metal mineralisation. *Ore Geol. Rev.* 33 (3–4), 451–489. <https://doi.org/10.1016/j.oregeorev.2006.10.010>.
- Groves, D.I., Bierlein, F.P., Meinert, L.D., Hitzman, M.W., 2010. Iron oxide copper-gold (IOCG) deposits through Earth history: implications for origin, lithospheric setting, and distinction from other epigenetic iron oxide deposits. *Econ. Geol.* 105 (3), 641–654.
- Haynes, D.W., 2000. Iron oxide copper (-gold) deposits: their position in the deposit spectrum and modes of origin. In: *Hydrothermal Iron Oxide Copper-gold and Related Deposits: A Global Perspective*, vol. 1. Australian Mineral Foundation, pp. 71–90.
- Haynes, D.W., Cross, K.C., Bills, R.T., Reed, M.H., 1995. Olympic Dam ore genesis: a fluid-mixing model. *Econ. Geol.* 90 (2), 281–307. <https://doi.org/10.2113/gsecongeo.90.2.281>.
- Hildebrand, R.S., Hoffman, P.F., Bowring, S.A., 1987. Tectono-magmatic evolution of the 1.9-Ga Great Bear magmatic zone, Wopmay orogen, northwestern Canada. *J. Volcanol. Geoth. Res.* 32 (1–3), 99–118. [https://doi.org/10.1016/0377-0273\(87\)90039-4](https://doi.org/10.1016/0377-0273(87)90039-4).
- Hitzman, M.W., 2000. Iron oxide-Cu-Au deposits: what, where, when and why?. In: Porter, T.M. (Ed.), *Hydrothermal Iron Oxide Copper-gold and Related Deposits: A Global Perspective*, vol. 1. Australian Mineral Foundation, pp. 9–25.
- Hitzman, M.W., Oreskes, N., Einaudi, M.T., 1992. Geological characteristics and tectonic setting of Proterozoic iron oxide (Cu-U-Au-REE) deposits. *Precambr. Res.* 58 (1–4), 241–287.
- Hoggard, M.J., Czarnota, K., Richards, F.D., Huston, D.L., Jaques, A.L., Ghelichkhan, S., 2020. Global distribution of sediment-hosted metals controlled by craton edge stability. *Nat. Geosci.* 13 (7), 504–510. <https://doi.org/10.1038/s41561-020-0593-2>.
- Hopper, D., Correa, A., 2000. The Panulcillo and Teresa de Colmo copper deposits: two contrasting examples of Fe-ox Cu-Au mineralization from the Coastal Cordillera of Chile. In: Porter, T.M. (Ed.), *Hydrothermal Iron Oxide Copper-gold and Related Deposits: A Global Perspective*, vol. 1. Australian Mineral Foundation, pp. 177–189.
- Huang, Q., Kamenetsky, V.S., Ehrig, K., McPhie, J., Kamenetsky, M., Cross, K., Meffre, S., Agangui, A., Chambeffort, I., Direen, N.G., Maas, R., Apukhtina, O., 2016. Olivine-phryric basalt in the Mesoproterozoic Gawler silicic large igneous province, South Australia: examples at the Olympic Dam iron oxide Cu-U-Au-Ag deposit and other localities. *Precambr. Res.* 281, 185–199. <https://doi.org/10.1016/j.precamres.2016.05.019>.
- Huston, D., Cross, A., Skirrow, R., Champion, D., Whelan, J., 2020. The Tennant Creek mineral field and Rover fields: Many similarities but some important differences. In: AGES 2020 Conference Proceedings, Northern Territory Geological Survey, pp. 70–83.
- Huston, D.L., Bolger, C., Cozens, G., 1993. A comparison of mineral deposits at the Gecko and White Devil deposits: implications for ore genesis in the Tennant Creek district,

- Northern Territory, Australia. *Econ. Geol.* 88 (5), 1198–1225. <https://doi.org/10.2113/gsecongeo.88.5.1198>.
- Ismail, R., Ciobanu, C.L., Cook, N.J., Teale, G.S., Giles, D., Mumm, A.S., Wade, B., 2014. Rare earths and other trace elements in minerals from skarn assemblages, Hillside iron oxide-copper-gold deposit, Yorke Peninsula, South Australia. *Lithos* 184–187, 456–477. <https://doi.org/10.1016/j.lithos.2013.07.023>.
- Johnson, C.A., Day, W.C., Rye, R.O., 2016. Oxygen, hydrogen, sulfur, and carbon isotopes in the Pea Ridge magnetite-apatite deposit, Southeast Missouri, and sulfur isotope comparisons to other iron deposits in the region. *Econ. Geol.* 111 (8), 2017–2032. <https://doi.org/10.2113/econgeo.111.8.2017>.
- Johnson, J.P., Cross, K.C., 1995. U-Pb geochronological constraints on the genesis of the Olympic Dam Cu-U-Au deposit, South Australia. *Econ. Geol.* 90, 1046–1063.
- Johnson, J.P., McCulloch, M.T., 1995. Sources of mineralising fluids for the Olympic Dam deposit (South Australia): Sm-Nd isotopic constraints. *Chem. Geol.* 121 (1–4), 177–199. [https://doi.org/10.1016/0009-2541\(94\)00125-R](https://doi.org/10.1016/0009-2541(94)00125-R).
- Kirschbaum, M.J., Hitzman, M.W., 2016. Guelb Moghrein: an unusual, carbonate-hosted iron oxide copper-gold deposit in Mauritania, northwest Africa. *Econ. Geol.* 111 (3), 763–770.
- Knipping, J.L., Bilenker, L.D., Simon, A.C., Reich, M., Barra, F., Deditius, A.P., Lundstrom, C., Bindeman, I., Munizaga, R., 2015. Giant Kiruna-type deposits form by efficient flotation of magmatic magnetite suspensions. *Geology* 43 (7), 591–594. <https://doi.org/10.1130/G36650.1>.
- Kolb, J., Meyer, M., Vennemann, T., Sindern, S., Prantl, S., Bottcher, M.E., 2010. Characterisation of the hydrothermal fluids of the Guelb Moghrein iron oxide-Cu-Au deposit, Mauritania: ore mineral chemistry, fluid inclusions and isotope geochemistry. In: Porter, T.M. (Ed.), *Hydrothermal Iron Oxide Copper-gold and Related Deposits: A Global Perspective*, vol. 4. PGC Publishing, pp. 553–572.
- Kolb, J., Petrov, N., 2016. The Guelb Moghrein Cu-Au deposit: Neoproterozoic hydrothermal sulfide mineralization in carbonate-facies iron formation. *Ore Geol. Rev.* 78, 573–577. <https://doi.org/10.1016/j.oregeorev.2015.09.003>.
- Krnetta, S., Cook, N.J., Ciobanu, C.L., Ehrig, K., Kontonikas-Charos, A., 2017. The Wirra Well and Acropolis prospects, Gawler Craton, South Australia: insights into evolving fluid conditions through apatite chemistry. *J. Geochem. Explor.* 181 (May), 276–291. <https://doi.org/10.1016/j.gexplo.2017.08.004>.
- Lahtinen, R., Huhma, H., Lahaye, Y., Jonsson, E., Manninen, T., Lauri, L.S., Bergman, S., Hellström, F., Niiranen, T., Nironen, M., 2015. New geochronological and Sm-Nd constraints across the Pajala shear zone of northern Fennoscandia: reactivation of a Paleoproterozoic suture. *Precambr. Res.* 256, 102–119. <https://doi.org/10.1016/j.precamres.2014.11.006>.
- Lahtinen, R., Huhma, H., Sayab, M., Lauri, L.S., Hölttä, P., 2018. Age and structural constraints on the tectonic evolution of the Paleoproterozoic Central Lapland Granitoid Complex in the Fennoscandian Shield. *Tectonophysics* 745 (January), 305–325. <https://doi.org/10.1016/j.tecto.2018.08.016>.
- Large, R.R., 1975. Zonation of hydrothermal minerals at the Juno Mine, Tenant Creek goldfield, central Australia. *Econ. Geol.* 70, 1387–1413. <https://doi.org/10.2113/gsecongeo.71.8.1615>.
- Li, W., Audétat, A., Zhang, J., 2015a. The role of evaporites in the formation of magnetite-apatite deposits along the Middle and Lower Yangtze River, China: evidence from LA-ICP-MS analysis of fluid inclusions. *Ore Geol. Rev.* 67, 264–278. <https://doi.org/10.1016/j.oregeorev.2014.12.003>.
- Li, X.C., Zhou, M.F., 2018. The nature and origin of hydrothermal REE mineralization in the Sin Quyen deposit, northwestern Vietnam. *Econ. Geol.* 113 (3), 645–673. <https://doi.org/10.5382/econgeo.2018.4565>.
- Li, X., Zhao, X., Zhou, M.F., Chen, W.T., Chu, Z., 2015b. Fluid inclusion and isotopic constraints on the origin of the Paleoproterozoic Yinachang Fe-Cu-(REE) deposit, Southwest China. *Econ. Geol.* 110 (5), 1339–1369. <https://doi.org/10.2113/gsecongeo.110.5.1339>.
- Lin, L., Chen, R., Pang, Z., Chen, H., Xue, J., Jia, H., 2020. Sulfide Rb-Sr, Re-Os and in-situ S isotopic constraints on two mineralization events at the large Hongnipo Cu deposit, SW China. *Minerals* 10 (5), 1–24. <https://doi.org/10.3390/min10050414>.
- Lu, C., Grand, S.P., Lai, H., Garner, E.J., 2019. TX2019slab: a new P and S tomography model incorporating subducting slabs. *J. Geophys. Res. Solid Earth* 124 (11), 11549–11567. <https://doi.org/10.1029/2019JB017448>.
- Maksaev, V., Zentilli, M., 2002. Chilean strata-bound Cu-(Ag) deposits: an overview. In: Porter, T.M. (Ed.), *Hydrothermal Iron Oxide Copper-gold and Related Deposits: A Global Perspective*, vol. 2. PGC Publishing, pp. 185–205.
- Mark, G., Oliver, N.H.S., Williams, P.J., 2006. Mineralogical and chemical evolution of the Ernest Henry Fe oxide-Cu-Au ore system, Cloncurry district, northwest Queensland, Australia. *Mineralium Deposita* 40 (8), 769–801. <https://doi.org/10.1007/s00126-005-0009-7>.
- Marschik, R., Fontboté, L., 2001. The Candelaria-Punta del Cobre iron oxide Cu-Au (-Zn-Ag) deposits, Chile. *Econ. Geol.* 96 (8), 1799–1826. <https://doi.org/10.2113/gsecongeo.96.8.1799>.
- Martinsson, O., Billström, K., Broman, C., Weiher, P., Wanhaugen, C., 2016. Metallogeny of the Northern Norrbotten Ore Province, Northern Fennoscandian Shield with emphasis on IOCG and apatite-iron ore deposits. *Ore Geol. Rev.* 78, 447–492. <https://doi.org/10.1016/j.oregeorev.2016.02.011>.
- McLean, R.N., 2002. The Sin Quyen iron oxide-copper-gold-rare earth oxide mineralisation of north Vietnam. In: Porter, T.M. (Ed.), *Hydrothermal Iron Oxide Copper-gold and Related Deposits: A Global Perspective*, vol. 2. PGC Publishing, pp. 293–301.
- McPhie, J., Ehrig, K.J., Kamenetsky, M.B., Crowley, J.L., Kamenetsky, V.S., 2020. Geology of the Acropolis prospect, South Australia, constrained by high-precision CA-TIMS ages. *Aust. J. Earth Sci.* 67 (5), 699–716. <https://doi.org/10.1080/08120099.2020.1717617>.
- Meinert, L.D., Dipple, G.M., Nicolescu, S., 2005. World skarn deposits. In: Hedenquist, J.W., Thompson, J.F.H., Goldfarb, R.J., Richards, J.P. (Eds.), *One Hundredth Anniversary Volume*. Society of Economic Geologists. <https://doi.org/10.5382/AV100.11>.
- Meyer, C., 1988. Ore deposits as guides to geologic history of the Earth. *Ann. Rev. Earth Planet. Sci.* 16 (1), 147–171.
- Myano, T., Klein, C., 1989. Phase equilibria in the system $K_2O - FeO - MgO - Al_2O_3 - SiO_2 - H_2O - CO_2$ and the stability limit of stilpnomelane in metamorphosed Precambrian iron-formations. *Contrib. Miner. Petro.* 102 (4), 478–491.
- Monteiro, L.V.S., Xavier, R.P., de Carvalho, E.R., Hitzman, M.W., Johnson, C.A., de Souza Filho, C.R., Torresi, I., 2008. Spatial and temporal zoning of hydrothermal alteration and mineralization in the Sossego iron oxide-copper-gold deposit, Carajás Mineral Province, Brazil: paragenesis and stable isotope constraints. *Miner. Deposita* 43 (2), 129–159. <https://doi.org/10.1007/s00126-006-0121-3>.
- Montreuil, J.F., Corriveau, L., Davis, W.J., 2016a. Tectonomagmatic evolution of the southern Great Bear magmatic zone (Northwest Territories, Canada): implications for the genesis of iron oxide-alkali-altered hydrothermal systems. *Econ. Geol.* 111 (8), 2111–2138. <https://doi.org/10.2113/econgeo.111.8.2111>.
- Montreuil, J.F., Corriveau, L., Potter, E.G., 2015. Formation of albitite-hosted uranium within IOCG systems: the Southern Breccia, Great Bear magmatic zone, Northwest Territories, Canada. *Mineralium Deposita* 50 (3), 293–325. <https://doi.org/10.1007/s00126-014-0530-7>.
- Montreuil, J.F., Corriveau, L., Potter, E.G., de Toni, A.F., 2016b. On the relationship between alteration facies and metal endowment of iron oxide-alkali-altered systems, southern Great Bear magmatic zone (Canada). *Econ. Geol.* 111 (8), 2139–2168. <https://doi.org/10.2113/econgeo.111.8.2139>.
- Moreto, C.P.N., Monteiro, L.V.S., Xavier, R.P., Amaral, W.S., dos Santos, T.J.S., Juliani, C., de Filho, C.R.S., 2011. Mesoarchean (3.0 and 2.86 Ga) host rocks of the iron oxide-Cu-Au Bacaba deposit, Carajás Mineral Province: U-Pb geochronology and metallogenetic implications. *Miner. Deposita* 46 (7), 789–811. <https://doi.org/10.1007/s00126-011-0352-9>.
- Mukhopadhyay, S., Kumar, V., Sangwan, M., 2019. Sediment hosted stratiform copper (SSC) mineralization in Bhudoli-Basari area, North Delhi Fold Belt, Mesoproterozoic Delhi Supergroup, Rajasthan. *J. Geol. Soc. India* 93 (6), 663–674. <https://doi.org/10.1007/s12594-019-1245-2>.
- Mumin, A.H., Corriveau, L., Somarin, A.K., Ootes, L., 2007. Iron oxide copper-gold-type polymetallic mineralization in the Contact Lake belt, Great Bear magmatic zone, Northwest Territories, Canada. *Exploration Min. Geol.* 16 (3–4), 187–208.
- Mumin, A.H., Somarin, A.K., Jones, B., Corriveau, L., Ootes, L., Camier, J., 2010. The IOCG-porphry-epithermal continuum of deposit types in the Great Bear magmatic zone, Northwest Territories, Canada. In: Corriveau, L., Mumin, A.H. (Eds.), *Exploring for Iron Oxide Copper-gold Deposits: Canada and Global Analogues. Short Course Notes*, vol. 20. Geological Association of Canada, pp. 59–78.
- Ootes, L., Snyder, D., Davis, W.J., Acosta-Góngora, P., Corriveau, L., Mumin, A.H., Gleeson, S.A., Samson, I.M., Montreuil, J.F., Potter, E., Jackson, V.A., 2017. A Paleoproterozoic Andean-type iron oxide copper-gold environment, the Great Bear magmatic zone, Northwest Canada. *Ore Geol. Rev.* 81, 123–139. <https://doi.org/10.1016/j.oregeorev.2016.09.024>.
- Oreskes, N., Einaudi, M.T., 1990. Origin of rare earth element-enriched hematite breccias at the Olympic Dam Cu-U-Au-Ag deposit, Roxby Downs, South Australia. *Econ. Geol.* 85 (1), 1–28. <https://doi.org/10.2113/gsecongeo.85.1.1>.
- Oreskes, N., Einaudi, M.T., 1992. Origin of hydrothermal fluids at Olympic Dam: preliminary results from fluid inclusions and stable isotopes. *Econ. Geol.* 87 (1), 64–90. <https://doi.org/10.2113/gsecongeo.87.1.64>.
- OSNACA, 2020. Ore samples normalised to average crustal abundance. <http://www.cet.edu.au/projects/osnaca-ore-samples-normalised-to-average-crustal-abundance>.
- Oyarzún, R., Oyarzún, J., Méndez, J.J., Lillo, J., 2003. The Cretaceous iron belt of northern Chile: role of oceanic plates, a superplume event, and a major shear zone. *Miner. Deposita* 38 (5), 640–646. <https://doi.org/10.1007/s00126-003-0359-y>.
- Oyunjargal, L., Hayashi, K., Teruyuki, M., 2020. Geological, mineralogical, and oxygen isotope studies of the Chandmani Uul iron oxide – copper – gold deposit in Dornogobi Province, southeastern Mongolia. *Resour. Geol.* 233–253. <https://doi.org/10.1111/rge.12232>.
- Page, R.W., 1983. Chronology of magmatism, skarn formation, and uranium mineralization, Mary Kathleen, Queensland, Australia. *Econ. Geol.* 78, 838–853.
- Perkins, C., Wyborn, L.A.I., 1998. Age of Cu-Au mineralisation, Cloncurry district, eastern Mt Isa Inlier, Queensland, as determined by $^{40}Ar/^{39}Ar$ dating. *Aust. J. Earth Sci.* 45 (2), 233–246. <https://doi.org/10.1080/0812009980728384>.
- Perring, C.S., Pollard, P.J., Dong, G., Nunn, A.J., Blake, K.L., 2000. The Lightning Creek Sill complex, Cloncurry district, northwest Queensland: a source of fluids for Fe oxide Cu-Au mineralization and sodic-calcic alteration. *Econ. Geol.* 95 (5), 1067–1089. <https://doi.org/10.2113/gsecongeo.95.5.1067>.
- Pestilho, A.L.S., Monteiro, L.V.S., de Melo, G.H.C., Moreto, C.P.N., Juliani, C., Fallick, A.E., Xavier, R.P., 2020. Stable isotopes and fluid inclusion constraints on the fluid evolution in the Bacaba and Castanha iron oxide-copper-gold deposits, Carajás Mineral Province, Brazil. *Ore Geol. Rev.* 126 (April 2019) <https://doi.org/10.1016/j.oregeorev.2020.103738>.
- Polito, P.A., Kyser, T.K., Stanley, C., 2009. The Proterozoic, albite-hosted, Valhalla uranium deposit, Queensland, Australia: a description of the alteration assemblage associated with uranium mineralisation in diamond drill hole V39. *Miner. Deposita* 44 (1), 11–40. <https://doi.org/10.1007/s00126-007-0162-2>.
- Porter, T.M., 2010a. Current understanding of iron oxide associated-alkali altered mineralised systems: Part I – An overview. In: Porter, T.M. (Ed.), *Hydrothermal Iron Oxide Copper-gold and Related Deposits: A Global Perspective*, vol. 3. PGC Publishing, pp. 5–32.

- Porter, T.M., 2010b. The Carrapateena iron oxide copper gold deposit, Gawler Craton, South Australia: a review. In: Porter, T.M. (Ed.), *Hydrothermal Iron Oxide Copper-gold and Related Deposits: A Global Perspective*, vol. 3. PGC Publishing, pp. 191–200.
- Prevato, M., Monteiro, L.V.S., Bello, R.M.da.S., Gonçales, L.C.G., 2020. Evolution of brines and CO₂-rich fluids and hydrothermal overprinting in the genesis of the Borrachudo copper deposit, Carajás Province. *Ore Geol. Rev.* 121 (March) <https://doi.org/10.1016/j.oregeorev.2020.103561>.
- Sharma, P.J., Sahoo, P.R., Mahanta, H., Venkatesh, A.S., Babu, E.V.S.S.K., John, M.M., 2020. Constraints on the genesis of the Proterozoic bornite dominated copper deposit from Nim ka Thana, western India: an IOCG perspective. *Ore Geology Reviews* 118 (May 2019). <https://doi.org/10.1016/j.oregeorev.2020.103338>.
- Ramírez, L.E., Palacios, C., Townley, B., Parada, M.A., Sial, A.N., Fernandez-Turiel, J.L., Gimeno, D., García-Valles, M., Lehmann, B., 2006. The Mantos Blancos copper deposit: an Upper Jurassic breccia-style hydrothermal system in the Coastal Range of northern Chile. *Miner. Deposita* 41 (3), 246–258. <https://doi.org/10.1007/s00126-006-0055-9>.
- Reeve, J.S., Cross, K.C., Smith, R.N., Oreskes, N., 1990. Olympic Dam copper-uranium-gold-silver deposit. In: Hughes, F.E. (Ed.), *Geology of the Mineral Deposits of Australia and Papua New Guinea*. Australasian Institute of Mining and Metallurgy, Monograph 14, pp. 1009–1035.
- Reich, M., Simon, A.C., Deditius, A., Barra, F., Chrysoulis, S., Lagas, G., Tardani, D., Knipping, J., Bilenker, L., Sánchez-Alfaro, P., Roberts, M.P., Munizaga, R., 2016. Trace element signature of pyrite from the Los Colorados iron oxide-apatite (IOA) deposit, Chile: a missing link between Andean IOA and iron oxide copper-gold systems? *Econ. Geol.* 111 (3), 743–761.
- Richards, J.P., Lopez, G.P., Zhu, J.J., Creaser, R.A., Locock, A.J., Mumin, A.H., 2017. Contrasting tectonic settings and sulfur contents of magmas associated with Cretaceous porphyry Cu ± Mo ± Au and intrusion-related iron oxide Cu-Au deposits in northern Chile. *Econ. Geol.* 112 (2), 295–318. <https://doi.org/10.2113/econgeo.112.2.295>.
- Richards, J.P., Mumin, A.H., 2013. Magmatic-hydrothermal processes within an evolving Earth: iron oxide-copper-gold and porphyry Cu ± Mo ± Au deposits. *Geology* 41 (7), 767–770. <https://doi.org/10.1130/G34275.1>.
- Rieger, A.A., Marschik, R., Díaz, M., Hözl, S., Chiaradia, M., Akker, B., Spangenberg, J. E., 2010. The hypogene iron oxide copper-gold mineralization in the Mantoverde district, northern Chile. *Econ. Geol.* 105 (7), 1271–1299. <https://doi.org/10.2113/econgeo.105.7.1271>.
- Rodríguez-Mustafa, M.A., Simon, A.C., del Real, I., Thompson, J.F.H., Bilenker, L.D., Barra, F., Bindeman, I., Cadwell, D., 2020. A continuum from iron oxide copper-gold to iron oxide-apatite deposits: evidence from Fe and O stable isotopes and trace element chemistry of magnetite. *Econ. Geol.* 115 (7), 1443–1459. <https://doi.org/10.5382/econgeo.4752>.
- Rojas, P.A., Barra, F., Deditius, A., Reich, M., Simon, A., Roberts, M., Rojo, M., 2018. New contributions to the understanding of Kiruna-type iron oxide-apatite deposits revealed by magnetite ore and gangue mineral geochemistry at the El Romeral deposit, Chile. *Ore Geol. Rev.* 93 (January), 413–435. <https://doi.org/10.1016/j.oregeorev.2018.01.003>.
- Rotherham, J.F., 1997. A metasomatic origin for the iron-oxide Au-Cu Starra orebodies, Eastern Fold Belt, Mount Isa Inlier. *Mineral. Deposita* 32 (3), 205–218. <https://doi.org/10.1007/s001260050086>.
- Rotherham, J.F., Blake, K.L., Cartwright, I., Williams, P.J., 1998. Stable isotope evidence for the origin of the Mesoproterozoic Starra Au-Cu deposit, Cloncurry district, northwest Queensland. *Econ. Geol.* 93, 1435–1449.
- Salazar, E., Barra, F., Reich, M., Simon, A., Leisen, M., Palma, G., Romero, R., Rojo, M., 2020. Trace element geochemistry of magnetite from the Cerro Negro Norte iron oxide-apatite deposit, northern Chile. *Miner. Deposita* 55 (3), 409–428. <https://doi.org/10.1007/s00126-019-00879-3>.
- Schlegel, T.U., Heinrich, C.A., 2015. Lithology and hydrothermal alteration control the distribution of copper grade in the Prominent Hill iron oxide-copper-gold deposit (Gawler Craton, South Australia). *Econ. Geol.* 110 (8), 1953–1994. <https://doi.org/10.2113/econgeo.110.8.1953>.
- Schlegel, T.U., Wagner, T., Wälle, M., Heinrich, C.A., 2018. Hematite breccia-hosted iron oxide copper-gold deposits require magmatic fluid components exposed to atmospheric oxidation: evidence from Prominent Hill, Gawler Craton, South Australia. *Econ. Geol.* 113 (3), 597–644. <https://doi.org/10.5382/econgeo.2018.4564>.
- Sillitoe, R.H., 2003. Iron oxide-copper-gold deposits: an Andean view. *Miner. Deposita* 38 (7), 787–812. <https://doi.org/10.1007/s00126-003-0379-7>.
- Sillitoe, R.H., 2010. Porphyry copper systems. *Econ. Geol.* 105 (1), 3–41. <https://doi.org/10.2113/gsecongeo.105.1.3>.
- Sillitoe, R.H., Magaranov, G., Mladenov, V., Creaser, R.A., 2020. Rosen, Bulgaria: a newly recognized iron oxide-copper-gold district. *Econ. Geol.* 115 (3), 481–488. <https://doi.org/10.5382/ECON GEO.4731>.
- Simon, A.C., Knipping, J., Barra, F., Deditius, A.P., Bilenker, L.D., Childress, T., 2018. Kiruna-type iron oxide-apatite (IOA) and iron oxide copper-gold (IOCG) deposits form by a combination of igneous and magmatic-hydrothermal processes: evidence from the Chilean Iron Belt. *Soc. Econ. Geol. Spec. Publ.* 21, 89–114.
- Skirrow, R.G., 1993. The Genesis of gold-copper-bismuth deposits, Tennant Creek, Northern Territory. Unpubl. PhD thesis, Australian National University.
- Skirrow, R.G., 2000. Gold-copper-bismuth deposits of the Tennant Creek district, Australia: a reappraisal of diverse high-grade systems. In: Porter, T.M. (Ed.), *Hydrothermal Iron Oxide Copper-gold and Related Deposits: A Global Perspective*, vol. 1. Australian Mineral Foundation, pp. 149–160.
- Skirrow, R.G., 2010. "Hematite-group" IOCG±U ore systems: tectonic settings, hydrothermal characteristics, and Cu-Au and U mineralizing processes. *Short Course Notes* In: Corriveau, L., Mumin, H. (Eds.), *Exploring for Iron Oxide Copper-gold Deposits: Canada and Global Analogues*, vol. 20. Geological Association of Canada, pp. 39–58.
- Skirrow, R.G., Ashley, P.M., McNaughton, M.J., Suzuki, K., 2000. Time-space framework of Cu-Au-(Mo) and regional alteration systems in the Curnamona Province. *AGSO Record* 2000 (10), 83–86.
- Skirrow, R.G., Bastrakov, E.N., Davidson, G.J., Raymond, O.L., Heithersay, P., 2002. The geological framework, distribution and controls of Fe-oxide Cu-Au mineralisation in the Gawler craton, South Australia: Part II – Alteration and mineralisation. In: Porter, T.M. (Ed.), *Hydrothermal Iron Oxide Copper-gold and Related Deposits: A Global Perspective*, vol. 2. PGC Publishing, pp. 33–47.
- Skirrow, R.G., Murr, J., Schofield, A., Huston, D.L., van der Wielen, S., Czarnota, K., Coghlan, R., Hight, L.M., Connolly, D., Doublier, M., Duan, J., 2019. Mapping iron oxide Cu-Au (IOCG) mineral potential in Australia using a knowledge-driven mineral systems-based approach. *Ore Geol. Rev.* 113, 103011. <https://doi.org/10.1016/j.oregeorev.2019.103011>.
- Skirrow, R.G., van der Wielen, S.E., Champion, D.C., Czarnota, K., Thiel, S., 2018. Lithospheric architecture and mantle metasomatism linked to iron oxide Cu-Au ore formation: multidisciplinary evidence from the Olympic Dam region, South Australia. *Geochem. Geophys. Geosyst.* 19 (8), 2673–2705. <https://doi.org/10.1029/2018GC007561>.
- Skirrow, R.G., Walshe, J.L., 2002. Reduced and oxidized Au-Cu-Bi iron oxide deposits of the Tennant Creek Inlier, Australia: an integrated geologic and chemical model. *Econ. Geol.* 97 (6), 1167–1202. <https://doi.org/10.2113/gsecongeo.97.6.1167>.
- Su, Z.-K., Zhao, X.-F., Li, X.-C., Zhou, M.-F., Kennedy, A.K., Zi, J.-W., Spandler, C., Yang, Y.-H., 2021. Unraveling mineralization and multistage hydrothermal overprinting histories by integrated in-situ U-Pb and Sm-Nd isotopes in a Paleoproterozoic breccia-hosted iron oxide copper-gold deposit, SW China. *Econ. Geol.* 116 (7), 1687–1710. <https://doi.org/10.5382/econgeo.4840>.
- Sun, X.J., Ni, P., Yang, Y.L., Qin, H., Chen, H., Gui, C.J., Jing, S., 2018. Formation of the Qixiashan Pb-Zn deposit in Middle-Lower Yangtze River Valley, eastern China: insights from fluid inclusions and in situ LA-ICP-MS sulfur isotope data. *J. Geochem. Expl.* 192 (June 2017), 45–59. <https://doi.org/10.1016/j.gexplo.2018.03.011>.
- Teale, G.S., Fanning, C.M., 2000a. The Portia - North Portia Cu-Au-(Mo) prospect, South Australia: timing of mineralisation, albitisation and origin of ore fluid. In: Porter, T. M. (Ed.), *Hydrothermal Iron Oxide Copper-gold and Related Deposits: A Global Perspective*, vol. 1. Australian Mineral Foundation, pp. 137–147.
- Teale, G.S., Fanning, C.M., 2000b. The timing of Cu-Au mineralisation in the Curnamona Province. *AGSO Rec.* 2000 (10), 98–100.
- Tiddy, C.J., Giles, D., 2020. Suprasubduction zone model for metal endowment at 1.60–1.57 Ga in eastern Australia. *Ore Geol. Rev.* 122 (March), 103483. <https://doi.org/10.1016/j.oregeorev.2020.103483>.
- Tornos, F., Velasco, F., Hanchar, J.M., 2016. Iron-rich melts, magmatic magnetite, and superheated hydrothermal systems: the El Laco deposit, Chile. *Geology* 44 (6), 427–430. <https://doi.org/10.1130/G37705.110.1130/2016141>.
- Wang, S., Williams, P.J., 2001. Geochemistry and origin of Proterozoic skarns at the Mount Elliott Cu-Au-(Co-Ni) deposit, Cloncurry district, NW Queensland, Australia. *Mineralium Deposita* 36 (2), 109–124. <https://doi.org/10.1007/s001260050292>.
- Wanhainen, C., Martinsson, O., 2010. The hybrid character of the Aitik deposit, Norrbotten, Sweden: a porphyry Cu-Au-Ag-(Mo) system overprinted by iron-oxide Cu-Au hydrothermal fluids. In: Porter, T.M. (Ed.), *Hydrothermal Iron Oxide Copper-gold and Related Deposits: A Global Perspective*, vol. 4. PGC Publishing, pp. 415–426.
- Wedge, M.R., Large, R.R., Williams, B.T., 1989. Controls on high-grade gold mineralization at Tennant Creek, Northern Territory, Australia. *Econ. Geol. Monogr.* 6, 168–179.
- Whitney, D.L., Evans, B.W., 2010. Abbreviations for names of rock-forming minerals. *Am. Mineral.* 95 (1), 185–187. <https://doi.org/10.2138/am.2010.3371>.
- Williams, M.R., Holwell, D.A., Lilly, R.M., Case, G.N.D., McDonald, I., 2015. Mineralogical and fluid characteristics of the fluorite-rich Monakoff and E1 Cu-Au deposits, Cloncurry region, Queensland, Australia: implications for regional F-Barich IOCG mineralisation. *Ore Geol. Rev.* 64 (1), 103–127. <https://doi.org/10.1016/j.oregeorev.2014.05.021>.
- Williams, P.J., 2010. Classifying IOCG deposits. In: Corriveau, L., Mumin, H. (Eds.), *Exploring for Iron Oxide Copper-gold Deposits: Canada and Global Analogues*. Geological Association of Canada, Short Course Notes, vol. 20, pp. 13–21.
- Williams, P.J., Barton, M.D., Johnson, D.A., Fontboté, L., de Haller, A., Mark, G., Oliver, N.H.S., Marschik, R., 2005. Iron oxide copper-gold deposits: geology, space-time distributions, and possible modes of origin. *Econ. Geol.* 100, 371–405.
- Williams, P.J., Skirrow, R.G., 2000. Overview of iron oxide-copper-gold deposits in the Curnamona Province and Cloncurry district (Mount Isa Block), Australia. In: Porter, T.M. (Ed.), *Hydrothermal Iron Oxide Copper-gold and Related Deposits: A z*, vol. 1. Australian Mineral Foundation, pp. 105–122.
- Wilson, N.S.F., Zentilli, M., Reynolds, P.H., Boric, R., 2003. Age of mineralization by basinal fluids at the El Soldado manto-type copper deposit, Chile: ⁴⁰Ar/³⁹Ar geochronology of K-feldspar. *Chem. Geol.* 197 (1–4), 161–176. [https://doi.org/10.1016/S0009-2541\(02\)00350-9](https://doi.org/10.1016/S0009-2541(02)00350-9).
- Wyborn, L.A.I., Heinrich, C.A., Jaques, A.L., 1994. Australian Proterozoic mineral systems: essential ingredients and mappable criteria. *Aust. Inst. Min. Metall. Publ. Ser. 5 (94)*, 109–115.
- Zhao, X.F., Zhou, M.F., 2011. Fe-Cu deposits in the Kangdian region, SW China: a Proterozoic IOCG (iron-oxide-copper-gold) metallogenic province. *Miner. Deposita* 46 (7), 731–747. <https://doi.org/10.1007/s00126-011-0342-y>.
- Zhao, X.F., Zhou, M.F., Hitzman, M.W., Li, J.W., Bennett, M., Meighan, C., Anderson, E., 2012. Late Paleoproterozoic to early Mesoproterozoic Tangdan sedimentary rock-

- hosted strata-bound copper deposit, Yunnan province, southwest China. *Econ. Geol.* 107 (2), 357–375. <https://doi.org/10.2113/econgeo.107.2.357>.
- Zhao, X.F., Zhou, M.F., Su, Z.K., Li, X.C., Chen, W.T., Li, J.W., 2017. Geology, geochronology, and geochemistry of the Dahongshan Fe-Cu-(Au-Ag) deposit, southwest China: implications for the formation of iron oxide copper-gold deposits in intracratonic rift settings. *Econ. Geol.* 112 (3), 603–628. <https://doi.org/10.2113/econgeo.112.3.603>.
- Zhou, M.F., Zhao, X.F., Chen, W.T., Li, X.C., Wang, W., Yan, D.P., Qiu, H.N., 2014. Proterozoic Fe-Cu metallogeny and supercontinental cycles of the southwestern Yangtze Block, southern China and northern Vietnam. *Earth Sci. Rev.* 139, 59–82. <https://doi.org/10.1016/j.earscirev.2014.08.013>.
- Zhou, T., Fan, Y., Yuan, F., Zhang, L., Qian, B., Ma, L., Yang, X., 2013. Geology and geochronology of magnetite – apatite deposits in the Ning-Wu volcanic basin, eastern China. *J. Asian Earth Sci.* 66, 90–107. <https://doi.org/10.1016/j.jseaes.2012.12.030>.